

ABSTRACT

Title of Dissertation: REMOTE SENSING OF CLOUDS AND PRECIPITATION: EVENT-BASED CHARACTERIZATION, LIFE CYCLE EVOLUTION, AND AEROSOL INFLUENCES

Rebekah Bradley Esmaili, Doctor of Philosophy, 2016

Dissertation directed by: Dr. Kyu-Myong Kim, NASA Goddard Space Flight Center Code 613
Dr. Yudong Tian, Earth System Science Interdisciplinary Center
Professor Ning Zeng, Department of Atmospheric and Oceanic Science

Global climate models, numerical weather prediction, and flood models rely on accurate satellite precipitation products, which are the only datasets that are continuous in time and space across the globe. While there are more earth observing satellites than ever before, gaps in precipitation retrievals exist due to sensor and orbital limitations of low-earth (LEO) satellites, which are overcome by merging data from different sensors in satellite precipitation products (SPPs).

Using cloud tracking at higher resolutions than the spatio-temporal scales of LEO satellites, this thesis examines how clouds typically form in the atmosphere, the rate that cloud size and temperature evolve over the life cycle, and the time of day that cloud development take place. This thesis found that cloud evolution was non-linear, which disagrees with the linear interpolation schemes used in SPPs. Longer lasting

clouds tended to achieve their temperature and size maturity milestones at different times, while these stages often occurred simultaneously in shorter lasting clouds.

Over the ocean, longer lasting clouds were found to occur more frequently at night, while shorter lasting clouds were more common during the daytime.

This thesis also examines whether large-scale Saharan dust outbreaks can impact the trajectories and intensity of cloud clusters in the tropical Atlantic, which is predicted by modeling studies. The presented results show that proximity to Saharan dust outbreaks shifts Atlantic cloud development northward and intense storms becoming more common, whereas on days with low dust loading small-scale, warmer clouds are more common.

A simplified view of cloud evolution in merged rainfall retrievals is a possible source of errors, which can propagate into higher level analysis. This thesis investigates the difference in the intensity, duration, and frequency of precipitation in IMERG, a next-generation satellite precipitation product with ground radar observations over the contiguous United States. There was agreement on seasonal totals, but closer examination shows that the average intensity and duration of events is too high, and too infrequent compared to events detected on the ground. Awareness of the strengths and limitations, particularly in context of high-resolution cloud development, can enhance SPPs and can complement climate model simulations.

REMOTE SENSING OF CLOUDS AND PRECIPITATION: EVENT-BASED
CHARACTERIZATION, LIFE CYCLE EVOLUTION, AND AEROSOL
INFLUENCES

by

Rebekah Bradley Esmaili

Dissertation submitted to the Faculty of the Graduate School of the
University of Maryland, College Park, in partial fulfillment
of the requirements for the degree of
Doctor of Philosophy
2017

Advisory Committee:
Professor Ning Zeng, Chair
Dr. Kyu-Myong Kim, Advisor
Dr. Yudong Tian, Advisor
Professor James Carton
Professor Marla McIntosh
Professor Fernando Miralles-Wilhelm

© Copyright by
Rebekah Bradley Esmaili
2017

Acknowledgements

“We learned about gratitude and humility - that so many people had a hand in our success, from the teachers who inspired us to the janitors who kept our school clean... and we were taught to value everyone's contribution and treat everyone with respect.”

Michelle Obama

I would first like to acknowledge my research funding sources, the NASA Earth System Data Records Uncertainty Analysis Program and NASA’s Precipitation Measurement Missions (PMM) program. Without these grants, I would have been unable to devote my time to scientific pursuits.

I am grateful to the many people who helped me prepare my thesis and mentored me during my time as a PhD student. I especially want to thank my two research advisors, Dr. Yudong Tian and Dr. Kyu-Myong Kim. Under their guidance, I not only grew professionally but on a personal level as well.

From day one, Dr. Tian had complete faith that the world was my oyster and that I could do great things. He made sure that I had all the best resources – a new laptop, all the server disc space that I needed, a website for my research, travel funding, and best of all, a window seat at NASA/GSFC. He introduced me to senior scientists, encouraged me to present my work at any available opportunity, and always had time to answer my questions. At first I did not think I was capable, but over time I found that my confidence grew and that I developed a “yes I can” attitude, which empowered me to transition from a student to a professional.

I am very thankful for the advising and encouragement of Dr. Kim, who taught me what it means to have integrity as a scientist, because he is someone of impeccable character. He showed me how to clearly present my arguments, to think critically about the limitations of my work, and to hold yourself to the highest standards. He is also very kind, patient, and constantly had my best interests at heart; he always had encouraging words to say when I looked worried or stressed. His guidance helped me to understand the ethos of scientific research.

I want to extend thanks to my other committee members: Professors Ning Zeng, Jim Carton, Fernando Miralles-Wilhelm, and Marla McIntosh. I am grateful to Dr. Zeng for providing me with both academic and research guidance during my studies and for serving as chair, even while on sabbatical overseas. Similarly, Dr. Carton was always available to give me candid advice as I progressed through the program. His suggestions regarding Chapter 4 of this thesis allowed me to submit a much stronger manuscript for review. As someone from an interdisciplinary background, I appreciate Dr. Miralles-Wilhelm's professional advice and his anecdotes from working in both social and scientific fields. I appreciate the time he spent editing my introduction and conclusion chapters, as these were the most difficult for me to write. I am grateful to Dr. McIntosh for serving as Dean's Representative for my defense. As a scientist from another discipline, her insights helped me to learn how to explain myself more clearly.

There are several colleagues and friends that I would like to specifically acknowledge for reading drafts, listening to my practice talks, giving me career advice, or providing moral support: Daniel Vila, Nai-Yu Wang, Viviana Maggioni, Patrick

Meyers, Amy McNally, Grey Nearing, Kristi Arsenault, Ken Harrison, Thomas Stanley, Shelagh Johnson, and the “Metogurlz” (Cathy Thomas, Clare Flynn, and Erin Lynch). I have truly had a village of support in my studies.

I want to thank my husband Eric Hoppmann for his unwavering support and my parents, Tracie and Farid Esmaili, who encouraged me from a young age to get my education (advice that I perhaps took too far). My family has always been supportive even the going got tough; knowing that they had my back is what allowed me keep looking forward. Even my loyal pets, Shino the cat and Xena the dog, supported me through the writing process.

If you have read this far rather than jumping to the figures, then it is likely you know me personally and had an influence on my life. In the spirit of Michelle Obama’s words which opened this section: Thank you to all the teachers, professors, co-workers, friends, and family members who helped me every step of the way. You all gave me a part of hearts and share credit for my success.

Table of Contents

Acknowledgements.....	ii
Table of Contents.....	v
List of Figures.....	vii
List of Abbreviations.....	xi
CHAPTER 1. INTRODUCTION.....	1
1.1 Background.....	1
1.1.1 Combining passive microwave and infrared observations in satellite precipitation products increases resolution, but compromises data quality.....	2
1.1.2 Cloud tracking can enable more realistic data combination by answering larger scientific questions.....	4
1.1.3 Event-based evaluation of precipitation datasets can show the downstream effects of uncertainty in instantaneous measurements.....	5
1.2 Research objective.....	7
1.3 Survey of existing literature.....	8
1.3.1 Review for scientific question 1: structural cloud characteristics, cloud life cycle evolution, and diurnal cycle of clouds and rainfall.....	8
1.3.2 Review for scientific question 2: the impact of large-scale Saharan dust outbreaks on the trajectories and the intensity of cloud clusters.....	17
1.3.3 Review for scientific question 3: rainfall products and validation with ground observations.....	18
1.4 Roadmap.....	21
CHAPTER 2. A LAGRANGIAN ANALYSIS OF COLD CLOUD CLUSTERS AND THEIR LIFE CYCLES WITH SATELLITE OBSERVATIONS.....	24
Abstract.....	24
2.1 Introduction.....	25
2.2 Data.....	27
2.3 Methodology.....	29
2.3.1 Identification using temperature and morphology.....	29
2.3.2 Tracking using area overlap.....	31
2.3.3 Collocation of clusters with passive microwave rainfall estimations.....	33
2.4 Results and Discussion.....	34
2.4.1 Mean trajectories and statistical properties of cloud clusters.....	34
2.4.2 Cloud cluster climatology.....	37
2.4.3 Interannual variability.....	39
2.4.4 Life cycle of cloud clusters.....	40
2.4.5 Cloud clusters and rainfall.....	44
2.4.6 Diurnal cycle of cluster evolution.....	47
2.5 Summary.....	52
CHAPTER 3. INFLUENCE OF LARGE-SCALE SAHARAN DUST PLUMES ON THE DEVELOPMENT OF CLOUD CLUSTERS IN THE ATLANTIC AND WEST AFRICA.....	55
Abstract.....	55

3.1 Introduction.....	55
3.2 Data and Methods	59
3.3 Results and Discussion	60
3.3.1 Dust outbreak index	60
3.3.2. Cloud tracks and frequency	62
3.3.3. Mature cloud states	65
3.4 Summary and Future Work.....	66
CHAPTER 4. EVALUATION OF THE INTENSITY, DURATION, AND FREQUENCY OF IMERG RAINFALL ESTIMATES OVER THE CONTINENTAL UNITED STATES	69
Abstract	69
4.1. Introduction.....	70
4.2. Data	73
4.2.1 IMERG.....	73
4.2.2 MRMS	74
4.3. Methods.....	76
4.4. Results.....	77
4.4.1 Seasonal average and event-based IDF characterization.....	77
4.4.2 Probability distribution of event-based characteristics over CONUS	81
4.4.3 The diurnal cycle of rainfall.....	84
4.5. Summary and Discussion.....	86
CHAPTER 5. CONCLUSION	90
5.1 Summary and contribution to the scientific community.....	90
5.2 Future Work	93
APPENDIX A. COMPARING SATELLITE-BASED AND GEOS-5 CLOUD TRACKS, CHARACTERISTICS, AND DIURNAL CYCLE OVER THE ATLANTIC OCEAN.....	98
A.1 Datasets and methods.....	98
A.2 Differences in cluster properties	99
A.3 Diurnal cycle.....	99
REFERENCES	101

List of Figures

- Figure 1-1** (a) Precipitation retrievals from passive microwave satellites overpasses during a 30 min interval (light swaths), for January, 31 2016 23:30 from the IMERG retrieval algorithm. There are large spatial and temporal gaps between these overpasses (white regions). (b) The same snapshot as Figure 1a, but with combined PMW-IR estimates. Keeping track of the continuous storm evolution with geostationary observations will help to fill the gaps and to produce more consistent precipitation estimates for GPM-era datasets. 3
- Figure 1-2** A comparison of cloud trajectories in (a) brightness temperature and (b) OLR from the GEOS-5 “nature run” over the tropical Atlantic (June, 2005). 9
- Figure 1-3** A comparison of the $1^\circ \times 1^\circ$ average (a) size (b) lifetime and (c) the frequency of occurrence of cloud clusters obtained from NCEP cloud brightness temperatures and OLR from the MERRA-2 “nature run” (June, 2005). 10
- Figure 1-4** A comparison of diurnal timing of initiation of brightness temperature and OLR from the GEOS-5 nature run over the continental United States (June, 2005). Values fitted using LOESS regression and shading represent standard error. 10
- Figure 1-5** Flow chart of thesis roadmap and areas of future work. 22
- Figure 2-1** (a) Globally merged map of IR brightness temperature from NCEP/CPC Cloud brightness temperature dataset for 23:00 GMT June 28, 2012. (b) Cloud clusters captured by ForTraCC after applying temperature and size thresholds. Shading represents cloud brightness temperature. 28
- Figure 2-2** Schematic of area-overlap handling of continuous systems (c), merging systems (m), and splitting systems (s). The image was taken of thunderstorms developing over the American Midwest beginning at 3:00pm EST on June 30, 2012. Yellow represents the initial time, orange 1.5 hours later, and red 3.0 hours after initial detection. 30
- Figure 2-3** Cloud cluster tracks from Dec 1-4, 2001 produced from using the ForTraCC algorithm. A few days of tracking yield a large number of clusters and their movement begins to trace out large-scale atmospheric patterns. 30
- Figure 2-4** Climatology of cloud cluster trajectories in (a) DJF and (b) JJA, 2002-2012 with 6-9 hour lifetimes binned by $2^\circ \times 2^\circ$. Lines show average displacement of all cloud clusters that initiated at the same point over the 11-year period studied. Coloring indicates net zonal movement of clusters. Grid boxes with fewer than five initiations were not displayed. 33

Figure 2-5 (a) Number of detected events globally by lifetime and size for the entire record. (b) The kernel density estimate of cloud clusters at their maximum areal extent for each lifetime group over the entire study period (DJF and JJA, 2002-2012). 35

Figure 2-6 Mean seasonal frequency of clusters for (a) DJF and (b) JJA at their maximum areal extent. The figure shows the average seasonal count of events over the study period, binned by $2^\circ \times 2^\circ$ latitude-longitude. Warmer colors represent higher counts while cooler colors represent fewer observations. White grid boxes have ten or fewer cloud clusters across the 11-year period. 36

Figure 2-7 The composite of the 11-year DJF mean annual frequency of cloud cluster overpasses for El Niño and La Niña, binned by $2^\circ \times 2^\circ$ latitude-longitude, at their maximum areal extent. Warm or cool event years were selected based on the NINO3.4 sea surface temperature anomaly index. White grid boxes have three or fewer cloud clusters. 39

Figure 2-8 The global average life cycle evolution for new cloud clusters with varying life times. Each curve represents the average properties of millions of clusters grouped by life span. The shortest lines are short-lived events longer lines are long-lived. Curves show how the size changes as a function of the clusters' lifetime. Dashed curve is a regression fitted to the maximum of each curve. Seasons are defined by the $\pm 25^\circ$ latitude line. 42

Figure 2-9 Same as Figure 8, but showing how the average brightness temperature changes as a function of time and lifetime. 43

Figure 2-10 Total instantaneous rainfall contribution as a function of rain rate captured by clusters in the (a, b) Northern Hemisphere, (c, d) tropics, and (e, f) Southern Hemisphere in June and December 2014. The distribution is based on coincident cloud clusters and passive microwave-based rainfall estimates from the IMERG dataset. 46

Figure 2-11 Diurnal variation in local solar time (LST) cloud cluster initiation for (a) DJF and (b) JJA, binned by $2^\circ \times 2^\circ$ latitude-longitude. Each box shows the timing of maximum occurrence of cluster formation for the 11-year record. Only clusters with a lifetime greater than two hours are included. 48

Figure 2-12 The kernel density of local solar time of the life cycle stage in two regions, 0° - 30° N and 60° - 90° E (South Asia) and 0 - 40° N, 50° W- 20° E (West Africa). 49

Figure 2-13 The kernel density of local solar time of initiation in three-hourly lifetime bins for two regions, 0° - 30° N and 60° - 90° E (South Asia) and 0 - 40° N, 50° W- 20° E (West Africa). 49

Figure 3-1 Suomi-NPP/VIIRS true color corrected reflectance of Atlantic dust outbreaks, June 20-25, 2016.	59
Figure 3-2 Hovmueller diagram of (a) daily zonal average of AOD (5-25°W) and daily cloud cluster counts for (b) 0-20°W and (c) 20-40°W for JJASO 2006.	60
Figure 3-3 (a) Average JJASO AOD for 2006-2009 and (b) AOD index, calculated from the boxed region (10-20°N, 5-25°W) in Figure 3a. Days where the index was greater (less) than 1 are classified as high AOD (low AOD) index days. Missing values are due to no aerosol retrieval on cloudy days.	61
Figure 3-4 Trajectories of cloud clusters on (a) high AOD index days and (b) low AOD index days. Only clusters with a lifetime greater than or equal to one hour that developed from 9:00 – 15:00 LST, are included.	62
Figure 3-5 Composite of low AOD index days subtracted from high AOD index days for (a) AOD and (b) cloud cluster count. Only clusters with a lifetime greater than or equal to one hour which developed from 6:00 – 18:00 UTC are included.....	63
Figure 3-6 Frequency of lifetime and maximum cluster size (in pixels) for all events in study region, (b) 0-20°N, 0-20°W which is predominantly land, and (c) 0-20°N, 20-40°W which is predominantly ocean. Non-parametric LOESS regression was performed on data and shading represents the standard error	64
Figure 3-7 Probability density difference (AOD index – all days) of the maximum size and minimum temperature of high and low AOD days from the mean density cloud clusters for two regions. To choose bins, the temperature and size were grouped by 0-33%, 33-66% and 66-100% quantiles for each region (all days).	65
Figure 4-1 Average seasonal rainfall for (a) IMERG and (b) MRMS, from March 2014 to December 2015. Observations are shown for all radar quality index (RQI) values.	78
Figure 4-2 Mean intensity, duration, and frequency of rain events in JJA for (a) IMERG, (b) MRMS, and (c) IMERG-MRMS from March 2014 to December 2015. Data in regions with an average quality index below 80% were excluded from this analysis.	79
Figure 4-3 Mean intensity, duration, and frequency of rain events in DJF for (a) IMERG, (b) MRMS, and (c) IMERG-MRMS from March 2014 to December 2015. Data in regions with an average quality index below 80% were excluded from this analysis.	80
Figure 4-4 Total number of events detected for (a) CONUS and (b) for three subregions shown in (c) from March 2014 to December 2015.	81

Figure 4-5 Kernel density estimate showing the probability of average rainfall intensity (mm/h) for precipitation events maintaining a rain rate above 0.2 mm/h for (a) CONUS JJA and SJF combined, (b) DJF, and (c) JJA, from March 2014 to December 2015. Grey shading represents the standard error. 82

Figure 4-6 Kernel density estimate of duration (h) for precipitation events maintaining a rain rate above 0.2 mm/hr for (a) CONUS JJA and SJF combined, (b) DJF, and (c) JJA, from March 2014 to December 2015. Grey shading represents the standard error. 82

Figure 4-7 Kernel density estimate of intensity (mm/h) for precipitation events maintaining a rain rate above 0.2 mm/hr for (a) each region with JJA and SJF combined, (b) each region with DJF and JJA considered separately, from March 2014 to December 2015. Grey shading represents the standard error. 83

Figure 4-8 Kernel density estimate of duration (h) for precipitation events maintaining a rain rate above 0.2 mm/hr for (a) each region with JJA and SJF combined, (b) each region with DJF and JJA considered separately, from March 2014 to December 2015. Grey shading represents the standard error. 83

Figure 4-9 The JJA diurnal cycle maximum hourly rain in local solar time and the amplitude of the signal. Data in regions with an average quality index below 80% were excluded from this analysis, from March 2014 to December 2015. 84

Figure 4-10 JJA kernel density estimate of the diurnal cycle hourly phase in local standard time for (a) all CONUS and (b) each region considered separately. 85

Figure 4-11 Summary highlighting the major differences of IMERG vs MRMS between the magnitude of the intensity, duration, and frequency, based on primary features. Shading (red, grey, blue) and symbols (>, =, <) used in the table above indicate that IMERG events were larger, equal, or smaller in value than MRMS, respectively; mixed implies a great deal of regional variability or uncertainty in estimates. 87

Figure 5-1 Summary of questions and findings that were reached in this thesis. 91

List of Abbreviations

AOD Aerosol Optical Depth

CONUS Contiguous United States

EOS Earth observing Systems

ERB Earth Radiation Budget

GCM Global Climate Model

GEO Geostationary Orbit

GEOS-5 Goddard Earth Observing System Model, Version 5

GOES Geostationary Operational Environmental Satellite

GPM Global Precipitation Mission

IDF Intensity, Duration, Frequency

IPWG International Precipitation Working Group

IMERG Integrated Multi-satellitE Retrievals for GPM (IMERG)

IR Infrared

LEO Low Earth Orbit

MERRA Modern-Era Retrospective analysis for Research and Applications

MRMS Multi-Radar/Multi-Sensor

NASA National Aeronautics and Space Administration

NWP Numerical Weather Prediction

PMW Passive Microwave

SPP Satellite precipitation products

TPMA TRMM Multi-satellite Precipitation Analysis

TRMM Tropical Rainfall Measurement Mission

Chapter 1. Introduction

1.1 Background

NASA's Earth Observing System currently has 25 satellites in operation and development, providing long-term global observations of our planet's land, ocean, and atmosphere. Even in this golden era of Earth data, barriers to uninterrupted observation of clouds and rain remain due to coverage gaps between satellite overpasses, spatial limitations of instruments, and uncertainty in retrieval algorithms. Consequently, the quality of satellite datasets impacts the ability of global climate models (GCMs) and numerical weather prediction (NWP) systems to make future projections; simulations rely on having an accurate representation of cloud and rain characteristics, daily cycles, and climatology [Trenberth, 2003; Ebert et al, 2007; Stephens et al., 2010; Maggioni et al., 2016].

Interpolating observations from passive microwave (PMW) with measurements from infrared (IR) enabled satellite platforms drastically improves the spatial and temporal sampling between overpasses. Doing so utilizes the high temporal and spatial resolution IR observations of geostationary satellites with the less frequent, but more accurate, PMW measurements taken from low-earth orbit satellites.

Unlike fluid-like and Gaussian environmental parameters such as wind speed and temperature, clouds and rainfall behave as semi-coherent and distinct events [Skok et al., 2009]. As a result, we can characterize how systems grow, mature, and decay over their entire lifetime, as well as their structural changes, age, and trajectories. This

allows us to understand their behavior between PMW overpasses using IR observations and to quantify their discrepancies with more accurate ground observations. Since satellite records are now available for extended time periods, we can also composite clouds and precipitation characteristics on daily, seasonal, and intra-seasonal timescales. This understanding of event development can then be built back into models and algorithms to improve estimates.

A downside of the PMW-IR interpolation strategy is that, while errors from individual sensors can be examined, interpolating the results of the two measurements complicates error and uncertainty analysis. Most work has been done on shorter, instantaneous time scales (e.g. how does the satellite rain rate compare with the rain rate obtained from surface measurements; Ebert et al., 2007; Maggioni et al., 2016). However, short time scale errors can propagate into analysis at daily, seasonal, and intra-seasonal timescales.

1.1.1 Combining passive microwave and infrared observations in satellite precipitation products increases resolution, but compromises data quality

Figure 1-1a illustrates the coverage gaps in a typical 30 min interval hourly rain rate swath from the Integrated Multi-satellite Retrievals for GPM (IMERG) dataset, a state-of-the-art rainfall retrieval from the Global Precipitation Mission (GPM) core observatory satellite [Hou et al., 2014]. IMERG, as the name suggests, integrates PMW estimates with IR geostationary observations to “morph” or linearly interpolate the movement of the PMW estimate by using the IR-derived cloud motion vectors [Joyce et al. 2004; Huffman et al., 2015].

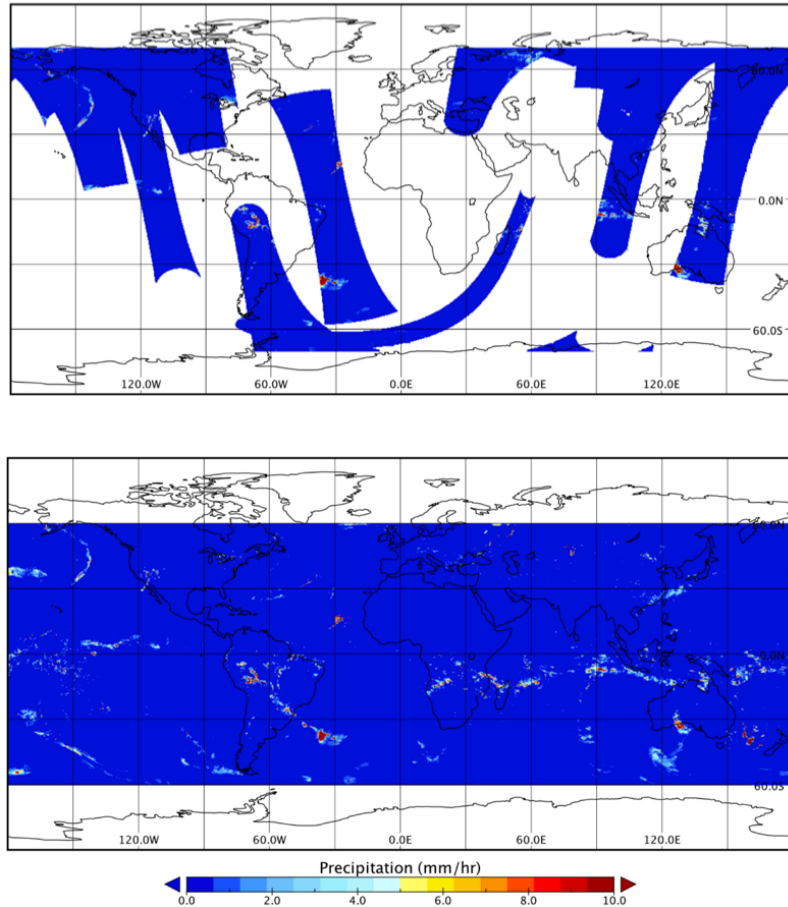


Figure 1-1 (a) Precipitation retrievals from passive microwave satellites overpasses during a 30-min interval (light swaths), for January, 31 2016 23:30 from the IMERG retrieval algorithm. There are large spatial and temporal gaps between these overpasses (white regions). (b) The same snapshot as Figure 1a, but with combined PMW-IR estimates. Keeping track of the continuous storm evolution with geostationary observations will help to fill the gaps and to produce more consistent precipitation estimates for GPM-era datasets.

While the morphing technique enables better coverage (Figure 1-1b), non-PMW estimate regions are lower quality and some of the assumptions upon reflection are simplistic. For instance, the evolution of rainfall and the clouds in which it is embedded are modulated by varying larger-scale environmental conditions such as sea surface temperature (SST), daytime solar heating, and subsidence from nearby storms, which can cause growth or decay to occur rather chaotically. As clouds propagate, they may split apart or merge to form larger systems. A linear interpolation of PMW with IR may thus be too simplistic an assumption. As shown in

Chapter 2, I examined how clouds evolve and found that growth is in fact a non-linear process that is both seasonally and regionally varying. These results encourage exploration of a more nuanced PMW-IR blending scheme, particularly in the context of cloud development.

1.1.2 Cloud tracking can enable more realistic data combination by answering larger scientific questions

Integrating IR observations in the Lagrangian framework is an effective strategy to study cloud development. Treating each cloud as a semi-coherent object across its lifespan results in a more realistic evolution of cloud systems properties than in the Eulerian view, which is essentially a series of snapshots [Machado et al., 1998].

While object-based (Lagrangian) cloud tracking has been an area of research for nearly three decades [Williams and Houze, 1987], there is renewed interest in cloud object-based evolution is partly due to the advancement of satellite-based multi-sensor high-resolution precipitation estimates [Li et al., 2015] and existence of long-term, near-global merged geostationary datasets.

In addition to retrieval algorithm applications, global climate models have difficulties reliably identifying and tracking smaller scale convective systems [Stephens et al. 2010; Westra et al., 2014]. This is in part because many cloud processes occur below the temporal and spatial resolutions of climate models. Thus, IR-based Lagrangian cloud tracking can be used to evaluate the abilities of models to reproduce both climatological cloud scaling features and trajectories, particularly at fine scales [Boer and Ramanathan, 1997].

Lagrangian cloud tracking also enables studying how large-scale environmental phenomena such as dust outbreaks can impact cloud development. During Saharan dust outbreaks, coarse aerosols travel deep into the atmosphere and interact with the clouds. Observational studies have shown that dust plumes can interact with and potentially weaken hurricanes [Dunion and Veldon, 2004; Wu, 2007]. Aerosols may also similarly affect smaller scale cloud and rainfall development, but the impact of dust outbreaks on cloud life cycles is not well known.

1.1.3 Event-based evaluation of precipitation datasets can show the downstream effects of uncertainty in instantaneous measurements

Stemming from imperfect understanding of precipitating processes and cloud development, error and uncertainty in satellite precipitation products can limit their usefulness in modeling applications. However, combining PMW and IR complicates quantification of sampling, measurement, and algorithm errors of instantaneous rainfall measurements [Maggioni et al., 2014]. The uncertainty and errors of both measurements have been individually assessed. PMW provides a more direct observation, but also systematically under and overestimates light and heavy rain, respectively [Anagnostou et al., 2010; Prakash et al., 2016]. IR-derived atmospheric motion vectors can overestimate advection rates and must be regionally corrected [Joyce and Xie, 2011]. The source of collective errors on the resulting rainfall estimate become difficult to diagnose.

Collectively, these short-time scale errors propagate into composited analysis on hourly, daily, seasonal, and climatological time scales [Tian et al., 2007]. Moving

beyond instantaneous or climatological rain totals to a more comprehensive examination of the intensity, duration, and frequency (IDF) characteristics of rain events can help pinpoint some of the sources of these errors. The IDF framework is beneficial because the impact of a single high-intensity storm is more societally significant than the same amount of rain spread out over a month. This therefore motivates the work described in Chapter 4, which evaluates event-based intensity, duration, and frequency of rainfall with surface observations.

Because radar and rain gauges are only available over a small fraction of the earth, satellite observations remain the only viable means of calibrating climate models. Models must reproduce present day precipitation for future precipitation and energy balance projections to be accurate [Hall and Vander Haar, 1999; Trenberth, 2003; Stephens, 2010]. However, models simulate precipitation character by overestimating the frequency and intensity, partly due to scaling (such sub-grid processes or averaging of intermittent precipitation) and also because of incorrect model physics, which create unrealistic vertical profiles in the cloud [Stephens et al., 2010]. In the cited studies and elsewhere, satellite observations are used as a reference to check the frequency, intensity, and daily timing of results. However, if satellite retrieval errors and uncertainty in instantaneous measurements impact composited analysis [Tian et al., 2014], observations become an imperfect reference for tuning the models and thus require further assessment.

1.2 Research objective

The objective of this thesis is to examine clouds and rainfall as semi-coherent and distinct events, to understand how their life cycle evolution unfolds in the time periods between overpasses. In carrying out this research objective, I sought to answer three principal scientific questions:

1. How many clouds typically form in the atmosphere, at what rate do cloud characteristics such as size and temperature evolve over the life cycle, and at what time of day does development take place?
2. Do large-scale Saharan dust outbreaks impact the trajectories and the intensity of cloud clusters in the tropical Atlantic, as predicted by modelling studies?
3. What are the differences between the intensity, duration, and frequency of satellite precipitation products and ground observations, which can inherit uncertainty and errors from instantaneous measurements?

To answer these questions, my goals were to:

1. Produce a large database of clouds tracks by clustering global IR-derived cold clouds and tracking their evolution and daily cycles through time to show how cloud size and temperature properties change with time, what the development differences are for large-scale storms versus small-scale clouds, and the daily timing when events take place. The results offer baseline global statistics to which models can be compared.
2. To use the object-based framework developed for this thesis to examine if coarse particles (larger than $1.0\ \mu\text{m}$) from dust outbreaks have an impact on cloud

growth and development. Clouds and rainfall can be both enhanced or inhibited by dust aerosols, which can alter the environment through radiative and microphysical effects. However, the impact on cloud development due to either effect is not well-researched.

3. To evaluate the quality of satellite rain events in the context of their intensity, duration, and frequency so that we, along with members of the community who rely on this data, can be aware of their current strengths and weaknesses.

As more GPM data is collected, precipitation observations are combined with tracked cloud clusters, so that in the future we can study how surface rain evolves within the cloud and in context of environmental phenomena like dust outbreaks. As retrieval measurement techniques mature, globally tracked rainfall becomes feasible and is a natural extension of this thesis.

1.3 Survey of existing literature

1.3.1 Review for scientific question 1: structural cloud characteristics, cloud life cycle evolution, and diurnal cycle of clouds and rainfall

1.3.1.1 Structural characteristics of cloud clusters

We show the usefulness of event tracking in Figure 1-3, which shows the differences in tracks produced by clustering outgoing longwave radiation from the GEOS-5 Nature Run (Figure 1-2a) and the tracks produced from cloud brightness temperature clusters (Figure 1-2b). Comparing the two Figures, the model has many more trajectories than what is observed. The model produces a more zonally extensive intertropical convergence zone (ITCZ), a semi-persistent band of heavy rainfall that

encircles the Earth. The resulting trajectories are a bit smoother and less chaotic in the model than in the observation results. A caveat of this comparison is that the model and observation are tracking two related but different environmental variables (Outgoing longwave radiation versus brightness temperature; see Appendix).

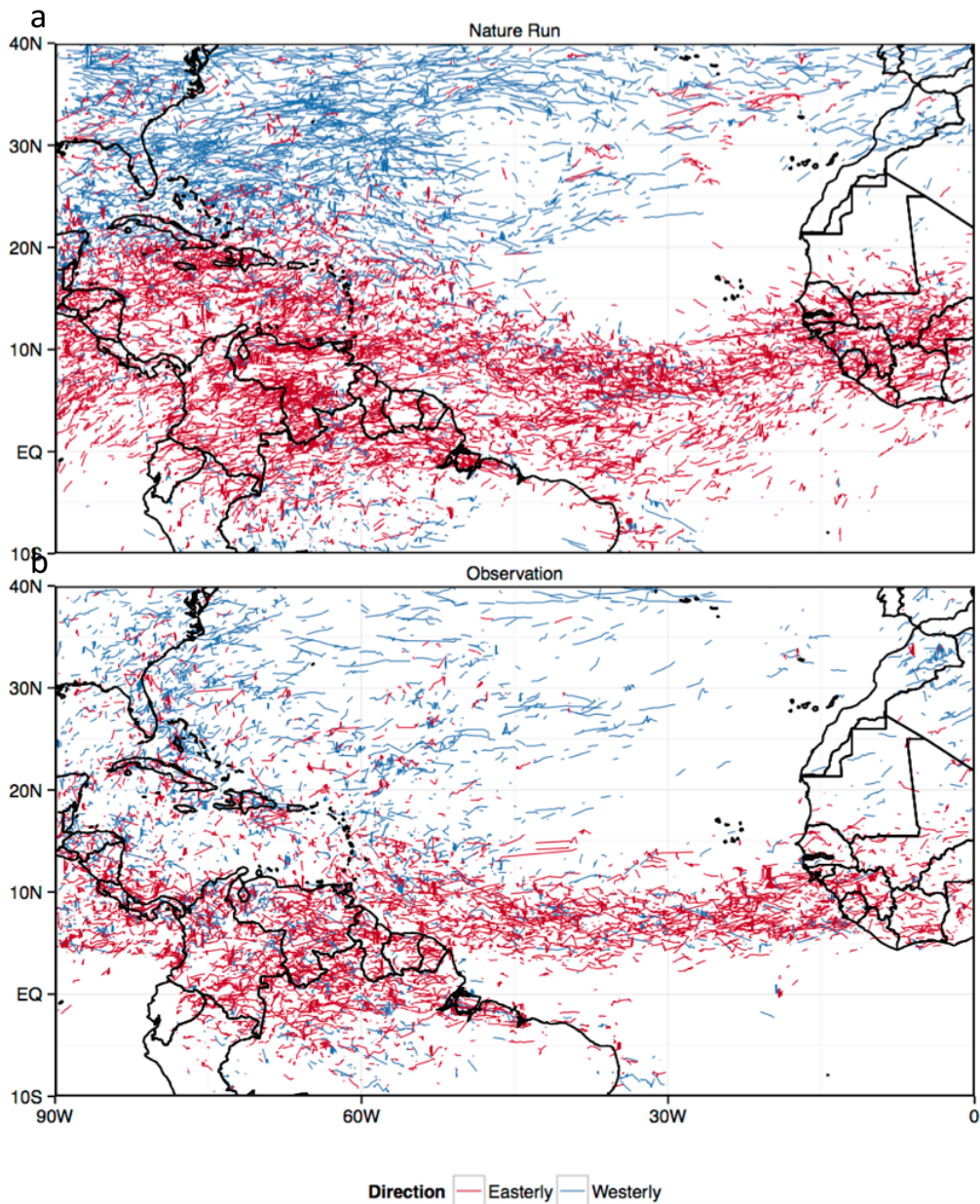


Figure 1-2 A comparison of cloud trajectories in (a) brightness temperature and (b) OLR from the GEOS-5 “nature run” over the tropical Atlantic (June, 2005).

Regardless, it does illustrate some of the disagreement.

There are also differences in the cluster characteristics. In Figure 1-3a, we can see that clusters are smaller in the model compared with observations, especially outside

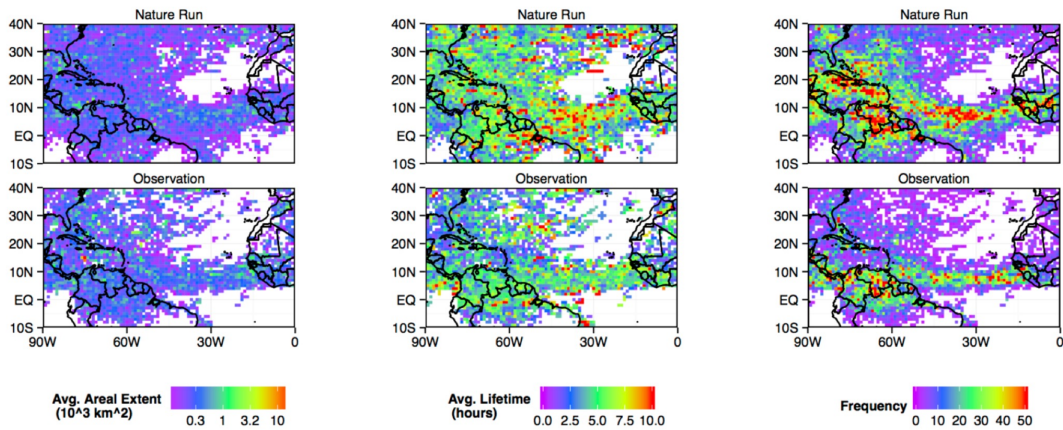


Figure 1-3 A comparison of the $1^\circ \times 1^\circ$ average (a) size (b) lifetime and (c) the frequency of occurrence of cloud clusters obtained from NCEP cloud brightness temperatures and OLR from the MERRA-2 “nature run” (June, 2005).

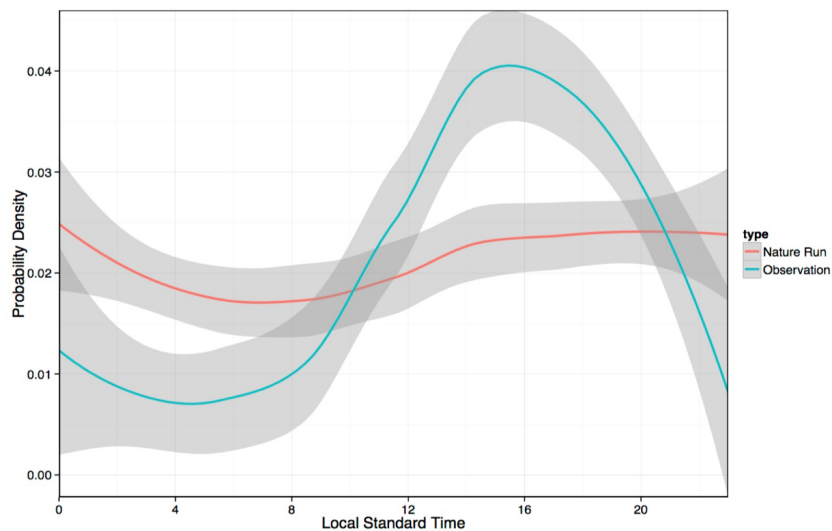


Figure 1-4 A comparison of diurnal timing of initiation of brightness temperature and OLR from the GEOS-5 nature run over the continental United States (June, 2005). Values fitted using loess regression and shading represent standard error.

of the ITCZ region. However, model clusters typically last longer (Figure 1-3b) across all locations than observed clusters. Finally, Figure 1-3c shows that the model produces a surplus of clusters, particularly over the Caribbean and the Southeastern United States.

A final divergence between models and observations can be seen in how they reproduce the diurnal cycle (Figure 1-4). Afternoon thunderstorms are common over Florida in June, however the model fails to reproduce this afternoon peak. Features of the shortest time scales are the most difficult for models to reproduce [Dai et al., 1999].

To evaluate how well models and algorithms characterize the atmosphere, it is necessary to survey past results and answer some basic questions about cloud tracking, characteristics, and the diurnal cycle. Some of the earliest studies sought to produce a census of cloud clusters using infrared observations to examine the scaling and lifetimes [Boer and Ramanathan, 1997]. Primarily focused in the tropics, infrared observations show that, while convection is commonly considered a chaotic process, there is in fact quite a bit of structure and regularity in terms of its regional size, frequency, and the timing of cluster formation. These represent basic features which are necessary to evaluate model quality.

1.3.1.1.1 Size distribution

Globally speaking, how large is a typical cloud? While the size of cloud clusters varies greatly, the few largest clouds (the 20% that are larger than $2 \times 10^4 \text{ km}^2$), rather than the numerous small clouds, are what contribute the most to cloud cover over the Western Pacific [Williams and Houze, 1987]. Events such as Mesoscale Convective

Systems (MCS) are 60% larger in the Southern Hemisphere, predominantly form over land, and are nocturnal; however, those that do form over the ocean tend to become tropical cyclones [Velasco and Fritsch, 1987; Machado, 1993]. In fact, clusters tend to have a lognormal sizing preference across different regions [Machado et al., 1992; Mapes and Houze, 1993; Esmaili et al., 2016].

But does rain follow similar scaling? While the presence of a cloud does not guarantee rain, the thresholds used in these studies (235-245K) are predominantly deep convection in the tropics. Studies that examine rain areas within the cloud clusters have shown that they scale similarly [Feng et al., 2013], and clusters can thus be used proxies for rain areas.

1.3.1.1.2 Frequency

How often do clouds form? Machado [1992] found that, across all size classes of clusters, the frequency distribution follows a power law and that there are preferential sizes for clusters with very cold cloud top temperatures. The highest concentration of clusters was found over land, particularly around high terrain. In the tropics, there was a high count of clusters over land in the summer hemisphere across all size scales [Machado et al., 1993].

Previous studies focused on West Africa, the tropical Atlantic [Machado et al. 1992], South America [Velasco and Fritsch, 1987; Machado et al. 2004] and the Maritime Continent [Mapes and Houze, 1993]. In Chapter 2 we present a global climatology of cluster count. We found regional agreement, but globally the highest occurrence of clusters took place over the Western Pacific, with high activity also taking place over the Amazon and the African Rainforest in the Austral Winter.

1.3.1.2 Cloud lifecycle evolution

The earliest studies examining cloud lifecycle evolution combined infrared satellite-based cloud cluster tracking with field campaign data, such as the Tropical Ocean Global Atmosphere (TOGA) field campaigns, to examine cloud evolution, structure, and the atmospheric and environmental conditions leading to development [Williams and Houze, 1987; Chen and Houze, 1997].

Past studies found that clouds undergo regular life cycle stages: initiation, growth, maturity, and decay [Williams and Houze, 1987; Chen and Houze, 1997]. The rate and timing at which these life cycle stages occur are related to their total lifetime, precipitation quantity, and diurnal cycle [Esmaili et al., 2016].

Past evolution studies have focused on Mesoscale Convective Systems (MCS) due to their ease of detection in radar and satellite images [Maddox, 1980; Laing and Fritsch, 1997; Blamey and Reason, 2011]. Because MCS display regularity in their life cycles, Machado et al. [2004] was able to develop a statistical life cycle model to predict MCS propagation, which was built into the Forecast and Tracking the Evolution of Cloud Clusters [ForTrACC; Vila et al., 2001] algorithm. This technique is presently in operational use by the Brazilian National Institute for Space Research for short-term forecasts of convective cloud systems.

Sophisticated combinations of infrared, PMW-based precipitation, and environmental reanalysis data can show nuanced details of evolution, such as which clouds contribute to total rainfall, during what development stage maximum precipitation occurs, and how rain features and their vertical reflectivity evolve. Hall and Vonder

Haar [1999] found that the coldest clouds were the largest contributors to total rainfall. Inoue et al. [2009] collocated PMW measurements and cloud clusters and found that rain rates tended to be more intense at earlier stages in their lifecycle, when clusters were also optically thicker. Feng et al [2012] took this one step further by separating clusters into distinct rain features: the convective core, the stratiform rain region, and non-raining anvil. They found that for clouds with lifetimes exceeding 6 hours, humidity and upper level wind shear were over 50% greater than among short duration clouds. The anvil size was well correlated with the convective core, stratiform rain area, and strong updraft speeds. In Yuan et al.'s [2011] analysis of the vertical profiles of MCS from CloudSat, the horizontal dropoff of reflectivity (and thus, internal rain intensity of the clouds) was more abrupt for the strongest supercluster events. Looking at environmental parameters as well, Duncan [2014] found that deep convective systems are the most easily tracked. While the system speed and duration didn't change significantly across ocean basins, the fastest systems caused sea surface temperature to decrease by reflecting solar radiation. By combining satellite observations with reanalysis data, we can see how deep convection and its local environment feed back into one another.

1.3.1.3 Lifecycle evolution and theories of cloud cluster development

Tracking these clusters with time and merging with other local environmental datasets enabled scientists to advance competing theories of how cloud clusters develop. Hall and Vonder Haar [1999] compare some of the primary theories. The “day versus night” subsidence (DNS) theory states that nocturnal development is driven by increased longwave cooling that leads to mass and moisture convergence,

making conditions prime for development. In the daytime, pressure gradients arise from differences in vertical heating in cloudy regions and adjacent clear-sky regions, but are more likely disrupted by solar heating.

Another theory is the direct radiative cloud forcing (DCF), which was promoted by Machado et al. [1992, 1993] and can be broken down into three components. First, daytime solar absorption leads to upper level heating in cloud tops, stabilizing the lapse rate, and discouraging development. However, nocturnal longwave emission is not offset by incoming solar radiation, and the net cooling destabilizes the lapse rate. At the base of the cloud, absorption of longwave emitted from the surface or lower level clouds is further destabilizing.

Finally, Chen and Houze's [1996] theory suggests that development is most favorable in the afternoon, but the longest lasting systems persist until the early morning, causing the peak. They also propose day-to-day variations in development, or "diurnal dancing," which suggest that regions that have strong development shade the underlying ocean surface and lower the SSTs. This, along with low humidity downdrafts, suppresses development for 1-2 days. However, neighboring "clear sky" regions will grow increasingly favorable for development.

In addition to local environmental influences, many of the above studies address the influence of the intraseasonal oscillations, as well as larger scale events like El Nino, on the results. Chen and Houze [1997] observed active and suppressed phases over the tropics. Velasco and Fritsch [1987] found that twice as many MCS clusters formed during the El Nino event in their study period. We similarly found a decrease

in cluster formation in South America and the Atlantic, along with other teleconnections such as an increase in the Northwestern United States and Indian Ocean and a decrease in the Atlantic Basin.

In spite of its rich history, a few gaps remain in our understanding of cloud cluster tracking. Few studies extended beyond the tropics or examined phenomena or target-specific phenomena such as tropical convection and MCS. Because there are many clouds, precipitation systems, and climate regimes, a goal of this thesis is to produce the first global study and also to extend analysis to all detectable events, rather than focusing on the most extreme.

1.3.1.4 Diurnal cycle of clouds and rainfall

When do clouds form? Velasco and Fritsch [1987] found that MCS were typically a nocturnal process. The early morning peak of the largest clusters was noted by Williams and Houze [1987] and Mapes and Houze [1993]. In the Williams and Houze [1987] study, land and ocean clusters frequencies were out of phase, with an early morning maximum over the ocean adjacent to the Maritime continent and a morning minimum over land. In the Mapes and Houze [1993] study, the early morning peak was made up of larger, colder clusters while the afternoon peak consisted of moderately cold clouds. Building on this, the work presented in Chapter 2 shows that double peak in development over the ocean is composed of long lasting clouds in the evening and the short lasting clouds in the morning.

1.3.2 Review for scientific question 2: the impact of large-scale Saharan dust outbreaks on the trajectories and the intensity of cloud clusters

Trans-Atlantic Saharan dust outbreaks can reach as far as the Caribbean, South America, and Eastern United States [Prospero and Lamb, 2003]. Dust outbreaks can be self-sustaining: Dust aerosols absorb shortwave solar radiation and emit in the longwave, heating the air but cooling the land and ocean below. This temperature gradient leads to the formation of the Saharan Air Layer (SAL). As the SAL rises, it creates a land-sea circulation which transports moisture from the Atlantic Ocean to the African continent, which then enhances rainfall along the Eastern Atlantic and coastal Africa. A Walker-type circulation forms in the Atlantic from the increase in deep convection closer to the Eastern Atlantic and the subsequent subsidence causes less convection in the West Atlantic and the Caribbean [Lau et al., 2009].

A northward shift of the intertropical convergence zone (ITCZ) can result from the enhancement of the African Easterly Jet in proximity to the SAL [Wilcox et al. 2010]. A high atmospheric loading of aerosols can decrease the sea surface temperatures of the underlying ocean, however this does not appear to shut down storm development [Wilcox et al., 2010; Lau and Kim, 2007]. Over the ocean, the SAL can enhance Easterly African Waves, which are a primary precursor to tropical cyclones.

The SAL can also enhance or inhibit clouds and rainfall through radiative effects or through microphysical effects from transported aerosols. Hurricanes can weaken or have intensification diminished when the SAL interacts with hurricanes [Dunion and Veldon, 2004; Wu, 2007]. A possible mechanism is that warm, dry air is intruded into

the cloud, which then weakens downdrafts thereby suppressing development. The presence of coarse aerosols in the SAL may inhibit development through microphysical effects. However, others claim that only a small fraction of dust is entrained [Twohy, 2014; Lawson, 2010].

The impact of dust outbreaks on cloud life cycles is not well known. The larger scale effects of aerosols may not only alter the location of clouds [Wilcox et al. 2010] but the induced large-scale circulation [Lau and Kim, 2007] may also affect how the lifecycle milestones occur and the local timing in which they take place. Heavy dust can cause the ocean surface to cool by absorbing solar radiation, possibly hindering the development of intense storms as convection shifts northward. While the indirect effects of aerosols are considered secondary, they could lead to some enhance or suppress of development in contaminated clouds.

1.3.3 Review for scientific question 3: rainfall products and validation with ground observations

Water naturally emits microwave radiation, a physical characteristic that enables both ground and satellite radar estimation. In the required 10-85 GHz window, observations can only be made in the low earth (400 km) polar orbit, at the expense of large gaps between satellite overpasses. Observations of far-infrared cloud brightness temperature (10.5 μm) from the much further away geostationary satellites (35,800 km) do not suffer from the same tunnel vision. However, longwave emission can only reveal cloud top characteristics and not the underlying rainfall [Sapiano and Arkin, 2009; Xie and Arkin, 1997].

Due to satellite orbits and sensor limitations, most major TRMM-era satellite precipitation products (e.g. TMPA, GSMaP, PERSIANN, CMORPH) relied to an extent on IR. Most products' algorithms operate using the following scheme: when a strong enough PMW signal is detected, the reflectivity is converted to a corresponding surface rain rate. Because the ocean surface has a more uniform temperature and composition than land, lower frequency channels (10-19 GHz) can be employed and the conversion can be more consistently and accurately applied. Measurements over land are more challenging because the surface is warmer, which saturates emission at lower microwave channels. The accuracy of PMW measurements are compromised due to the surface's inhomogeneity in time and space, and this inaccuracy can range from false detection of rain from the presence of surface snow and ice to overlooking the presence of light, warm rain altogether [Ebert et al., 2007; Agnostou et al., 2010]. Various datasets were thus developed during the TRMM-era to overcome these and other limitations by implementing a variety of innovative strategies.

Of the list of satellite precipitation datasets, CMORPH is of particular relevance to this thesis, in part because the morphing technique has been inherited by IMERG, the flagship retrieval algorithm for GPM. IMERG is built on CMORPH's ability to provide global, half hourly estimates by combining PMW scans with geostationary infrared observations. After a passive microwave overpass, cloud motion vectors are estimated from infrared data and then used to predict where the rainfall is propagating. A Kalman filter is used to decide which measurement to use (the PMW,

IR, or MORPHED data) to provide a weighted estimate, depending on the timing of the overpass [Joyce and Xie, 2011].

While improving the temporal resolution, morphing PMW and IR complicates sampling, measurement, and algorithm error quantification of instantaneous rainfall measurements [Maggioni et al., 2014]. PMW in general has difficulty characterizing extreme rainfall, both heavy and light. Convective rainfall in the detection is inhibited

While improving the temporal resolution, morphing PMW and IR complicates sampling, measurement, and algorithm error quantification of instantaneous rainfall measurements [Maggioni et al., 2014]. PMW in general has difficulty characterizing extreme rainfall, both heavy and light. Convective rainfall in the detection is inhibited partly due to rapid changes in rain rates over short periods of time. Lighter rain events are also challenging, because clouds are warmer and often lack ice particles and can therefore escape detection [Ebert et al., 2007]. However, even motion vectors can overestimate propagation in the extratropics and require adjustment [Sears and Velden, 2012]. IR can be used to indirectly measure rainfall, but because the highest levels of the cloud mask the underlying rainfall, estimates are only statistically significant for tropical deep convection [Xie and Arkin, 1997]. For this reason, it is preferable to use IR to calculate the atmospheric motion vectors in precipitation measurements, rather than to estimate rainfall whenever a recent PMW overpass is available.

While combining PMW, IR, and morphing enables the highest temporal and spatial sampling, CMORPH has a high bias and strong seasonality, with overestimation in

the summer and underestimation in the winter. CMORPH tends to overestimate the amplitude of the diurnal cycle in the summer. When examined on different time scales, there is a large positive bias in the summer and a small negative bias in the winter, resulting in high bias on yearly time scales. However, on shorter event time scales (1-5 days), errors were lower than when using other products [Tian et al., 2014]. Utilizing a Kalman filter to select the most appropriate technique improved the quality of estimations [Joyce and Xie, 2011]. Since the morphing technique is seen as the way forward into the GPM-era, continued refinement and validation of final products are areas of ongoing work [Sorooshian et al., 2011], and motivate the work in this thesis.

1.4 Roadmap

I provide a roadmap for how the dissertation is organized, which is also summarized in Figure 1-5. As I progressed through my research work, atmospheric scaling left a great impression on me. On that note, it is appropriate that my thesis starts with a global analysis of cold cloud clusters in Chapter 2. There, I show that clouds have regular development stages, and detail the local timing of when longer lasting clouds typically form.

In Chapter 3, I will present an early examination of how dust aerosols can modulate the location and development of clouds over the Atlantic in 2007. In the future, I will extend this work to longer time scales and put it in the context of environmental data from reanalysis results.

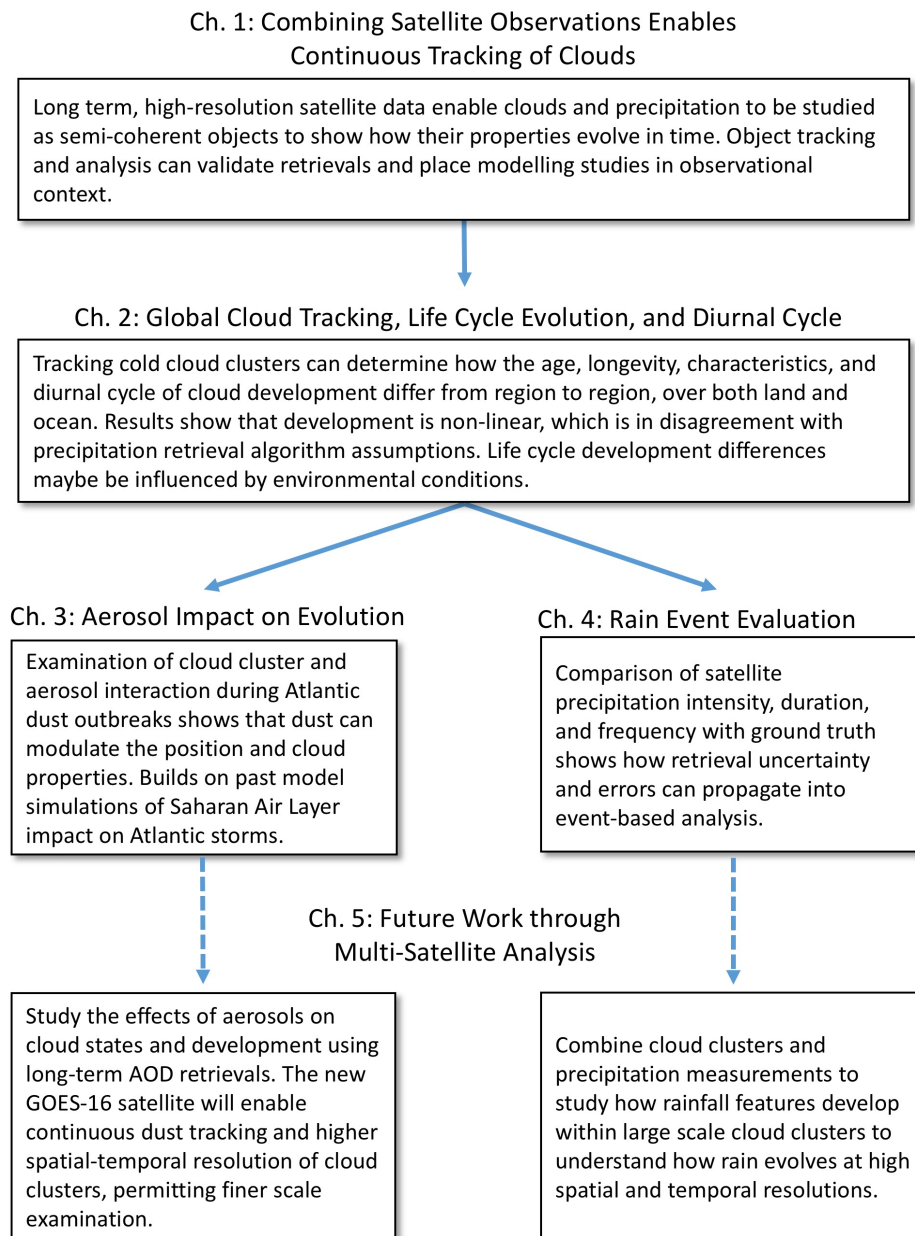


Figure 1-5 Flow chart of thesis roadmap and areas of future work.

In Chapter 4, I move from planetary to synoptic scales and from clouds to the rainfall that they contain. I characterize precipitation events produced by IMERG and compare them with ground observations over the contiguous United States. This work shows how well IMERG reproduces rainfall event characteristics and the daily cycle.

Developing awareness of the strengths and weaknesses of this next-generation product forms the basis of my future research, wherein I plan to examine rainfall in both time and space by combining IMERG with the cloud cluster data produced in Chapter 2.

By the end of this thesis, we can see how object-based tracking and analysis help us understand the paradox of scaling in our planet: even the smallest atmospheric constituents (1-2 μm) can impact a much larger cloud (1000 km or more). I will offer some closing thoughts as I conclude Chapter 5 and propose my vision for future work.

Chapter 2. A Lagrangian Analysis of Cold Cloud Clusters and their Life Cycles with Satellite Observations

Published in the Journal of Geophysical Research: Atmospheres, Oct 6, 2016

Rebekah Bradley Esmaili¹, Yudong Tian², Daniel Alejandro Vila³, Kyu-Myong Kim⁴

¹Dept. of Atmospheric and Oceanic Science, University of Maryland, College Park, Maryland

²Earth System Science Interdisciplinary Center, University of Maryland, College Park, Maryland

³National Institute for Space Research (INPE), São José dos Campos, Brazil

⁴NASA Goddard Space Flight Center, Greenbelt, Maryland

Abstract

Cloud movement and evolution signify the complex water and energy transport in the atmosphere-ocean-land system. Detecting, clustering, and tracking clouds as semi-coherent clusters enables study of their evolution which can complement climate model simulations and enhance satellite retrieval algorithms, where there are gaps between overpasses. Using a cluster tracking algorithm, in this study we examine the trajectories, size, and brightness temperature of millions of cloud clusters over their lifespan, from infrared satellite observations at 4 km, 30 min resolution, for a period of 11 years. We found that the majority of cold clouds were both small and short-lived and that their frequency and location are influenced by El Niño. Also, this large sample of individually tracked clouds shows their horizontal size and temperature evolution. Long-lived clusters tended to achieve their temperature and size maturity milestones at different times, while these stages often occurred simultaneously in short-lived clusters. On average, clusters with this lag also exhibited a greater rainfall contribution than those where minimum temperature and maximum size stages occurred simultaneously. Furthermore, by examining the diurnal cycle of cluster

development over Africa and the Indian subcontinent, we observed differences in the local timing of the maximum occurrence at different life cycle stages. Over land there was a strong diurnal peak in the afternoon while over the ocean there was a semi-diurnal peak composed of longer-lived clusters in the early morning hours and shorter-lived clusters in the afternoon. Building on regional specific work, this study provides a global long-term survey of object-based cloud characteristics.

2.1 Introduction

Clouds are the most visible vital sign of the atmosphere's dynamic water and energy transfer. They are responsible for the latent heat release that drives the atmospheric circulation. Their transport of water in the form of moisture and precipitation is critical for the Earth's hydrological cycle. On sub-synoptic scales, the cloud systems' movement, evolution, and spatial and temporal characteristics are remarkably turbulent and complex.

The Lagrangian framework is an effective approach to study cloud clusters. Treating each cloud as an object across its lifespan produces useful information on the evolution of cloud systems' properties, which is not available from the Eulerian view [Machado et al., 1998]. Renewed interest in cloud object-based evolution is partly due to the advancement of satellite-based multi-sensor high-resolution precipitation estimates [Li et al., 2015]. Currently, these estimates rely heavily on observations from passive microwave (PMW) sensors aboard polar-orbiting satellites [Kummerow et al., 2000; Joyce et al., 2004; Huffman et al. 2007; Huffman et al. 2013]. These PMW-based estimates are relatively accurate, but they do not correlate well with

surface observations when precipitation is very light, very heavy, or over saturated land surfaces, particularly during winter months [Ebert et al., 2007]. Additionally, these data have large spatial and temporal gaps.

One way to bridge these coverage gaps is to use cloud system advection information derived from high-resolution infrared observations to continuously “morph” the PMW-based rainfall [Joyce et al., 2004; Kubota et al., 2007; Xie and Xiong, 2011]. These approaches have been proven effective and are being incorporated into Integrated Multi-satellite Retrievals for GPM [IMERG; Huffman et al., 2013], the next-generation, Global Precipitation Measurement (GPM; Hou et al., 2014) era product suite. However, the accuracy of the PMW-based estimates is also influenced by the life cycle stage [Tadesse and Agnastou, 2011]. Developing a more detailed understanding of evolution can provide additional context.

Another critical application is the evaluation and diagnosis of global models. Currently atmospheric models still unrealistically reproduce observed precipitation [Ebert et al., 2007; Stephens et al. 2010]. The conventional Eulerian validation gives the spatial and temporal statistics on each individual grid box, which is the accumulation of many different cloud systems at various life stages. A Lagrangian comparison of modeled and observed cloud evolution statistics could produce additional insight on the modeling of individual cloud-precipitation processes [Boer and Ramanathan, 1997].

In the past, studies that combined infrared satellite-based cloud cluster tracking with Tropical Ocean Global Atmosphere (TOGA) field campaigns to examine cloud

evolution, anatomy, and development conditions [Williams and Houze, 1987; Chen and Houze, 1997]. On larger scales, Mesoscale Convective Systems (MCS) have in particular been studied due to their ease of detection in radar and satellite images and destructiveness [Maddox, 1980; Laing and Fritsch, 1997; Blamey and Reason, 2011]. MCS display regularity in their life cycles, enabling Machado et al. [2004] to develop a statistical life cycle model to predict MCS propagation with good forecasting skill.

As global, long-term, quality controlled IR data and precipitation data become available [e.g., Janowiak et al., 2001; Joyce et al., 2004], it becomes feasible to extend IR-based cloud tracking beyond regional scales and expand the scales of observed phenomena. By following a large number of cloud clusters on the global scale for over 11 years, we will be able to understand more systematically their large-scale dynamical and statistic characteristics.

In this paper, we present a near-global (60°S-60°N), high-resolution (4 km, 30 min.), long-term (11 year) study of cloud cluster tracks, life cycle evolution, and diurnal cycle. The high-resolution data used for the study and the methodology for storm tracking are described in Section 2.2 and 2.3, respectively. Section 2.4 presents the results, followed by summary and discussions in Section 2.5.

2.2 Data

For our study, we use the NCEP/CPC a 4-km, half hourly infrared (IR) brightness temperature dataset [Janowiak et al., 2001]. The dataset is merged from all available geostationary satellites (GMS, Meteosat-5, Meteosat-7, GOES-8 and GOES-10) to

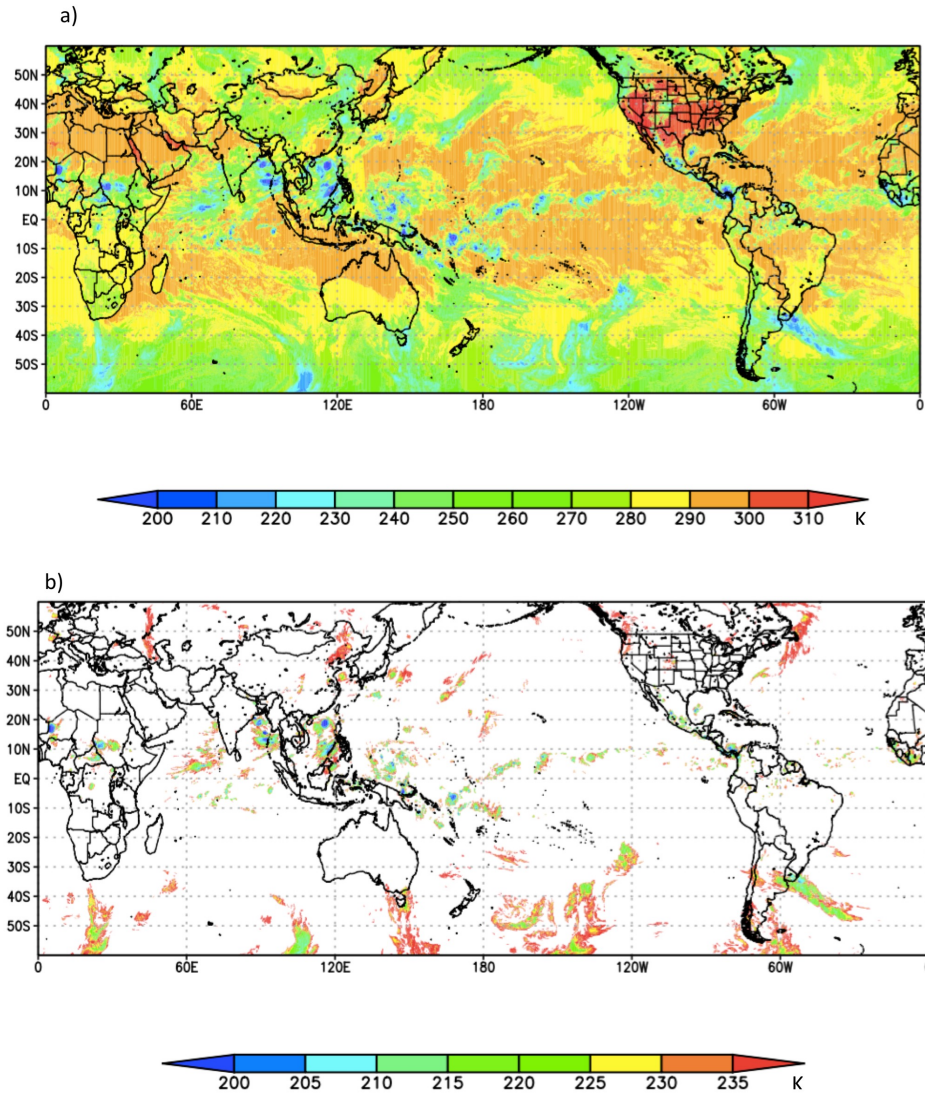


Figure 2-1 (a) Globally merged map of IR brightness temperature from NCEP/CPC Cloud brightness temperature dataset for 23:00 GMT June 28, 2012. (b) Cloud clusters captured by ForTraCC after applying temperature and size thresholds. Shading represents cloud brightness temperature.

form near-global (60°N-60°S) coverage on a uniform latitude-longitude grid. We used 11 years of data from 2002 to 2012 for our study.

We have performed additional quality control of the IR data. There are gaps in the IR data in regions covered by the GMS satellite in the Western Pacific (120°-170°E), so we filled the missing data by interpolating the preceding and following 30 min

snapshots, to produce more seamless coverage. Our tests show that this interpolation helps to prevent early termination of the cloud lifespan due to missing data.

2.3 Methodology

The techniques for tracking clouds are mature and largely similar, albeit there are many implementations. Most of those techniques involve IR geostationary satellite imagery to follow classes of convective events. The primary dissimilarities in algorithms involve the detection criteria, such as through the selection of brightness temperature or size parameter thresholds [Carvalho and Jones, 2001; Morel and Senesi, 2002], usage of more nuanced detection schemes [Lakshmanan, 2009], or the treatment of splits and merges [Fiolleau and Roca, 2013].

Despite a variety of implementations, Machado et al. [1998] found that most of the life cycle statistics are not overly sensitive to the tracking method used. For this paper, we selected Forecast and Tracking the Evolution of Cloud Clusters [ForTrACC; Vila et al., 2001] which has a single temperature and system size threshold and merges and splits are treated as special cases for tracking systems (this will be explained in the Section 2.3.2). ForTrACC's simplicity enabled us to capture a broader range of cloud species.

Tracking clouds involves the following two major steps:

2.3.1 Identification using temperature and morphology

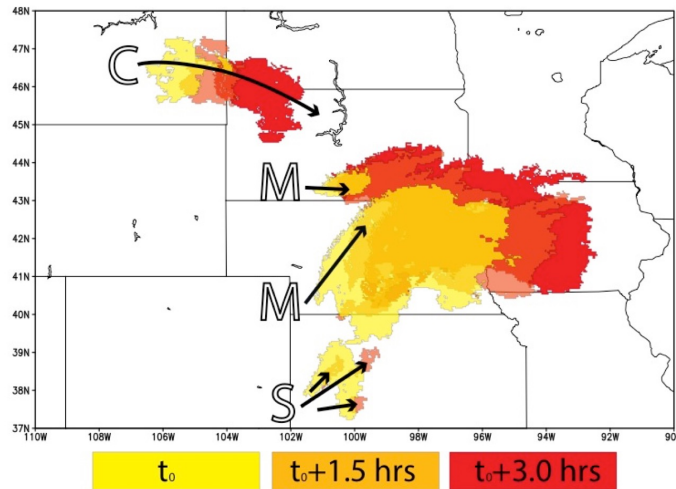


Figure 2-2 Schematic of area-overlap handling of continuous systems (c), merging systems (m), and splitting systems (s). The image was taken of thunderstorms developing over the American Midwest beginning at 3:00pm EST on June 30, 2012. Yellow represents the initial time, orange 1.5 hours later, and red 3.0 hours after initial detection.

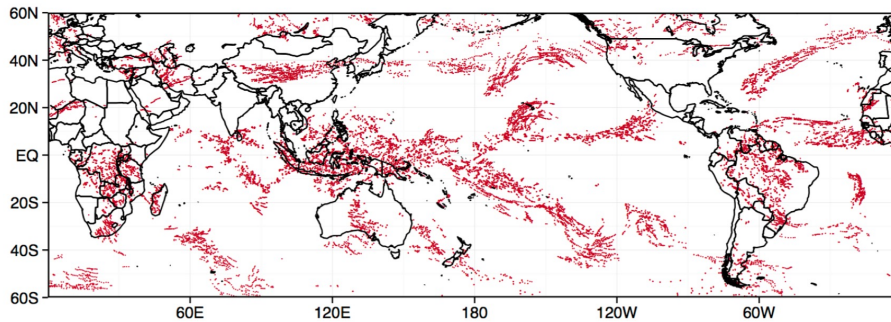


Figure 2-3 Cloud cluster tracks from Dec 1-4, 2001 produced from using the ForTrACC algorithm. A few days of tracking yield a large number of clusters and their movement begins to trace out large-scale atmospheric patterns.

Using brightness temperature thresholds to capture clouds has been used in past studies and typically empirically derived to satisfy the research goals [e.g. Blamey and Reason, 2001; Velasco and Fritch, 1987; Williams and Houze, 1987]. In general, brightness temperature detection thresholds vary between 235-255 K and tended to be subjectively chosen. However, the cluster areal extent was found to be linearly

dependent on cluster threshold and thus not overly sensitive to the exact threshold chosen [Machado et al. 1992; Mapes and Houze, 1993].

To capture a variety of cloud clusters, we used a single 235 K brightness temperature threshold, which in the upper atmosphere corresponds to a height of roughly 10 km (9 km) in the tropics (midlatitudes), which is well into the free atmosphere.

Additionally, we applied a minimum size threshold of 100 contiguous pixels (1,600 km² at the equator) at all time steps, thus limiting the study to events at the upper bounds of mesoscale or larger. We excluded smaller scale events because they would be more suitable for regional studies. Figure 2-1 shows this selection criteria being applied to a typical IR snapshot. A temperature range of 235-245 K has been used in the past to detect cloud clusters (e.g. Williams and Houze, 1987; Mapes and Houze, 1993; Carvalho and Jones, 2001; Machado et al., 2004); the colder threshold is utilized to avoid capturing frozen, high altitude surfaces. The size threshold reduces the number of tracked clouds by filtering out small-scale events and reducing the number of splits and merges. With only a temperature threshold, a single time step can yield over 17,000 cloud clusters. Applying the size threshold decreased to the number to 800-1000 events.

2.3.2 Tracking using area overlap

ForTrACC uses an area overlap technique to track the cloud clusters, both forward and backward in time. If two cloud clusters identified in different time steps have any shared pixels, they were considered the same system and assigned a family number. If more than one match was found, the largest overlapping system was tracked.

Using infrared data, we show in Figure 2-2 a schematic of the area-overlap handling in ForTrACC. The area overlap technique produces several cloud cluster merge scenarios: one-to-one (continuous), one-to-many (split), many-to-one (merge), or no match (initialization or dissipation). Most systems undergo merging or splitting in their life cycle, the prior occurs before maturation, and the latter more frequently towards the end of the life cycle. Only one cluster is followed at each time step to keep features well defined. When clusters split, the largest cloud continues to be tracked while the smaller split clusters are treated as a new family and the lifetime clock is reset. All merging clusters are considered a dissipation and their life cycle ends. ForTrACC's handling of split and merge segments is different from earlier work; in other schemes, the segments remain part of the cloud cluster system rather than considered a new systems [Mapes and Houze, 1993; Chen and Houze, 1996; 1997)].

A sample output of the resulting cloud cluster tracks are shown in Figure 2-3. In addition to showing centroid location, statistics related to the size or areal extent, the mean brightness temperature, and travel distance of the cluster are also calculated. Colder temperatures indicate higher cloud tops while areal extent shows the relative scale of the observed system. All clusters achieve a minimum temperature and maximum size, which we use as criteria for developmental maturity in Section 2.4.5. We use this information to study the ForTrACC-based cloud clusters' statistical properties, climatology, life cycle, rainfall contribution, and diurnal cycle.

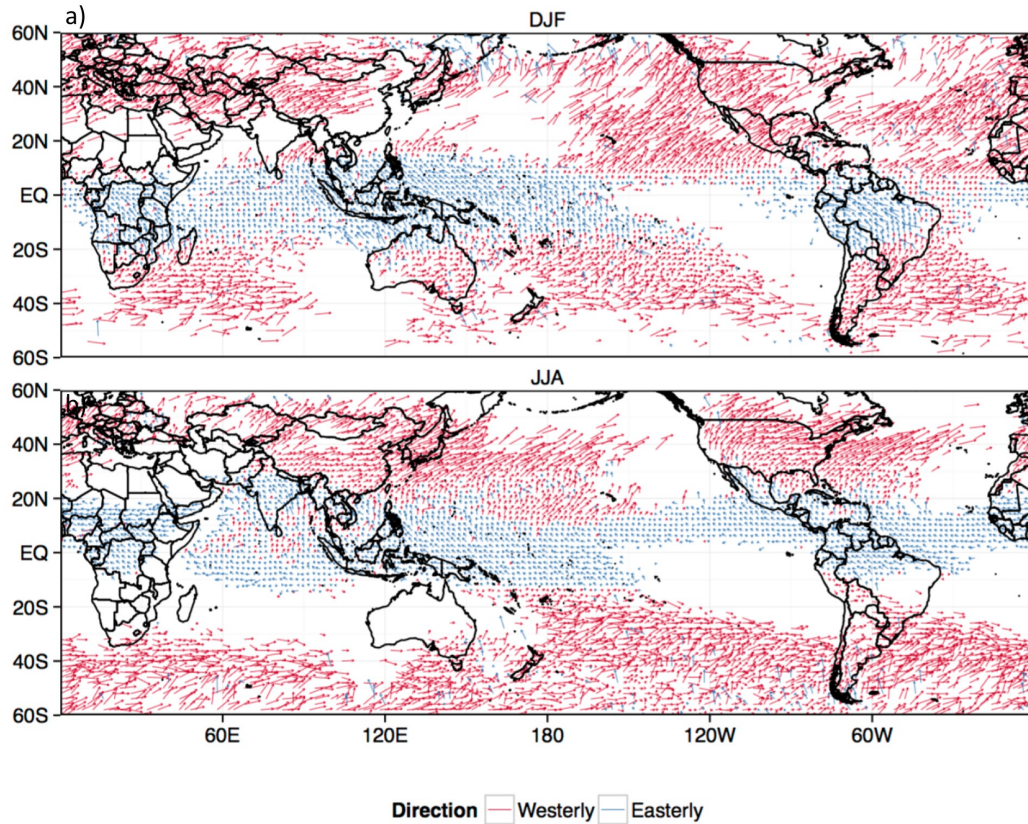


Figure 2-4 Climatology of cloud cluster trajectories in (a) DJF and (b) JJA, 2002-2012 with 6-9 hour lifetimes binned by $2^\circ \times 2^\circ$. Lines show average displacement of all cloud clusters that initiated at the same point over the 11-year period studied. Coloring indicates net zonal movement of clusters. Grid boxes with fewer than five initiations were not displayed.

2.3.3 Collocation of clusters with passive microwave rainfall estimations

To examine the rainfall contribution of cloud clusters, we matched PMW precipitation estimates from IMERG [Huffman et al., 2013] with spatially and temporally collocated cloud clusters.

While Tropical Rainfall Measuring Mission (TRMM)-based products have a longer data record, GPM has global coverage so we selected two months of data to examine

(June and December 2014). Both datasets were scaled to a common grid ($0.1^\circ \times 0.1^\circ$) and the available rainfall totals were summed for clusters at various life cycle stages.

2.4 Results and Discussion

2.4.1 Mean trajectories and statistical properties of cloud clusters

Tracking on the global scale builds on regional studies and enables us to document many fundamental statistical characteristics of cloud clusters. At any instant, there are on average 800 clusters larger than $1,600 \text{ km}^2$ in the Earth's atmosphere between 60°S and 60°N . Figure 2-4 shows the global distribution of clusters with lifetimes between 6 and 9 hours, for both December through February (DJF) and June through August (JJA). The mean trajectories are calculated by averaging the endpoints of all cluster centroids that initiate at the same $2^\circ \times 2^\circ$ binned latitude and longitude coordinates. The colors represent the net zonal direction of the flow.

Regarding the zonal average distance travelled by 6-9 hour lifetime clusters in Figure 2-4, we found that cloud clusters travel further in the Northern Hemisphere during DJF; the average distance traveled peaks at 644.8 km at 36°N , which is likely due to influence of the climatological jet stream on development and propagation. In the Southern Hemisphere the maximum occurs near 52°S at a lower 419.8 km. Movement in the tropics doesn't vary drastically from each season, but the peak (189.1 km) occurs in JJA at 12°N . This is in part due to the persistence of the Intertropical Convergence Zone (ITCZ) and African Easterly Wave activity.

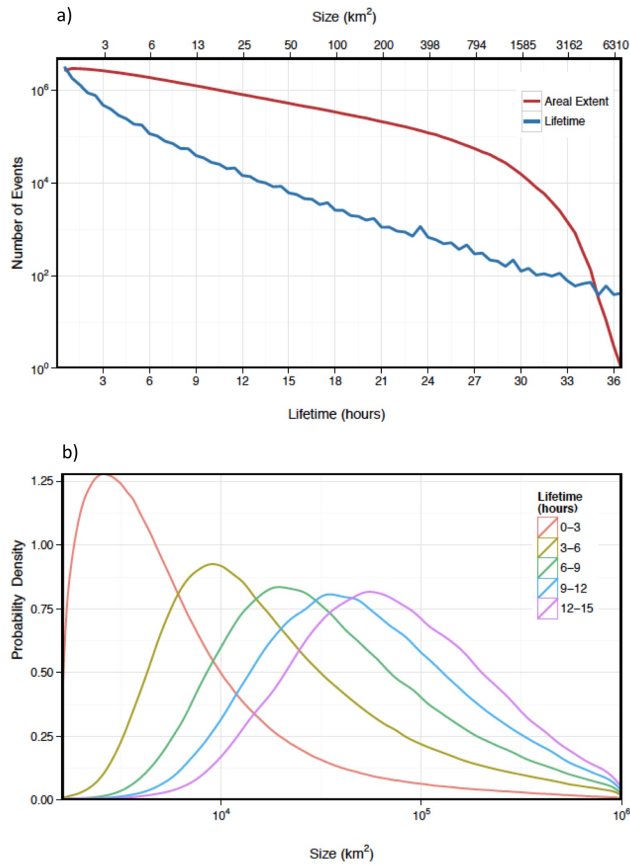


Figure 2-5 (a) Number of detected events globally by lifetime and size for the entire record. (b) The kernel density estimate of cloud clusters at their maximum areal extent for each lifetime group over the entire study period (DJF and JJA, 2002-2012).

Cloud clusters can last from a few hours up to two days, and their sizes range from our minimal threshold to more than 10^6 km² (Figure 2-5). Most of the clusters are short-lived and small (Figure 2-5a), with 90% of the clusters detected having a size less than 49,275 km² and a lifetime less than 5 hours. The cluster lifetime distribution follows roughly a log-linear distribution while the cluster size distribution appears to be lognormal at certain scales, the latter being consistent with some past findings [Machado et al. 1992; Mapes and Houze, 1993] but different from others [Lovejoy and Schertzer, 2006]. Figure 2-5b shows the kernel density estimate [Rosenblatt,

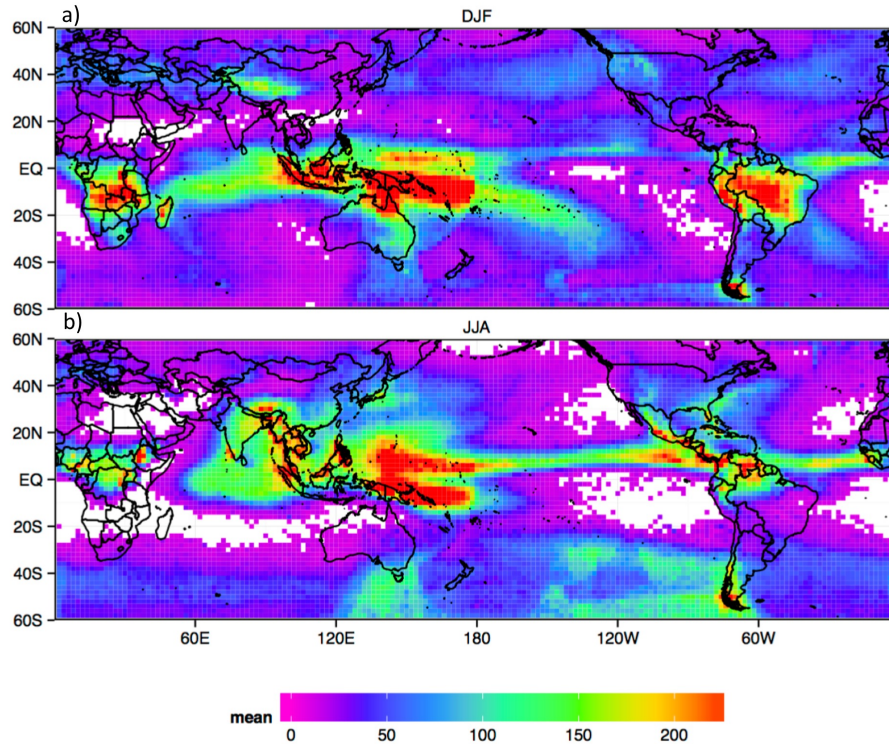


Figure 2-6 Mean seasonal frequency of clusters for (a) DJF and (b) JJA at their maximum areal extent. The figure shows the average seasonal count of events over the study period, binned by $2^\circ \times 2^\circ$ latitude-longitude. Warmer colors represent higher counts while cooler colors represent fewer observations. White grid boxes have ten or fewer cloud clusters across the 11 year period.

1956; Parzen, 1962], a non-parametric estimate of the probability density of maximum areal extent of each cluster across several lifetime bins.

Overall, Figure 2-5 shows that the frequency of cluster lifetime and size are proportional. This is similar to the results from Chen et al. [1997], who show a linear correlation between the count of tropical cloud clusters with respect to maximum size and lifetime in the western Pacific. This reinforces that shorter lived events tend to remain small in scale while longer-lived ones achieve greater horizontal scales.

These results can be compared with event tracking based on model data [e.g. Bengtsson et al., 2006; Bengtsson et al., 2009; Hoskins and Hodges, 2001; Neu et al., 2013; Sinclair, 1994]. Modelling studies typically use vorticity or sea level pressure

as the defining feature of midlatitude cyclone storm tracks. Coupled with lower temporal resolution data, this can result in smoother tracks and are larger and longer-lived than the ones shown in Figure 2-4. The differences are due to tracking definitions but may also be due to the prevalence of lighter rainfall typical in models as compared with observations [Stephens et al., 2010].

2.4.2 Cloud cluster climatology

On the global scale, the clusters exhibit many systematic spatial and temporal characteristics, as seen in the seasonal climatology map of clusters (Figure 2-6). The map produced is the frequency of clusters at their maximum areal extent for each $2^\circ \times 2^\circ$ latitude-longitude bin. During DJF, the intertropical convergence zone (ITCZ) is closer to the equator and South Pacific convergence zone is intensified. There is increased activity from the midlatitude storm tracks across the North American west coast and Europe. In JJA, tracks capture the northward placement of the ITCZ, Atlantic coastal storms, and the East Asian monsoon. Less activity is found in proximity of the semi-permanent high pressure systems (e.g. Pacific and Bermuda highs in JJA). Artifacts in south Pacific (40° - 60° S, 120° - 160° W) are due to calibration differences between geostationary platforms and the interface of the half-hourly and hourly sampling regions of the Geostationary Meteorological Satellite between 120° and 170° E. Note that in Figure 2-6a, we excluded data from DJF 2006 from 120° to 170° E due to intermittent noisy brightness temperature data in this region.

The frequency also reveals some regional subtleties in Figure 2-6b. Over the Southeast-Asia islands in the western Pacific Ocean, there are roughly twice as many clusters along coastlines than the surrounding oceanic areas. This region's combination of topography, land-sea thermal contrast, and available moisture generates storms that are both large in scale and deep, making it one of the rainiest places on Earth in TRMM-based object studies [Houze et al., 2015].

Interestingly, a high count of clusters does not necessarily correlate with intense rainfall. Outside the ITCZ, the Amazon, the Asian monsoon, and West African monsoon are among the most active continental regions in terms of cluster frequency. However, TRMM-based studies have shown that objects tend to be moderate in strength and larger scale in the Amazon while the latter two regions are composed of deep convection [Zipser et al. 2006; Houze et al., 2015]. In the Amazon, rainfall features have a lower mean height than those over the Asian and African monsoon regions and warm rain tends to be the greatest contributor of rainfall [Liu and Zipser, 2008]. While not shown, statistically, we found that clusters in our study were typically larger, colder, and longer-lived over Western Africa and the Indian Subcontinent (JJA), whereas shorter-lived, moderate sized clusters tended to occur over the Amazon (DJF).

Compared to results based on reanalysis-based tracking results, the JJA cluster counts shown in Figure 2-6b resemble vorticity-based African Easterly [Thorncroft and Hodges, 2001]. In both studies, initiation maxima occur along the West Africa coast and Ethiopian highlands as well as over the Pacific, downstream of Central America. We visually observed that our IR-based tracks are noisier than reanalysis derived ones

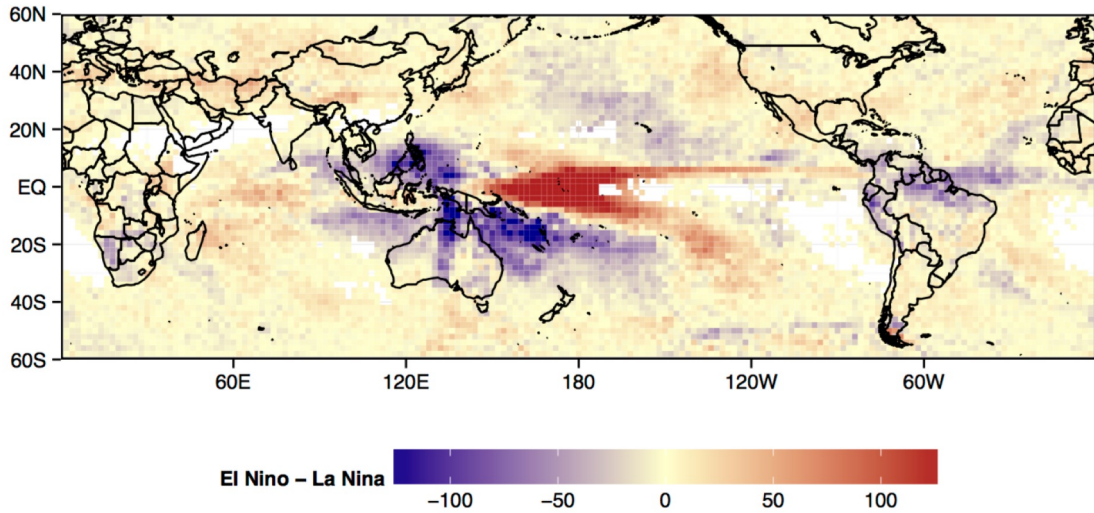


Figure 2-7 The composite of the 11-year DJF mean annual frequency of cloud cluster overpasses for El Niño and La Niña, binned by $2^\circ \times 2^\circ$ latitude-longitude, at their maximum areal extent. Warm or cool event years were selected based on the NINO3.4 sea surface temperature anomaly index. White grid boxes have three or fewer cloud clusters.

and are less exclusive. Tracking with 6-hourly data can skew results towards stronger, longer-lived events, and can miss younger events.

2.4.3 Interannual variability

There is significant inter-annual variability in cluster occurrence, particularly between El Niño and La Niña years. Figure 2-7 shows the composite of frequency difference of cluster overpasses at their maximum size during the El Niño phases for 11 years of DJF, binned by $2^\circ \times 2^\circ$ latitude-longitude boxes. This was produced by subtracting the annual average frequency of cluster occurrence during warm phases from the annual average of cool phases. Only seasons with weak, moderate, or strong phases based on the NINO3.4 sea surface temperature anomaly index are included.

El Niño has an expected effect on the frequency of cloud clusters in the tropics: more clusters are observed near the equator during the warm phase in the central pacific (160°E-160°W) and in the western pacific (110°-160°E) during the cool phase. However, teleconnections can also be observed; there is an increase in occurrence over the Northwest United States (25-55°N, 100-120°W) and Indian Ocean (10°S-10°N, 40°-80°E) and a decrease in the Atlantic basin (10°S-10°N, 60°-10°W) during El Niño. Teng et al. [2014] have shown that there are both increases in cloud cluster occurrence as well as their likelihood of forming tropical cyclones in the western North Pacific during El Niño.

2.4.4 Life cycle of cloud clusters

The advantage of continuous Lagrangian tracking is that it allows us to examine systematically the clusters' full life cycle and the associated evolution of their characteristics. Figures 2-8 and 2-9 show how the size and brightness temperature of clusters evolve throughout their lifespan. Each curve represents the average of the aggregated clusters that lived to the same age. For clarity, clusters that merged into or split off from existing clusters were not included in Figures 2-8 and 2-9. Shorter curves represent brief events while longer lines represent clusters with longer lifespans. The observed mean life cycles have well-defined stages of development – initial detection, intensification, maturity, and decay. This can be seen in both their size evolution (Figure 2-8) and brightness temperature evolution (Figure 2-9). With respect to size, clusters initiate, grow, and achieve their areal maximum closer to the end of their life cycle (Figure 2-8). At their size maximum, longer-lived clusters can double or triple their initial areal extent. Shorter-lived ones undergo rapid decay early

in their cycle. In contrast, during their brightness temperature life cycle, clusters cool to a minimum and then begin to warm for the rest of the life cycle (Figure 2-9). While an individual clusters' evolution usually appears erratic and unpredictable, collectively their mean behavior computed from the ensemble of 10 million clusters shows regularity.

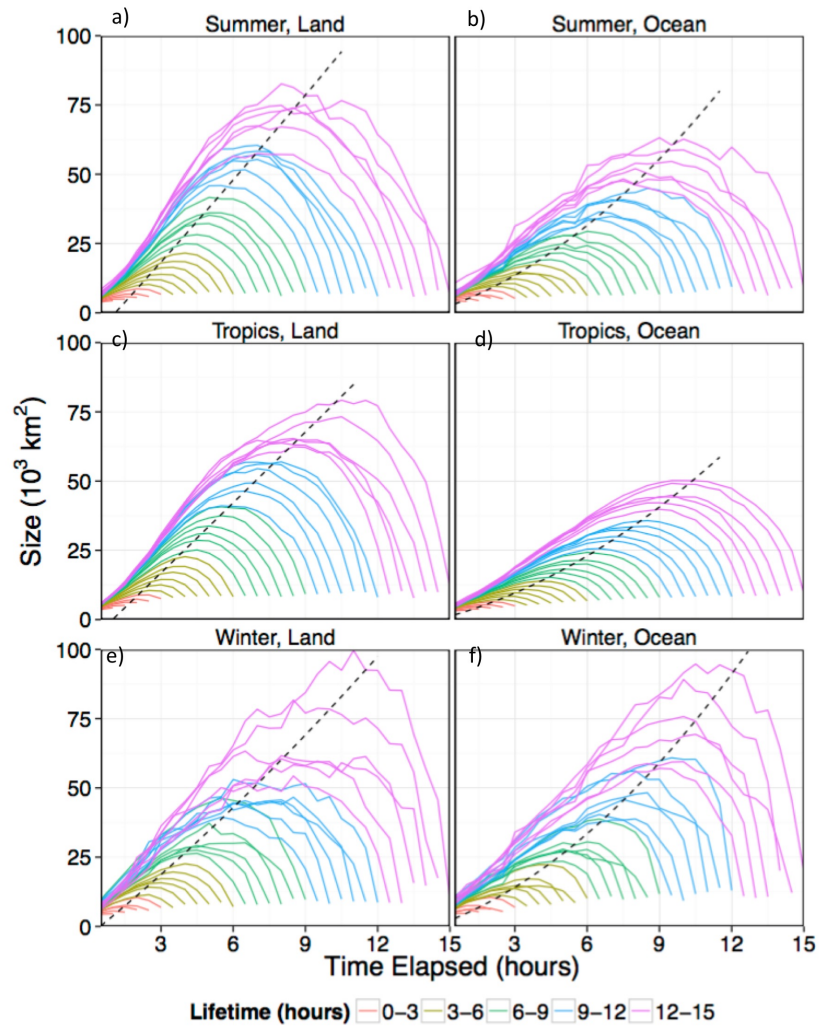


Figure 2-8 The global average life cycle evolution for new cloud clusters with varying life times. Each curve represents the average properties of millions of clusters grouped by life span. The shortest lines are short-lived events longer lines are long-lived. Curves show how the size changes as a function of the clusters' lifetime. Dashed curve is a regression fitted to the maximum of each curve. Seasons are defined by the $\pm 25^\circ$ latitude line.

The minimum brightness temperature is reached at an earlier point in the clusters life cycle than the size maximum. This could be due to overshooting tops, which reach deep into the troposphere or lower stratosphere first, and then expand to form anvils as they cool, and thus attaining their minimum brightness temperature before their

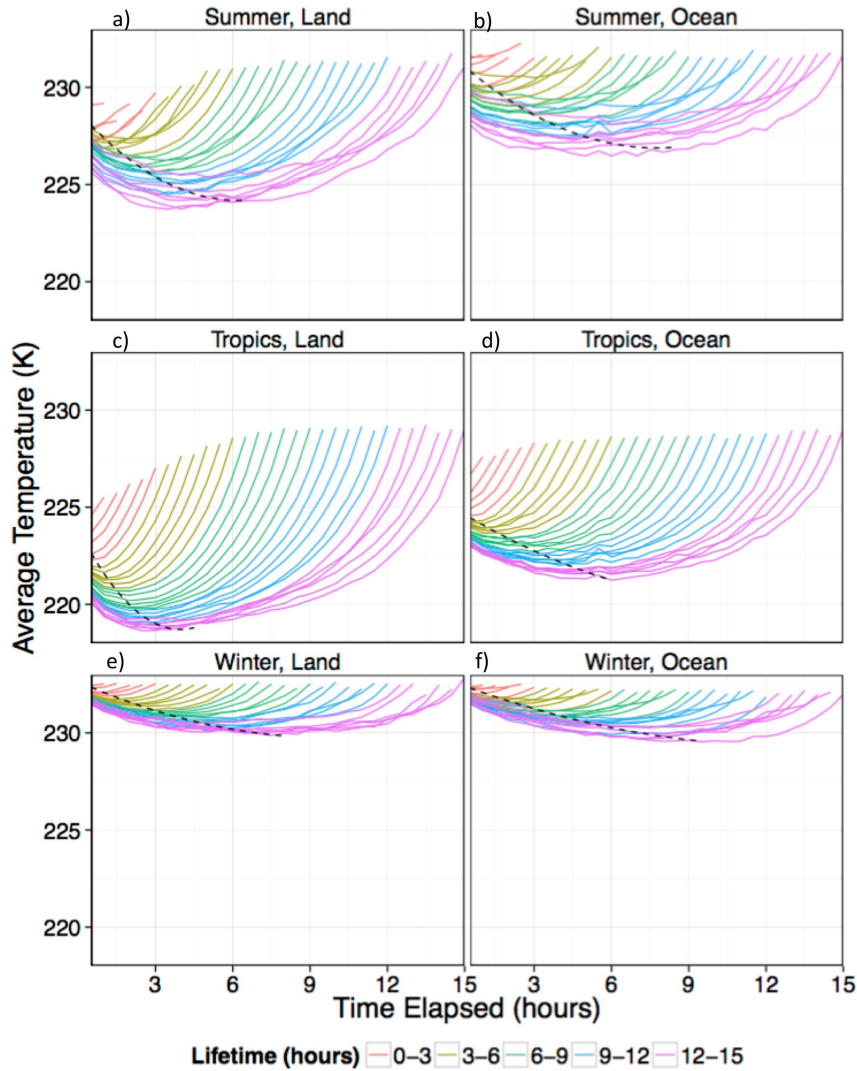


Figure 2-9 Same as Figure 8, but showing how the average brightness temperature changes as a function of time and lifetime.

maximum areal extent. Additionally, clusters at their maximum areal extent produce cirrus shields that can also conceal the true extent of the clusters underneath.

On the global scale, the life cycle evolution shows substantial differences over contrasting seasons and land surfaces. Due to their similarity, in Figures 2-8 and 2-9 regions are divided into seasons along the $\pm 25^\circ$ latitude line, where Northern and Southern winters (summers) are during DJF and JJA (JJA and DJF), respectively. The

tropics use data from both seasons. Generally, growth is more vigorous in summer than in winter (e.g., compare Figures 2-8b and 2-8f to Figures 2-9b and 2-9f), over land than over ocean (e.g., compare Figures 2-8a and 2-8b to Figures 2-9a and 2-9b). In addition, the wintertime clusters are much larger than summertime (e.g., Figures 2-8a and 2-8e). In the summer, the midlatitude size curves (Figures 2-8a and 2-8b) are more similar to the tropics (Figures 2-8c and 2-8d). Regarding brightness temperature, there is a larger spread during the summer (Figures 2-9a and 2-9b) and in tropics (Figures 2-9c and 2-9d) than during the winter for both land and ocean (Figures 2-9e and 2-9f). Clusters in the tropics (Figures 2-9c and 2-9d) are significantly cooler than higher latitudes due to deep convection (Figures 2-9a and 2-9b).

The peaks in Figures 2-8 and 2-9 were fitted to a quadratic linear regression model to show the general trend of size and temperature maturity across different lifetimes. Shorter-lived clusters tended to be already at maturity at the time of detection – that is, the shortest lines in Figures 2-8 and 2-9 show that these clusters total area decreased and temperatures rapidly increased. For longer-lived clusters, the timing of the maximum areal extent and minimum temperature was asynchronous and larger than that for shorter-lived events. We will examine some of the implications of this in the following sections.

2.4.5 Cloud clusters and rainfall

In raining cloud clusters, the differences in the timing of the minimum brightness temperature and maximum size contribute varying amounts to total precipitation. In

Figure 2-10, we identified several distinct life cycle stages (initiation, mixed maturity, minimum brightness temperature, maximum size, and dissipation) and the instantaneous total volumetric rainfall that is attributed to each rain rate bin. Using the procedure detailed in Section 2.3.3, this was determined by collocating the cloud clusters with available microwave-only rainfall estimations from IMERG [Huffman et al., 2013], for June and December 2014.

Due to the lower temporal resolution of polar orbiting satellites, most clouds could only be sampled once, so results are examined in a statistical sense rather than as totals by individual objects. Here we define the minimum temperature (maximum size) as the lowest average temperature (largest areal extent) achieved by a clusters. We also divide contribution into two mutually exclusive maturity states, synchronous and asynchronous occurrence of minimum temperature and maximum areal extent. The prior is denoted as mixed maturity, while the latter is broken down into the two stages of its variables. Collectively, the Figure shows the rainfall contribution of the beginning, mature, and final life cycle stage.

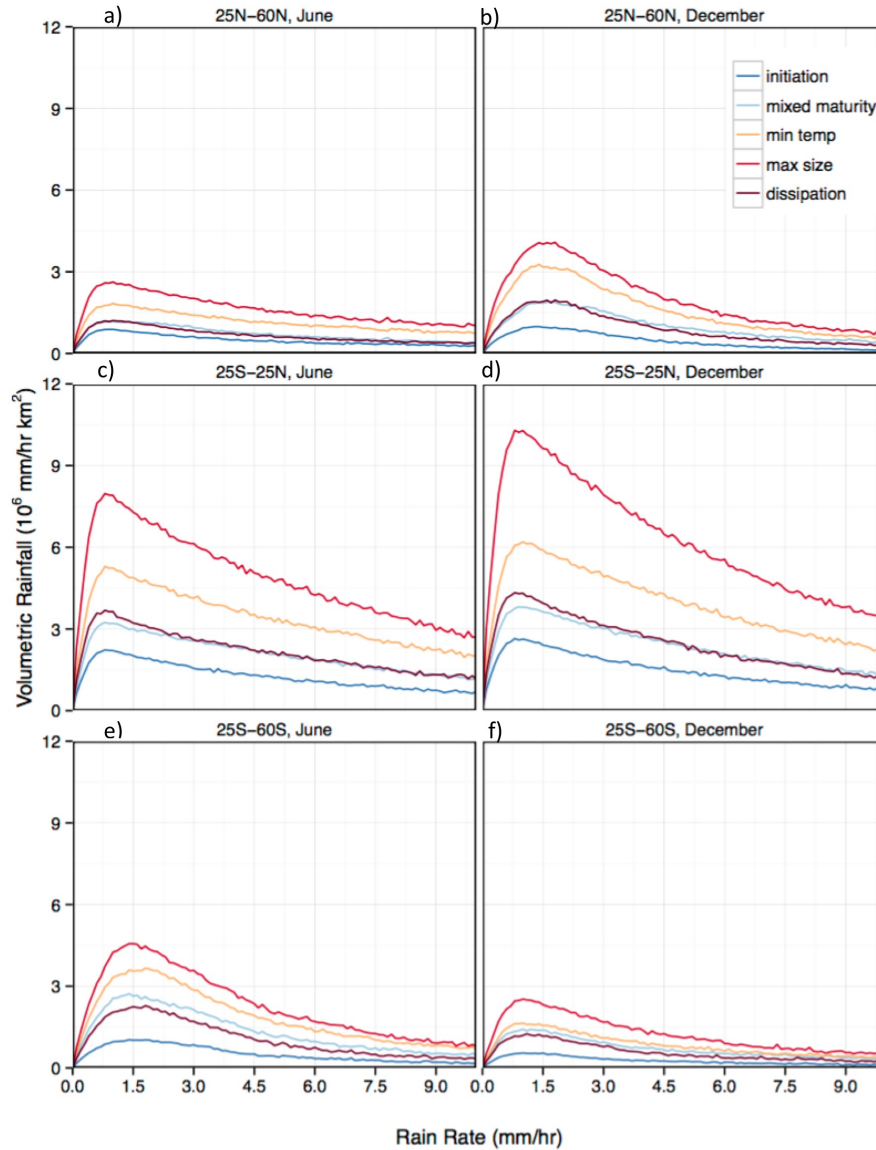


Figure 2-10 Total instantaneous rainfall contribution as a function of rain rate captured by clusters in the (a, b) Northern Hemisphere, (c, d) tropics, and (e, f) Southern Hemisphere in June and December 2014. The distribution is based on coincident cloud clusters and passive microwave-based rainfall estimates from the IMERG dataset.

Initially, raining clusters are composed of lighter rain and produce less of it. As development continues, they produce larger volumes of rain as the areal extent of the cloud increases. It is interesting that in all cases, mixed maturity clusters contribute less rainfall than those with asynchronous stages. These cases tended to be shorter lived on average (1.9 hours) than those with larger differences in timing (2.9 hours).

There are seasonal differences in these values. The winter midlatitudes (Figures 2-10b and 2-10e) produced more overall rain than their corresponding summer hemisphere (Figures 2-10a and 2-10f) and were more heavily skewed towards lighter rainfall. The tropics had less seasonal variation in rainfall contribution (Figures 2-10c and 2-10d).

Precipitation retrieval algorithms may benefit from incorporating information on the life cycle stage, season, and hemisphere of the IR cloud cluster. In morphing techniques, the shape and intensity of rain clusters is held constant between overpasses [Joyce et al., 2004], while in Figures 2-8 and 2-9 we show that both horizontal size and temperature growth rates are not constant during cloud cluster evolution. Biases in hourly rain volume estimates vary across life cycle stages, lifetimes, and precipitation algorithm [Tadesse and Anagnostou, 2009]. Knowing the age of the cloud could be useful in devising the next-generation multi-sensor algorithms.

2.4.6 Diurnal cycle of cluster evolution

By continuously tracking cloud clusters, we can study when and where they reach their life cycle milestones. Figure 2-11 shows the local solar time (LST) of the maximum in the frequency of cluster initiation. This was calculated from frequency maximum at each hourly, $2^\circ \times 2^\circ$ bin for clusters with a lifetime greater than two hours. Over land, peak cloud initiation occurs in the afternoon, especially in the summer hemisphere. Over the ocean, there is greater prevalence of early morning and afternoon clouds, but the timing of peak activity depends on region. This double peak was also previously found in the West Pacific warm pool by Chen and Houze (1997).

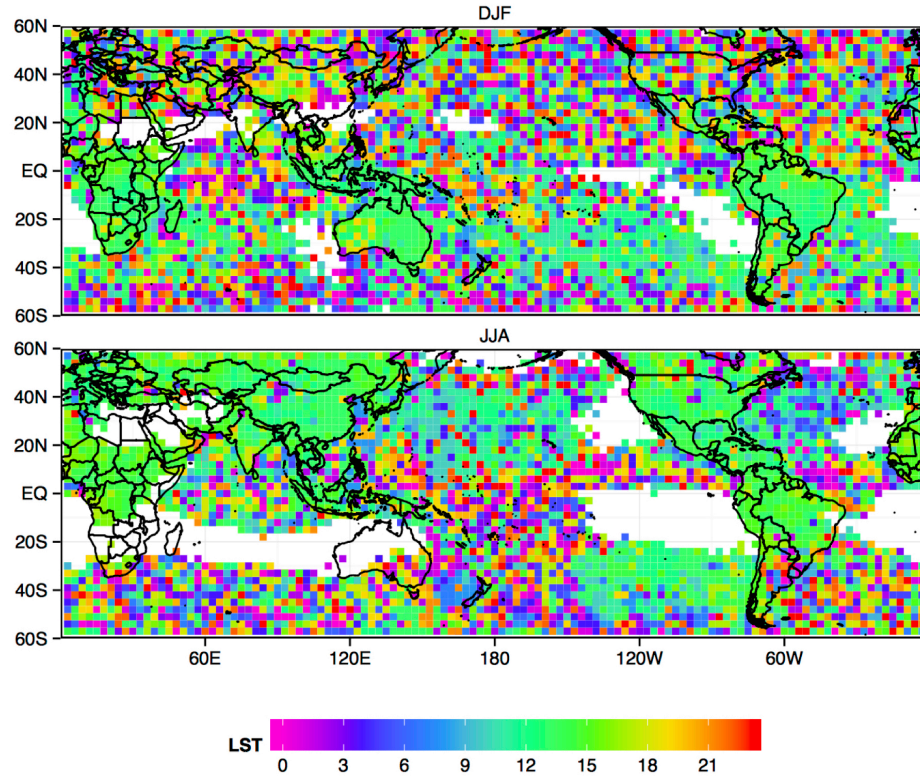


Figure 2-11 Diurnal variation in local solar time (LST) cloud cluster initiation for (a) DJF and (b) JJA, binned by $2^\circ \times 2^\circ$ latitude-longitude. Each box shows the timing of maximum occurrence of cluster formation for the 11-year record. Only clusters with a lifetime greater than two hours are included.

To examine these differences in context of development stage, we examine two regions centered over West Africa ($0^\circ\text{-}40^\circ\text{N}$, $50^\circ\text{W}\text{-}20^\circ\text{E}$) and the South Asian peninsula ($0^\circ\text{-}30^\circ\text{N}$ and $60^\circ\text{-}90^\circ\text{E}$).

In Figure 2-12, we examine the kernel density of the LST by cluster life cycle stage in these two regions for both seasons. Over land, there is a strong diurnal cycle and a lag in the local timing of initiation, minimum temperature, and maximum size. The timing differences are much smaller over the ocean in both regions and there is a semi-diurnal cycle over the ocean. The timing of peak initiation over land is earlier in the South Asian region (1300 LST) than in the Western Africa region (1500 LST).

This is possibly due to the windward side of the Indian subcontinent skewing the the population to lower initiation times. Over the ocean, the early morning peaks have similar timing (0200 LST), but the afternoon peak in Western Africa is earlier (1100

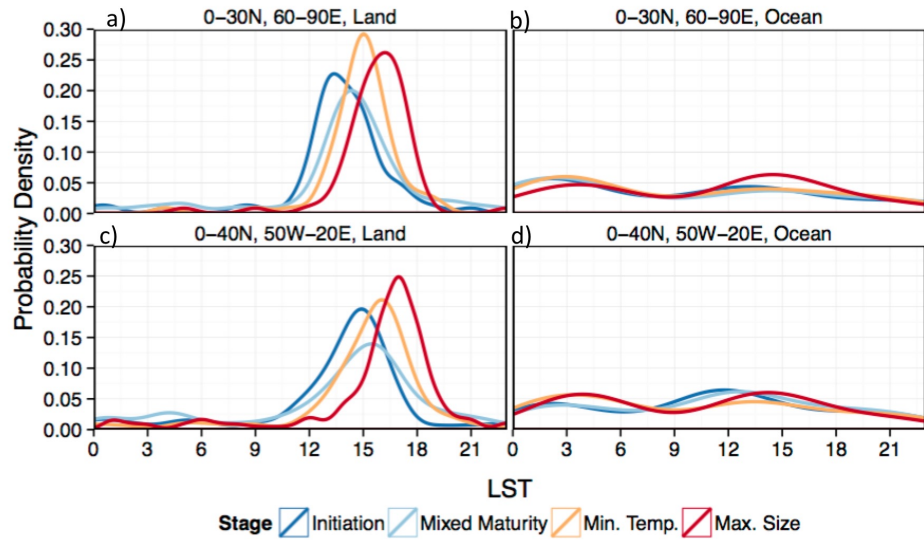


Figure 2-12 The kernel density of local solar time of the life cycle stage in two regions, 0°-30°N and 60°-90°E (South Asia) and 0-40°N, 50°W-20°E (West Africa).

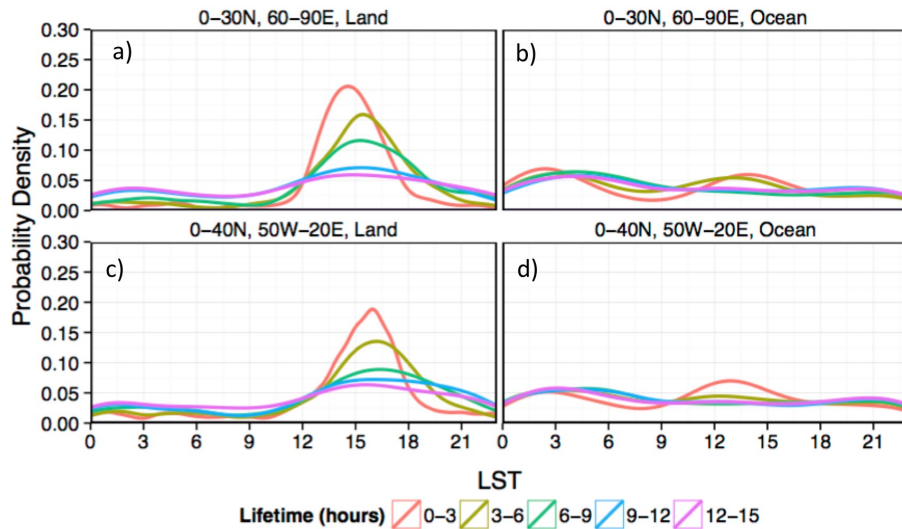


Figure 2-13 The kernel density of local solar time of initiation in three-hourly lifetime bins for two regions, 0°-30°N and 60°-90°E (South Asia) and 0-40°N, 50°W-20°E (West Africa).

versus 1300 LST). Kikuchi and Wang [2008] observed this semi-diurnal cycle over the Pacific, Indian, and Atlantic Oceans in empirical orthogonal modes of TRMM datasets. We can take advantage of the known lifetime and further inspect the duration of these cloud clusters at different times of the day.

In Figure 2-13, we show the kernel density for the LST grouped by the three-hourly binned lifetime. Over land, the timing differences were delayed by not more than an hour for all lifetime groups. Shorter-lived clusters (those with lifetimes 6 hours or less) had a sharper peak than longer-lived events (those with lifetimes greater than 6 hours). There are trivial differences in the onset of short versus long-lived events in the South Asia region than over West Africa.

However, over the ocean, longer-lived clusters had a greater tendency to occur in the early morning hours, peaking between 0300-0400 and 0400-0500 LST in South Asia and West Africa, respectively. Shorter-lived events peaked both in the early morning and afternoon, but were the primary type in the afternoon between 1200 and 1300 LST for both regions. In South Asia, the maxima of short-lived clusters precede that of long-lived ones by an hour, partly due to rapid growth and decay of isolated convective cells which upon visual inspection are more numerous in this region than in West Africa.

These results are interesting considering previous examination of TRMM-based precipitation and features, which show that nocturnal storms are more intense over the ocean while over land the strongest storms are observed during the day [Zipser, 2006]. Also using TRMM datasets, Kikuchi and Wang [2008], found three major

diurnal regimes in the tropics, with the India and West Africa adjacent ocean regions having a mixture of open ocean and coastal regimes. The oceanic coastal regime showed significant phase propagation into the following day, which may account for secondary peaks in the diurnal cycle in Figures 2-12 and 2-13.

The causes of the different diurnal cycle regimes are an area of ongoing study. Over inland continents, the diurnal cycle is primarily driven by the daily heating cycle (Silva Dias et al. 1987). Over open ocean, Sui et al. (1997) connect the daytime peak to the daily cycle in SSTs, particularly in subsidence regions, where winds are weak and solar heating is strong due to the absence of clouds overhead. The nocturnal peak is primarily driven by moisture provided from large-scale convergence, (e.g during MJO over the maritime continent region). Convective development takes place both in the day and nighttime, whether a region is experiencing subsidence or convergence. However, the amplitude of the phase will be dependent on the respective large scale atmospheric conditions.

In tropical coastal continental regions, Kikuchi and Wang [2008] speculate that land-sea breezes are largely responsible for development. Several studies identify the main candidates for coastal oceanic nocturnal development to be monsoonal flow and convergence due to gravity waves produced from deep convection and high terrain of adjacent continental regions [Yang and Slingo, 2000; Zuidema, 2002; Mapes et al. 2003]. The resulting oceanic nocturnal storms that develop in this regime then show maximum propagation the next day, from noon to late evening.

Our results show that results from Chen and Houze (1997), who found that large scale, long lived clusters follow a two-day cycle, can extend beyond their West Pacific study region to other regions and over longer time periods. The formation of long-lived clusters suppresses subsequent development in that area due to dry downdrafts from strong storms and the reduction in sea surface temperatures due to cloud canopy shading. Examining the development-suppression cycle of cloud clusters in other oceanic regions could be an interesting future direction for this work.

2.5 Summary

In this study, we tracked cloud clusters on the global scale to study the climatology and life cycles across a broad class of clusters using 11 years of the high-resolution, satellite-based globally merged cloud brightness temperature data. We examined the trajectories, climatology, life cycles, and diurnal cycle of clusters in context of their life cycle stage and lifetime.

We found that the vast majority of clusters are short lived and small, demonstrating the need to work with high-resolution data to fill in coverage gaps. Differences in the shapes and scales of life cycle curves reflect the variety of clouds captured and show that evolution is a complex process. Development over the oceans is less intense compared to land, where strong thermal contrast, orography, and aerosols can influence evolution. We observe a larger lag in the occurrence of minimum temperature and maximum size for longer-lived cloud clusters, particularly over land. The diurnal cycle of cloud clusters over the South Asia and West Africa revealed a strong diurnal peak over land and a semi-diurnal cycle over the ocean, the latter of

which showed greater prevalence of shorter lived cloud clusters in the afternoon and dominance of longer lived events in the early morning.

The capability for infrared data to reliably identify and track smaller scale convective systems is an aspect in which global climate models still have difficulties [Stephens et al. 2010; Westra et al., 2014]. Thus, IR-based cloud tracking can be used to evaluate the effectiveness of the downscaling abilities of models [Boer and Ramanathan, 1997]. On the other hand, the infrared data can only depict the two-dimensional, cloud-top characteristics of the clusters. To address the complex three-dimensional hydro-thermo-dynamics of cloud systems, one has to combine observations from other satellites, such as CloudSat and CALIPSO, with reanalysis data.

There are several limitations to this study that represent an area of ongoing work, particularly regarding thresholds. Being too selective on size scales can exclude these events; being too relaxed produces too many splits, which prematurely terminates the cluster. Cold surfaces are a particular challenge, such as the Tibetan Plateau which is dry in the northern winter. However, the relatively high frequency over this region in Figure 2-6a indicates that mountain glacier surfaces are incorrectly being captured in this region. This poses a challenge to other tracking studies, and mountainous areas are sometimes removed from analysis [Neu et al., 2013]. As a future improvement, we could develop a dynamic threshold criteria rather than a fixed brightness temperature value. [Hennon et al., 2011].

Another challenge lies in the early termination of cloud clusters due to splits and mergers. As clouds evolve, they continuously split and merge, each of which resets

the lifetime clock to zero. Only the largest, most well defined clusters avoid this in their lifetimes. This is a limitation of this specific technique but the tracking algorithm could be refined in the future to track features that do not have an easily defined shape, such as wintertime midlatitudes storms or the movement of clouds that are part of atmospheric rivers.

Despite such limitations, there are many promising areas of future work. The cluster tracking provided in this study can be combined with other event based datasets, such as the TRMM precipitation feature (TRMM-PF) dataset developed by Liu et al. [2008]. TRMM-PF has been extensively used to study the scale and intensity of rainfall events and can infer life cycle stage from the vertical profiles obtained from the precipitation radar. By combining TRMM-PF with our IR-based cloud tracks, rain features can be studied in context of their entire life cycle and trajectory, overcoming the sampling limits of polar orbiting satellites, to further our understanding of precipitating cloud systems.

Chapter 3. Influence of Large-Scale Saharan Dust Plumes on the Development of Cloud Clusters in the Atlantic and West Africa

In preparation, to be submitted in early 2017

Rebekah Bradley Esmaili¹ and Kyu-Myong Kim²

¹Dept. of Atmospheric and Oceanic Science, University of Maryland, College Park, Maryland

²NASA Goddard Space Flight Center, Greenbelt, Maryland

Abstract

Clouds and rainfall can be enhanced or inhibited by dust aerosols, which can alter the environment through radiative and microphysical effects. Modeling studies predict that during Saharan dust outbreaks, the African Easterly Jet is enhanced, which can increase convection to the south of the outbreak region. However, observational evidence is limited. Using cloud tracks from brightness temperature observations and measurements of aerosol optical depth to create a dust outbreak index, this study examines cloud cluster evolution over the Atlantic on during high and low aerosol days from June-October, 2006-2009. Early results show that cloud clusters in close proximity to dust outbreaks can be shifted northward. On average, there are more cloud clusters on low dust days than on high dust days, but longer lived clusters become more likely during dust outbreaks days. is an increase in the distribution of Additionally, during dust outbreaks, deep convection and intense storms become more common, whereas on days with low dust loading small-scale, warmer clouds are more likely.

3.1 Introduction

Under the right summertime conditions, the Sahara can produce large volumes of mineral dust which can travel across the Atlantic all the way to the Caribbean and

Southern United States. These Saharan dust plumes can influence both the ocean and atmosphere, sometimes with negative societal consequences. Transported dust can cause summer air quality to exceed Environmental Protection Agency standards in Southern Florida [Prospero, 1999]. The deposition of dust can fertilize the ocean, leading to phytoplankton blooms [Walsh and Steidinger, 2001]. Additionally, dust suspended in the atmosphere can indirectly impact cloud development as far as Southern Florida [Sassen et al., 2003]. Modeling studies suggest that the dust outbreaks can influence rainfall and convection in West Africa [Lau et al., 2009; Kim et al., 2010; Wilcox et al., 2010], however the actual impact on the cloud life cycles is unknown. Greater examination of dust on convection is important because of the wide scale circulation effects of the region and because the Sahara is projected to experience warming in the future [IPCC 5th report]. Additionally, the timing and location of African monsoons can impact rainfall in the Sahel, which is sensitive to slight changes in rainfall [Prospero and Lamb, 2003].

During dust outbreaks, the thick aerosol layer absorbs shortwave solar radiation and emits in the longwave, heating the air but cooling the land and ocean below. The warm, dry air is also called the Saharan Air Layer (SAL) and ultimately makes its journey across the Atlantic in the course of a week [Prospero and Lamb, 2003].

However, at its genesis, the SAL rises and creates a land-sea circulation, which draws moisture from the adjacent Atlantic Ocean and enhances rainfall along coastal Africa. The increase in deep convection closer to the Eastern Atlantic causes less convection in the West Atlantic and the Caribbean due to subsidence, resulting in a Walker-type circulation [Lau et al., 2009].

The feedbacks of the Saharan air layer can have a strong regional impact. Wilcox et al. 2010 show that advection of the SAL can enhance the African Easterly Jet, which can cause 1-4° northward shift of the intertropical convergence zone (ITCZ), a semi-persistent band of intense equatorial storms. This happens in spite of the cooler waters, which is attributed to the net surface cooling of aerosols [Wilcox et al., 2010; Lau and Kim, 2007]. Over the ocean, the SAL can enhance Easterly African Waves, a major precursor to tropical cyclones.

Because the dust can propagate deep into the atmosphere, it can also interact with the clouds. Observational studies have shown that, when the SAL interacts with hurricanes, many weaken or no longer intensify [Dunion and Veldon, 2004; Wu, 2007]. A possible mechanism is that warm, dry air is intruded into the cloud, which then weakens downdrafts thereby suppressing development. The presence of coarse aerosols may inhibit development through microphysical effects. However, others claim that only a small fraction of dust is entrained [Twohy, 2014; Lawson, 2010], and that any effects are likely secondary to direct aerosol effects and other environmental factors such as vertical shear, sea surface temperatures, and humidity. Regardless, if there is reason to suspect that aerosols can stunt the growth of large scale events such as hurricanes, they may also impact smaller scale cloud and rainfall development, which provides needed rainfall to drought-prone regions.

The impact of dust outbreaks on cloud life cycles is not well known. In cloud tracking studies, clouds undergo regular life cycle stages: initiation, growth, maturity, and decay [Williams and Houze, 1987; Chen and Houze, 1997]. The rate and timing at which these life cycle stages occur are related to their total lifetime, precipitation

quantity, and diurnal cycle [Esmaili et al., 2016]. The larger scale effects of aerosols may not only alter the location of clouds but also affect how the lifecycle milestones occur and the local timing in which they take place. Heavy dust can cool the ocean surface, possibly reducing intensity when convection shifts northward. The indirect effects of aerosols on cloud development, albeit secondary, could enhance or suppress contaminated clouds.

In this study, we examine how environmental feedbacks caused by dust outbreaks can influence the location and the intensity of mature cloud clusters in the tropical Atlantic. To do so, we examine four years of cloud track data from Jun 2006-October 2009 in conjunction with remotely sensed AOD observations. The boreal summer months are the peak season for dust outbreak, which is made airborne from convective outflows and the morning disruption nocturnal low level jets [Engelstaedter and Washington, 2006; Heinold et al., 2013].

In Section 4.2, we identify the data and methods used for this study. We use AOD observations from MODIS to create an index to detect days where dust outbreaks are likely and days that are anomalously clear, in order to examine the impact on cloud cluster development detected from cloud brightness temperatures. In Section 4.3, we show early results related to the differences in the longevity and cloud characteristics during high and low dust index days. In Section 4.4, we summarize early results and lay out the future direction of this work.

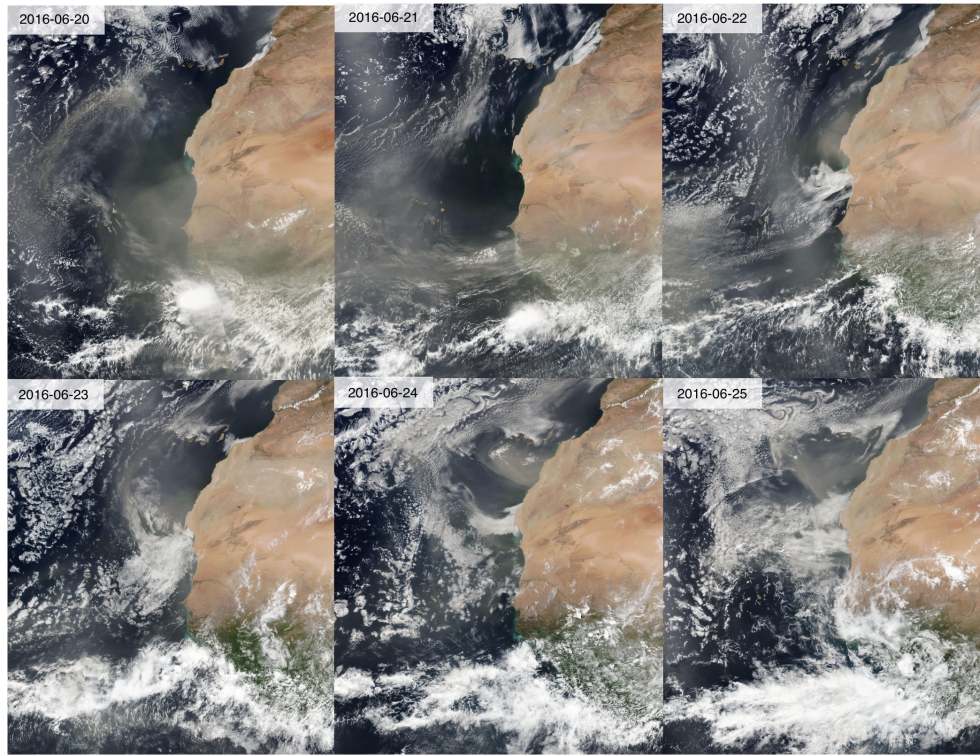


Figure 3-1 Suomi-NPP/VIIRS true color corrected reflectance of Atlantic dust outbreaks, June 20-25, 2016.

3.2 Data and Methods

To understand how clouds develop, we must be able to know their age and total duration, which is obtained by continuously tracking over their lifetimes. For this study, we use a global cloud tracking and development database produced by Esmaili et al. 2016 (see Chapter 2). This storm database was generated by using geostationary infrared data to cluster clouds with a brightness temperature below a temperature of 235 K, and to track using cluster area overlap in high resolution (30 min, 4km). This database generates a variety of cloud statistics, including temperature, areal extent, velocity, and convective fraction. Over our four year study period, this method detected 3,483,669 instantaneous cloud clusters which made up 610,425 distinct events.

Large scale dust outbreaks can be easily seen in visible satellite images (Figure 3-1). For this reason, we use the Sea-viewing Wide Field-Of View Sensor (SeaWiFS) Deep Blue aerosol product [Hsu et al., 2004] to detect

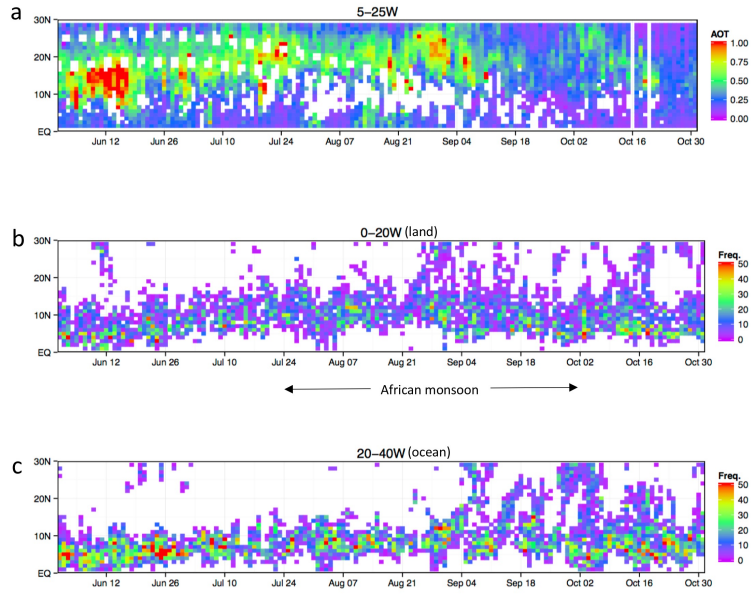


Figure 3-2 Hovmueller diagram of (a) daily zonal average of AOT (5-25°W) and daily cloud cluster counts for (b) 0-20°W and (c) 20-40°W for JJASO 2006.

outbreak days. Deep Blue estimates AOD from retrievals in shorter wavelengths because deserts are less reflective in blue bands compared to aerosols. This dataset is advantageous because it has retrievals over both land and ocean for a 13 year period. After 2010, the SeaStar satellite, which carried SeaWiFS, was retired. SeaStar passed the equator once daily at noon local standard time (LST), so clusters that developed between 9:00-15:00 LST are considered in this study.

3.3 Results and Discussion

3.3.1 Dust outbreak index

In Figure 3-2, we show the Hovmueller diagrams for AOD and clusters in 2007 (Figure 3-2). In Figure 3-2a, we can see distinct dust outbreaks of varying strength centered around June 12, August 21, and Sept 1. Over a typical season, dust extends further to the south and is highest in concentration in June-July and thereafter

decreases in concentration and shifts further north. As higher AOD values shift northward, cloud development from 0-20°W follows (Figure 3-2b), reaching its furthest northward extent in late July and August. The ITCZ is well formed between June and August, and becomes less organized and broader from September to October. From late June to early October, the monsoon rains begin and AOD concentration decreases. Over the ocean region (20-40°W), the ITCZ position is less variable.

Figure 3-3a shows the average AOD for the entire 2006-2009 study period. Concentration is heaviest over land, but AOD remains high even as dust is transported across the Atlantic. To classify days as having a dust outbreak or not, we

constructed an index (Figure 3-3b) from the boxed region in Figure 3-3a. This was defined by the normalized daily departure from the monthly mean AOD.

We identified the local maximum as potential high and low dust days, however we only considered days with an index absolute value

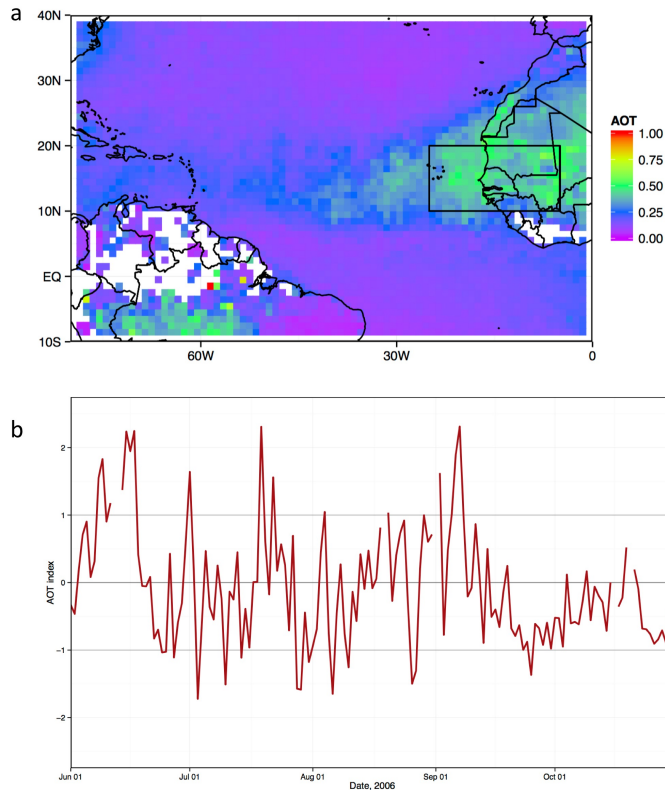


Figure 3-3 (a) Average JJASO AOT for 2006-2009 and (b) AOT index, calculated from the boxed region (10-20°N, 5-25°W) in Figure 3a. Days where the index was greater (less) than 1 are classified as high AOT (low AOT) index days. Missing values are due to no aerosol retrieval on cloudy days.

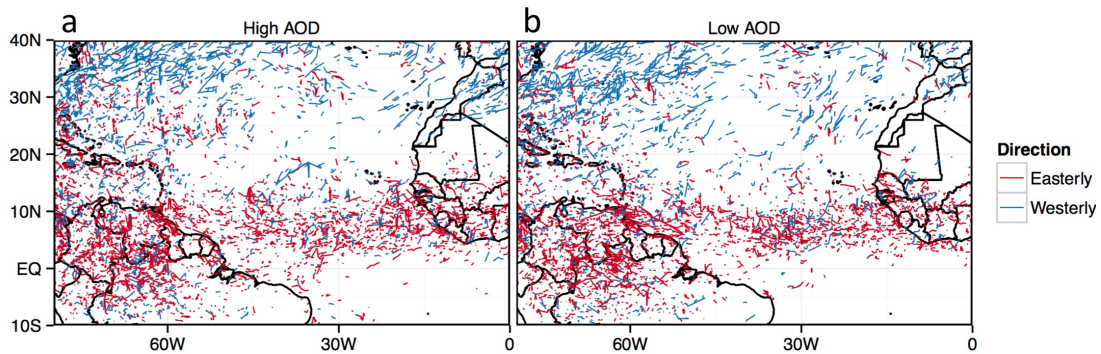


Figure 3-4 Trajectories of cloud clusters on (a) high AOT index days and (b) low AOT index days. Only clusters with a lifetime greater than or equal to one hour that developed from 9:00 – 15:00 LST, are included.

greater than one. Using this method, we identified 50 high index, dust outbreak days and 88 low index days.

3.3.2. Cloud tracks and frequency

The cloud tracks for DJFSO 2006-2009 are shown in Figure 3-4 for high and low index days. On high AOD index days, there are fewer clouds in the central Atlantic and more coastal storms over southern Senegal and Gambia (10°N, 17°W). The ITCZ is broader, whereas it is more defined on lower AOD index days. On low AOD days, there are more tracks through the north central Atlantic, centered over 25°N, 15°W.

Composite maps of low index days subtracted from high index days (Figure 3-5) show that the aerosol loading is significantly higher during high index days, particularly over ocean waters adjacent to Senegal and Mauritania (near 15°N, 17°W). There is an overall decrease in the activity south of the central ITCZ axis near the West African Coast and a slight increase in the Northern part of the ITCZ. There is also decreased activity over parts of the southeast Caribbean and Venezuela (10°N,

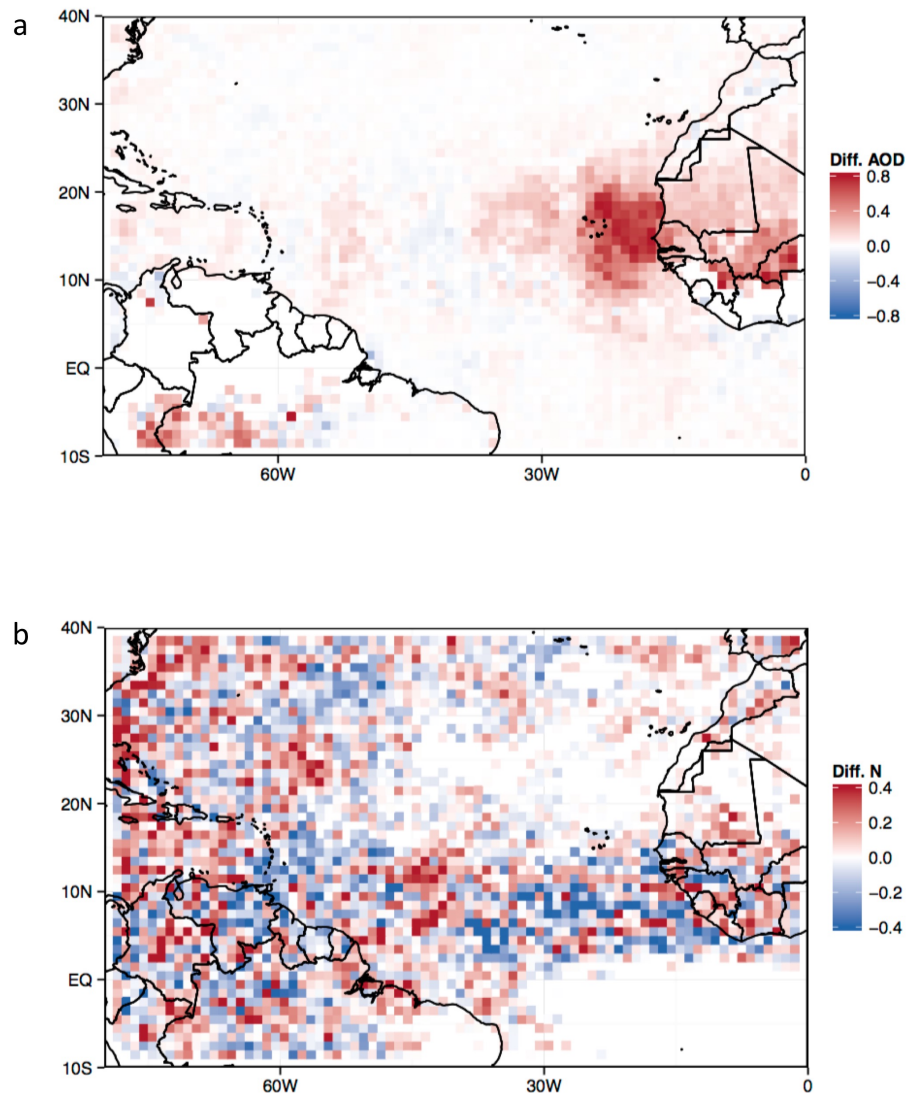


Figure 3-5 Composite of low AOT index days subtracted from high AOT index days for (a) AOT and (b) cloud cluster count. Only clusters with a lifetime greater than or equal to one hour which developed from 6:00 – 18:00 UTC are included.

60°W).

Over regions closer to the dust source (0-40°W, 0-20°N), fewer clusters formed on high index days (247 clusters/day) than on low index days (265 clusters/day). Figure 3-6 shows the kernel density estimate of cluster lifetime frequency and maximum cluster size frequency on high and low index days. We further divide the study region into two parts: one that is predominantly land (0-20°N, 0-20°W) and one that is

predominantly ocean (0-20°N, 20-40°W). Figure 3-6a shows that, for lower lifetimes, low and high AOD days had roughly the same composition of short-lived events, but that there are more moderate length events on low AOD days. The scaling (Figure 3-6b) is roughly the same for both, although during high AOD days, larger clouds are more probable (3.25-3.6, and > 4.0). Figure 3-6c shows that, over the ocean, there are more clusters with longer lifetimes on high AOD days (> 7 h). In terms of size (Figure 3-3d), there are a greater number of large sized clusters (> 3.0) on low AOD days except at the largest scales.

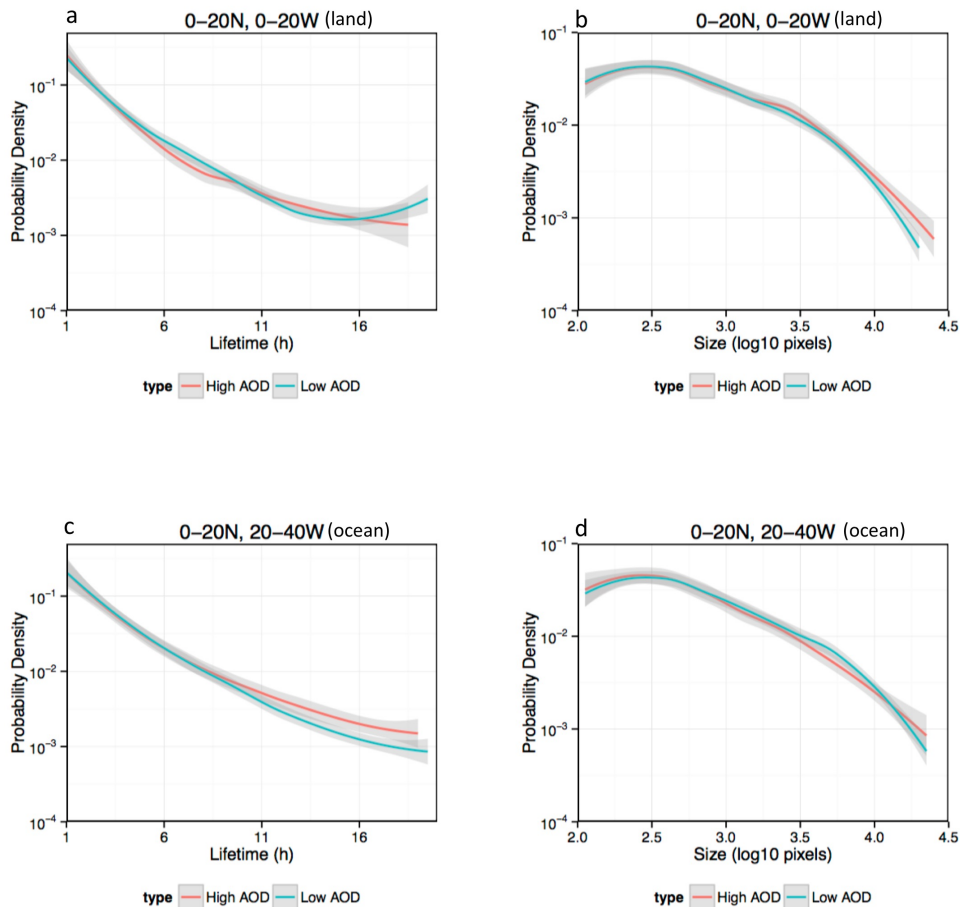


Figure 3-6 Frequency of lifetime and maximum cluster size (in pixels) for all events in study region, (b) 0-20°N, 0-20°W which is predominantly land, and (c) 0-20°N, 20-40°W which is predominantly ocean. Non-parametric loess regression was performed on data and shading represents the standard error.

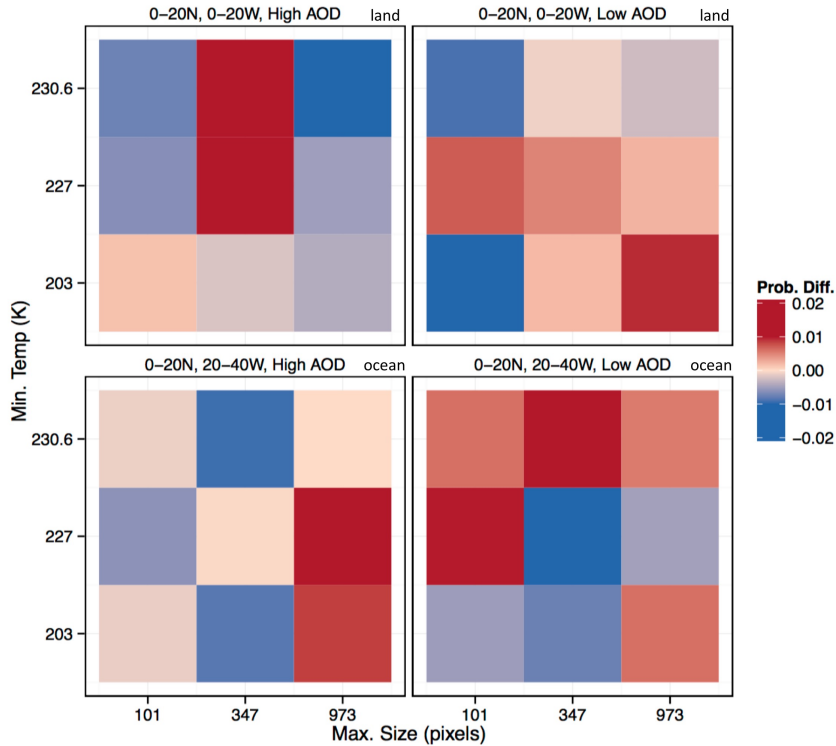


Figure 3-7 Probability density difference (AOD index – all days) of the maximum size and minimum temperature of high and low AOD days from the mean density cloud clusters for two regions. To choose bins, the temperature and size were grouped by 0-33%, 33-66% and 66-100% quantiles for each region (all days).

3.3.3. Mature cloud states

We hypothesize that dust outbreaks can modulate cloud development, either through environmental factors or from aerosol interactions. Cloud states for low and high AOD index days (Figure 3-7) show that dust outbreaks can affect the minimum temperature and maximum size of clouds, which are indicators of maturity and storm severity [Esmaili et al., 2016]. In the diagrams, cells in the top left can be interpreted as weaker events (warmer cloud tops, small scale) and the lower right as more intense (cold cloud tops, large scale). Cells parallel to the x-axis likely deep convection at various scales. Shading represents the difference between the probability density of high and low AOD days from all days, where blue represents a net decrease in

probability of occurrence and red a net increase.

Over land, the effects are mixed, but with a noticeable shift toward midsized warmer clouds and a strong decrease in larger warm clouds on high AOD days. Low AOD days have more intense storms but also a shift toward small- to moderate-scale, moderate temperature events.

Over the ocean, there is a pronounced increase in clouds that are larger and colder, and a decrease in clouds that are warmer and moderate-scale. On Low AOD days, the inverse is observed: there is a shift to more small-scale, warmer cloud clusters.

Over the ocean region, the behavior is consistent with Wilcox et al. 2010's modeling study. They propose that the African Easterly Jet is enhanced due to the presence of dust in the SAL over the ocean, which absorb in the shortwave, cooling the ocean below while heating the atmosphere. The resulting vertical temperature gradient leads to an anti-cyclonic circulation and strengthens the easterly jet to the south of the SAL, which then increases convection and shifts the ITCZ northward [Wu et al., 2009]. Thus, convection is expected to be enhanced on high AOD days and less active on low AOD days.

3.4 Summary and Future Work

In this chapter, we track cloud clusters using satellite observations to examine evolution during dust outbreaks over the eastern Atlantic, to see if we can observe changes in the location and mature cloud characteristics.

The early results presented in this chapter show that the East Atlantic ITCZ increased

activity in the north, with decreased occurrence in the south during dust outbreaks. Overall, there are fewer cloud clusters present during high AOD days. Over land on high AOD days, these clusters tended to have a greater share that were larger and had lifetimes between 11-16 hours, but fewer that lasted 5-10 hours than on low AOD days. On high AOD days over the ocean, there are many more longer-lasting clouds than on low AOD days, but these clouds tended to be smaller except for at the largest scales.

Examining the probability differences in mature cloud states, over the ocean there is a significant increase in large-scale, cold clouds on high AOD days and an increase in warm, smaller-scale clouds on low AOD days.

Over land the patterns are less pronounced, but there is a shift toward more warm, moderate-scale events on high AOD days and towards stronger, more intense events on low AOD days.

Can dust outbreaks influence a shift in mature cloud states? While over land the message is more mixed, over the ocean there is evidence of a shift in cloud properties to more intense events during dust outbreaks. Utilizing a longer study period and examining environmental conditions will likely help elucidate some of the underlying causes. A northward shift in the ITCZ leads to cloud development over cooler sea surface temperatures, which could suppress deep convection on high AOD days near the dust source [Lau and Kim, 2007; Wilcox et al., 2010]. Additionally, examining precipitation, relative humidity, vertical motion, zonal wind, vertical shear, and sea surface temperatures would put cloud properties in context.

In the future, we can examine other development characteristics such as cloud fraction and the impact on full life cycle development. Integrating other satellites' observations, such as those from CloudSat, Cloud-Aerosol Lidar, and Infrared Pathfinder Satellite Observation (CALIPSO), would enable examination of the aerosol loading and vertical rain reflectivity within the cloud. Combined with the storm track database of Esmaili et al. [2016], we could put this information in the context of the cloud age.

There are some drawbacks to the current method. First, we solely rely on SeaWiFS, whose polar orbit crosses the equator at noon, limiting the number of comparable cloud observations to only a few hours before and after its overpass. Combining measurements from Aqua and Terra based Deep Blue and Dark Target would increase the number of useable observations. While current GOES channel differencing can only be examined at night [Dunion and Velden, 2004] when the circulation effects of aerosols become secondary to surface longwave cooling, next generation geostationary satellites will permit continuous day and night observation. GOES-16 data will be available in early 2017, which has the necessary channels to do daytime channel differencing to detect aerosols and the SAL, which would enable both high resolution cloud tracking and aerosol detection.

Chapter 4. Evaluation of the Intensity, Duration, and Frequency of IMERG Rainfall Estimates over the Continental United States

To be submitted to the Journal of Hydrometeorology, 2017

Rebekah Bradley Esmaili¹, Kyu-Myong Kim², Yudong Tian³

¹Dept. of Atmospheric and Oceanic Science, University of Maryland, College Park, Maryland

²NASA Goddard Space Flight Center, Greenbelt, Maryland

³Earth System Science Interdisciplinary Center, University of Maryland, College Park, Maryland

Abstract

A simplified view of cloud evolution can lead to errors in merged rainfall retrievals, which then propagate into higher level analysis. We investigate the intensity, duration, and frequency of precipitation events to see how the Integrated Multi-satellitE Retrievals for GPM (IMERG) algorithm compares with ground observations over the contiguous United States. The results show that while there was agreement on seasonal totals, closer examination of event details shows that IMERG overestimates rainfall duration and intensity, but underestimates frequency. Over Florida, IMERG overestimates the intensity and duration, but underestimates the frequency of rainfall in the winter. However, east of the Rocky Mountains, IMERG underestimates the intensity distribution and frequency but overestimates the duration. The timing of the summertime diurnal cycle is well represented across the continental United States, although the amplitude is weaker in the southwest. Moderate intensity events, which represent the majority of rain event cases, show more agreement than events that have significant amounts of light or heavy rain. Satellite-based precipitation datasets are rapidly improving, but awareness of their

strengths and limitations, as well as examination of precipitation datasets in a developmental context, can enhance satellite retrieval algorithms and can complement climate model simulations.

4.1. Introduction

While rare, severe weather is scientifically interesting because it indicates upper level divergence, moisture transport, and vertical heating rates in the atmosphere. The societal impact of heavy rainfall can be significant: on August 11, 2016, heavy rainfall led to flooding in Louisiana, which resulted in \$10 billion in damages and 13 deaths. To describe the character of such severe weather and storms, a rain event can be broken down into its corresponding intensity, duration, and frequency characteristics to provide a more complete description of its character than by examination of any of these parameters alone [Westra et al., 2014]. This event-based Intensity-Duration-Frequency (IDF) framework is useful for predicting regional susceptibility to extreme weather and flooding [Kendon et al., 2014]. Climate models predict that there will be shifts in the intensity, duration, frequency, and total precipitation due to climate change [Trenberth et al., 2003]. Satellite-based precipitation datasets are used to evaluate precipitation features in global climate models, which have been found to over predict the frequency of light rainfall [Stephens, 2010]. However, existing studies have not assessed satellite precipitation products in context of the IDF framework. Measurement uncertainty that results from sensor-level errors and algorithm assumptions at instantaneous scales propagates into longer, sub-daily timescales [Tian et al., 2014].

Integrated Multi-satellite Retrievals for the Global Precipitation Measurement [GPM; Hou et al., 2014] satellite mission [IMERG] is a state-of-the-art satellite precipitation dataset that integrates observations from passive microwave and infrared sensors across several satellite platforms to have global coverage in high space and time resolution (0.1°, 30 min) [Huffman et al., 2015]. Satellite precipitation products such as IMERG are evaluated against ground “truth” observations, which are typically national radar networks or rain gauges [Hourdin et al., 2016], but can also consist of field experiments or observations of surface water flow [Hou et al., 2014].

Uncertainty in precipitation measurements are compounded by regional, topographical, and seasonal dependencies [Tang, 2016; Tan, 2016; Oliveira et al., 2016]. Most validation work focused on comparing instantaneous rain rates from satellite sources to ground datasets on shorter, instantaneous time scales [Ebert et al., 2007; Maggioni et al., 2016], and not into IDF, which would more faithfully characterize the event.

Models also struggle to simulate the diurnal cycle of rainfall [Dai, 1999], in part because storms can occur at temporal and spatial scales below the model resolution. The diurnal cycle is typically well-captured in precipitation products, but complex terrain and arid or very moist regions can cause rainfall to be missing or overestimated, impacting the diurnal cycle. Compared with older PMW-based datasets, IMERG was found to better capture the diurnal cycle over China when compared with rain gauge networks [Tang, 2016]. However, this study found that the timing of the diurnal cycle was out of phase over the arid regions. Similarly, Oliveira et al [2016] examined the diurnal cycle over the Amazon during the CHUVA project

[Machado et al., 2016] and found that IMERG captures the wet season diurnal cycle, albeit with some overestimated rainfall in the morning. However, IMERG does not capture the daily cycle during the dry season due to underestimation of heavy rainfall (> 10 mm/h) during this season. Machado et al. attribute this to the surface characterization of the PMW retrieval algorithm, suggesting that more studies over different land surface types and climates are needed.

The goal of this study is to use the IDF framework to evaluate IMERG's ability to reproduce event-based characteristics and diurnal cycles with ground radar over the continental United States (CONUS). This study will permit us to examine how uncertainty in the rain estimate on instantaneous scales, which is a function of terrain, season, and regional climatology, can impact measurements at time-scales that extend to the duration of the event (< 4 days) and the daily cycles of rainfall. These results can improve understanding of the strengths and weaknesses of IMERG, a next-generation multi-satellite, merged satellite precipitation product, which will be beneficial to climate and flood modeling research.

In Section 4.2, we will explain the datasets, and in Section 4.3 we will describe the methods. We will present our results on precipitation seasonal mean, IDF analysis and statistics, and the diurnal cycle in Section 4.4. The discussion and conclusions will also be in Section 5.4.

4.2. Data

4.2.1 IMERG

IMERG (version 3, final product) is a gridded, $0.1^\circ \times 0.1^\circ$, half-hourly precipitation dataset [Huffman et al., 2015]. The final, research-grade product has been calibrated with surface gauges where available. IMERG unifies observations from passive microwave (PMW) and infrared (IR) sensors from GPM core and constellation satellites, and is calibrated using gauge corrections. We used all available IMERG data at the time of writing, which is from March 2014 to December 2015.

High resolution precipitation datasets are possible through the combined community effort to innovate, evaluate, and improve the many datasets from GPM's predecessor satellite, Tropical Rainfall Measurement Mission (TRMM) [Maggioni et al., 2016]. Many of the strengths from the TRMM-era datasets were integrated into IMERG, and as its acronym implies, most notably by merging passive microwave (PMW) measurements from the GPM constellation with infrared IR observations from geostationary satellites. PMW observations provide a higher quality rainfall estimate but because they are taken from low-earth orbit satellites, measurements have a lower temporal sampling rate (every 3 hours). Because IR cannot penetrate cloud tops to examine surface precipitation, IR observations provide lower quality rainfall estimates but because they come from geostationary satellites they have higher temporal sampling (every 30-60 min). The synthesized PMW-IR combination allows greater spatial and temporal coverage, although data quality suffers due to IR observations being significantly worse rainfall estimators than PMW [Tan et al.,

2016]. A third estimation method within IMERG is to combine the IR and PMW measurements using morphing.

Morphing is a Lagrangian technique that propagates PMW precipitation estimates using cloud motion vectors derived from geostationary infrared observations [Joyce et al., 2004]. The PMW estimate is translated both forward and backwards in time between PMW overpasses, filling in the gaps (within 90 minutes of an overpass) with a combined value of the later and earlier rain rate. The final rain rate is weighted by time closer to when the PMW observation was made.

Utilizing a Kalman filter to select the appropriate estimate (PMW, morphing, or IR) improved the quality of estimations [Joyce and Xie, 2011]. The Kalman filter assigns weights to minimize error variance in the rain estimate, which results in a blend between a PMW-only, morphed, or IR-derived rain estimate. Morphing can improve rainfall estimates on daily timescales. Past studies found that the Climate Prediction Center (CPC) morphing technique [CMORPH, Joyce et al., 2001] precipitation dataset, a TRMM-based dataset that pioneered the morphing technique, had a 10% smaller root mean square error than 3B42, a non-morphed precipitation dataset, at time scales less than four days. Beyond that errors were approximately 30% greater [Tian et al., 2014].

4.2.2 MRMS

As a reference, this study uses ground-based measurements from the Multi-Radar/Multi-Sensor (MRMS, gridded 1-km, hourly) dataset. MRMS is precipitation product produced by integrating base-level radar data with model, gauge, and satellite

observations over the continental United States [Zhang et al., 2011a]. There are advantages and drawbacks of using a radar-based dataset as a reference, which can be reduced through bias correction from gauge calibration and by only using pixels with a high radar quality index (RQI) to reduce uncertainty in the measured rain rate.

MRMS is useful as a reference dataset because ground-based radar observations are (1) more accurate than space-based observations, (2) available in high temporal and spatial resolution, and (3) quality controlled to reduce detection of non-precipitation such as noise, radar clutter, and complex terrain effects. Alternatively, rain gauges can be utilized for validation, but may not be representative of a large area and like radar, are not available in remote regions [Kidd, 2016]. Gauge calibration can lead to improvements in estimates [Zhang et al. 2011a].

However, there are some drawbacks to using MRMS as the ground reference. First, there are large gaps in the radar network due to beam blockage by topographical features. Radar measurements are advantageous in their spatial and temporal sampling; however, the reflectivity-rain-rate (Z-R) relationship is used to convert radar reflectivity into precipitation rate, and this relationship has a spatial and seasonal dependence which can lead to underestimation of rainfall in warm and wet conditions [Harrison, 2000; Dinku, 2003; Maggioni, 2016].

Using the gauge bias-corrected radar product (3B-HHR) can reduce bias and uncertainty that is due to inaccurate Z-R relationships, however terrain can introduce uncertainty in estimates due to beam blockage [Zhang et al. 2011b]. MRMS has a radar quality index (RQI), which ranges from 0 (worst) to 100 (best) to indicate the

degree of uncertainty in the measurement. To control for both these data voids and non-negligible biases in measurements, we only used radar in regions with an average quality index greater than 80%.

To make the datasets comparable, IMERG observations were averaged hourly and MRMS was binned to $0.1^\circ \times 0.1^\circ$ to match the IMERG resolution. We used the entire IMERG record that was available at the time of writing, from March 2014 to December 2015.

4.3. Methods

We define a rain event as the number of hours during which either IMERG or MRMS detects rainfall above 0.2mm/hour. This threshold is the minimum rain rate that Ka and Ku- band radars on GPM, which are used for PMW calibration, can detect; at lower values, the relative standard deviation can exceed 100% and the data are unreliable [Tian and Peters-Lidard, 2010]. For the remainder of this paper, we use the following definitions for rainfall characteristics of the events:

- Intensity: The average rain rate for an event.
- Duration: The number of hours that an event lasts.
- Frequency: The number of events.

We examined these events for the entire year and spatial domain, and also divided them into seasons: December-February (DJF), March-May (MAM), June-August (JJA), and September-November (SON).

To assess IMERG's ability to reproduce diurnal variability, we aggregated the IMERG and MRMS into a seasonal daily average rain rate and took a Fourier

transform of the result following a procedure similar to that of Bell et al., 2008. From the phase, we could estimate the local time of day of the daily maximum rain rate, as well as the amplitude of the signal.

4.4. Results

In this study, we examine the IDF characteristics of rain events detected using IMERG, which we evaluate against the MRMS dataset. Using the methods described in Section 2 resulted in the detection of over 2 million rain events, which were then compared. Additionally, we examine the diurnal cycle to further characterize the accuracy of IMERG at sub-daily timescales.

4.4.1 Seasonal average and event-based IDF characterization

In terms of seasonal average rain rates for 2014-2015, there is good agreement between IMERG and MRMS (Figure 4-1). Some of the spatial details are smoothed out in IMERG over the Midwest due to the lower native resolution in IMERG than in the MRMS dataset. MRMS has noticeable radar gaps, is caused by an absence of an available radar tower or because the measurement did not meet our 80% minimum RQI threshold, which is particularly over high terrain regions such as the Rocky Mountains.

However, on regional scales there are some noticeable differences, particularly in JJA and DJF. In DJF, IMERG produces less rain than MRMS over the Pacific Northwest (43-49°N, 119-126°W). Over Florida (23-31°N, 80-86°W) during JJA, some of the heaviest rainfall (>10 mm/day) present in the MRMS dataset is lighter (7.5 mm/day) in IMERG. The region east of the Rocky Mountains (35-40°N, 97-102°W) shows reasonable agreement. There is a large density of rain gauges east of the Rockies and both MRMS and IMERG are gauge-calibrated products, which could be responsible for the good agreement.

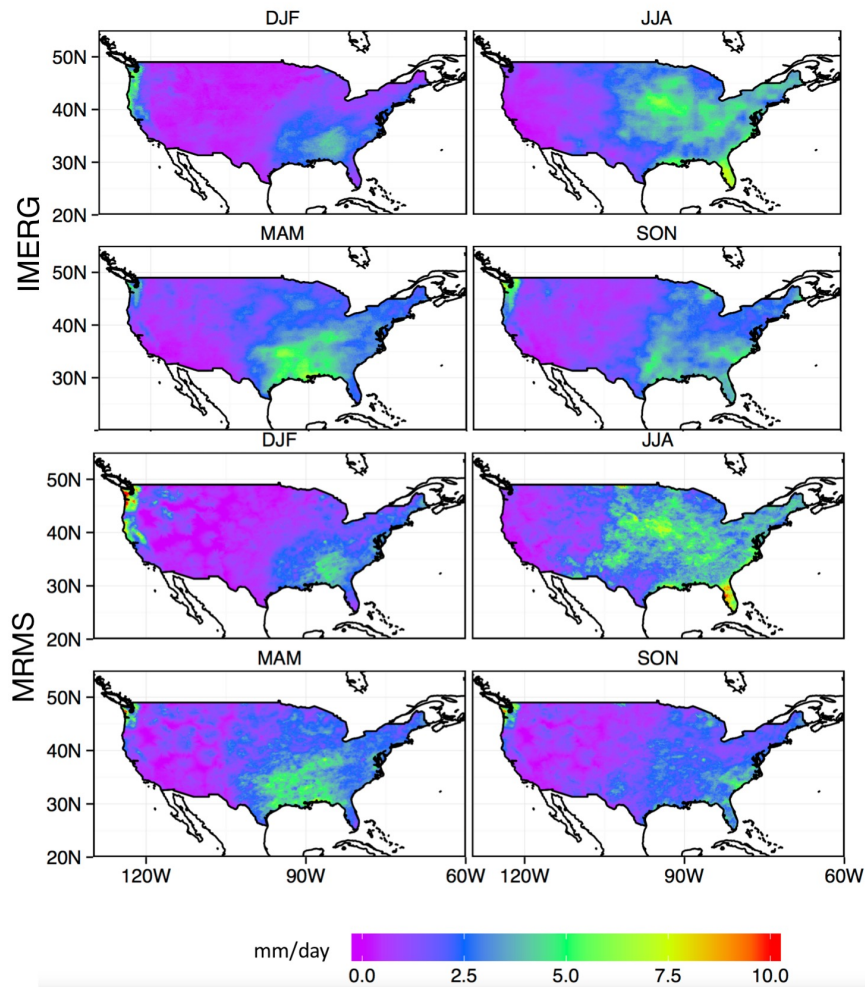


Figure 4-1 Average seasonal rainfall for (a) IMERG and (b) MRMS, from March 2014 to December 2015. Observations are shown for all radar quality index (RQI) values.

However, we can examine the characteristics of individual rain events to determine how disagreements in Figure 4-1 occur on shorter time scales. In JJA, the average event intensity is over or underestimated depending on the region (Figure 4-2a); there is underestimation in the Midwest, but overestimation in the north, near the Great Lakes region (45°N, 85°W). The duration of events was almost uniformly overestimated (Figure 4-2b). Distinguishing rain from land surfaces remains a challenge to PMW retrievals [Ferraro et al. 1996], and since rain rate is used as a threshold for duration, these values will be impacted as well.

In the wintertime (DJF), IMERG uniformly overestimates the maximum intensity of

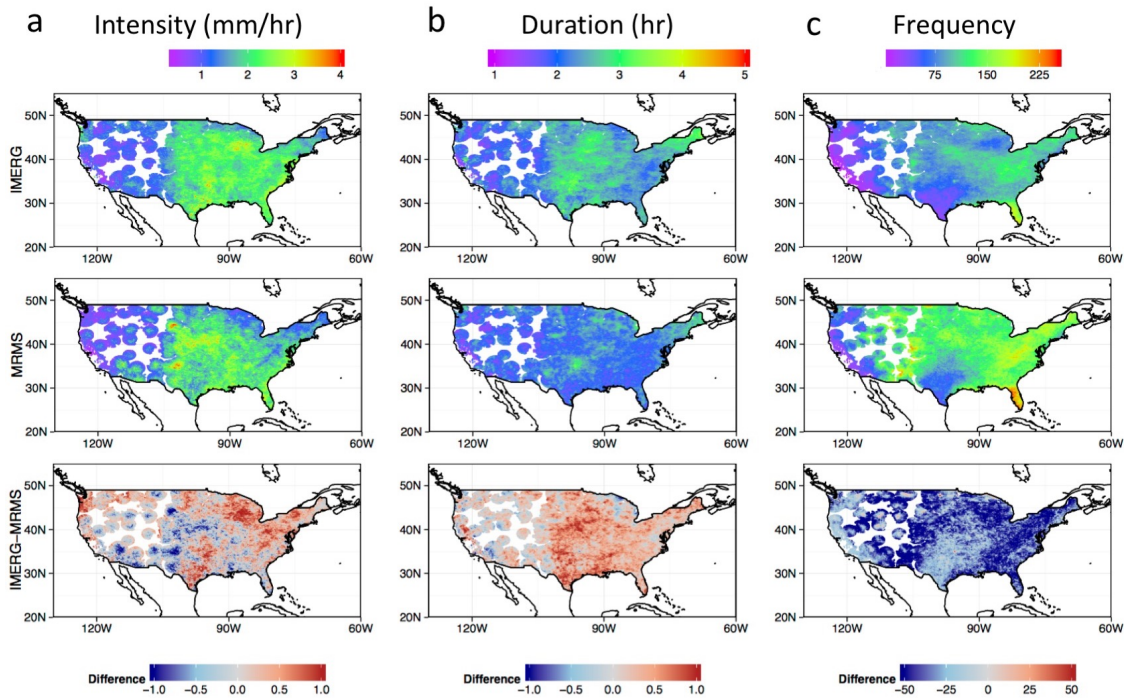


Figure 4-2 Mean intensity, duration, and frequency of rain events in JJA for (a) IMERG, (b) MRMS, and (c) IMERG-MRMS from March 2014 to December 2015. Data in regions with an average quality index below 80% were excluded from this analysis.

events (Figure 4-3a). Duration differences are more regionally specific, with underestimates of an hour mainly in higher latitudes in DJF. Over the Pacific Northwest, MRMS characterizes rain events as light, long lasting, and frequent. However, IMERG shows heavier, shorter-lived, and frequent rainfall in this region. IMERG underestimates the frequency of rain events across both seasons (Figure 4-2c and 4-3c). Radar limitations in the wintertime limit the scope of validations over more remote regions in the western United States. Typically, the west coast experiences its wet season in the winter and dry season in the summer, and the inverse is true for the eastern CONUS, leading to seasonally dependent biases in values. Note that while both 2014 and 2015 were combined in these figures, our examination

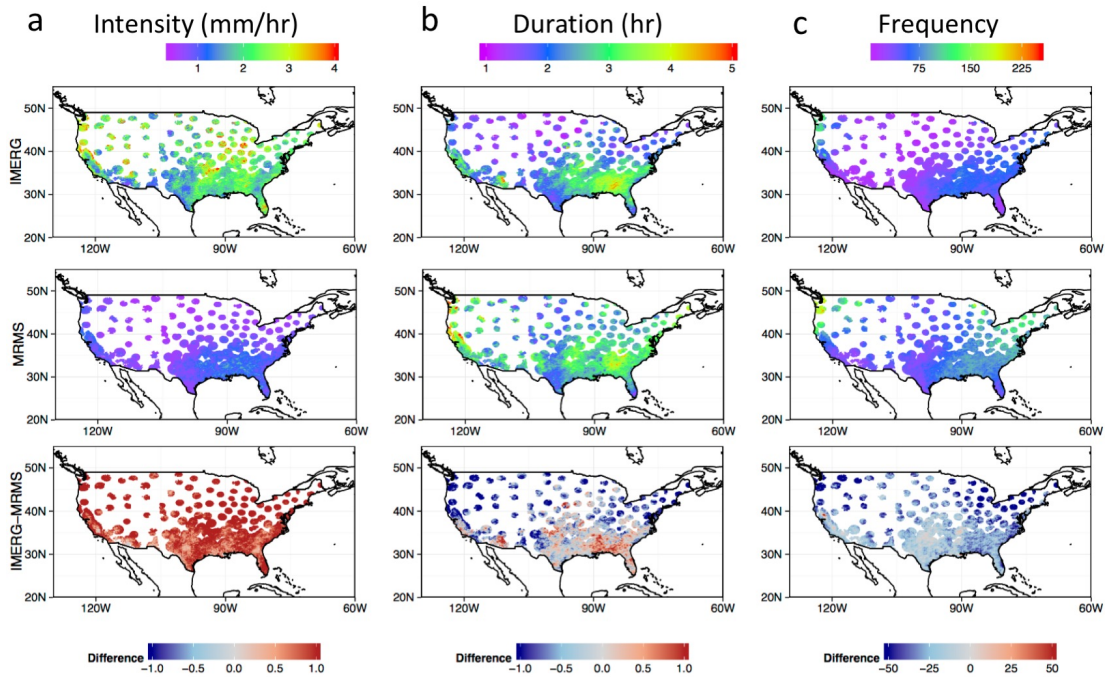


Figure 4-3 Mean intensity, duration, and frequency of rain events in DJF for (a) IMERG, (b) MRMS, and (c) IMERG-MRMS from March 2014 to December 2015. Data in regions with an average quality index below 80% were excluded from this analysis.

of year-to-year differences in MRMS and IMERG were smaller than differences in our comparison of the two datasets. While not shown, the spatial distribution of the standard errors of the intensity and duration in JJA (Figure 4-2) and DJF (Figure 4-3) were generally smaller than the differences between the two datasets. Errors were higher in DJF than JJA, in IMERG than MRMS, and in intensity measurements than in duration.

4.4.2 Probability distribution of event-based characteristics over CONUS

For the total number of detected events shown in Figure 4-4, we examine probability distribution of intensity and duration for all events in Figures 4-5 and 4-6, respectively. These figures are normalized by the total frequencies in Figure 4-4, so differences may not reflect a large number of events, particularly at the tail end of the distribution.

Overall, IMERG light rain events are less probable than in MRMS (Figure 4-5a). In

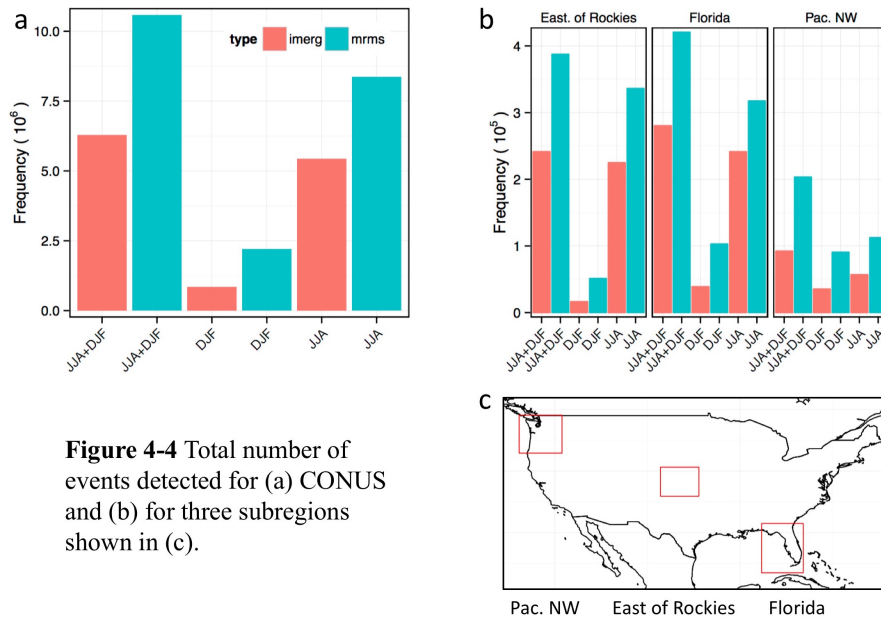


Figure 4-4 Total number of events detected for (a) CONUS and (b) for three subregions shown in (c).

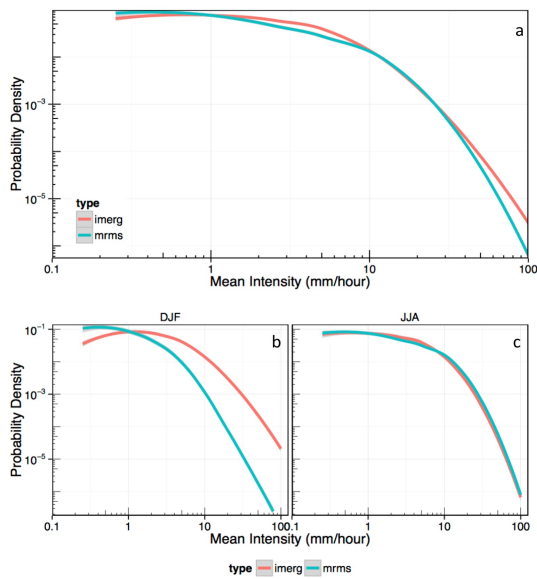


Figure 4-5 Kernel density estimate showing the probability of average rainfall intensity (mm/h) for precipitation events maintaining a rain rate above 0.2 mm/h for (a) CONUS JJA and SJF combined, (b) DJF, and (c) JJA, from March 2014 to December 2015. Grey shading represents the standard error.

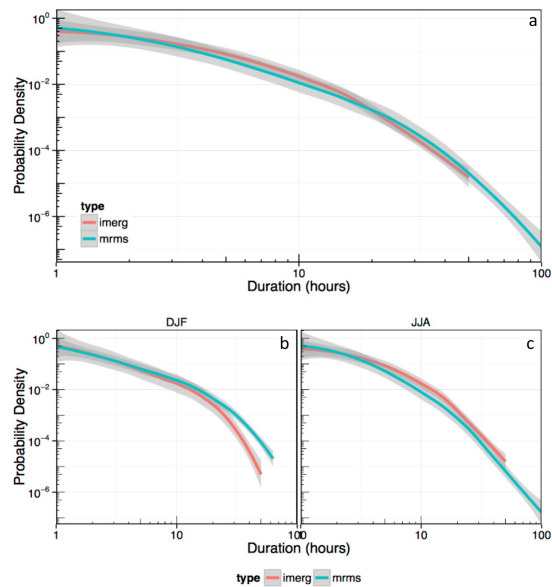


Figure 4-6 Kernel density estimate of duration (h) for precipitation events maintaining a rain rate above 0.2 mm/hr for (a) CONUS JJA and SJF combined, (b) DJF, and (c) JJA, from March 2014 to December 2015. Grey shading represents the standard error.

DJF (Figure 4-5b), we can see that this difference is more pronounced: the distribution is shifted toward stronger events than what is observed in IMERG. Performance is more consistent with MRMS in JJA (Figure 4-5c), when convective rainfall is typically more common over CONUS. However, the distribution shows an underestimation of higher intensity events (> 10 mm/h) and an overestimation at moderate intensities (1-10 mm/h). Grey shading represents the standard error of the plots, however the error ranges are fairly small for intensity.

Figure 4-6a shows that IMERG detects more moderate length events (2-11 h), and underestimates the Mean distribution of short-lasting (1-2 h) and longest-lasting (>11 h) events. However, error ranges are larger in duration than in the intensity probabilities (Figure 4-5), and there is overlap. In DJF, IMERG almost uniformly underestimates event duration, which is significant for the longest lasting rain events (Figure 4-6b). In contrast, during JJA there is an overestimation of events longer than an hour

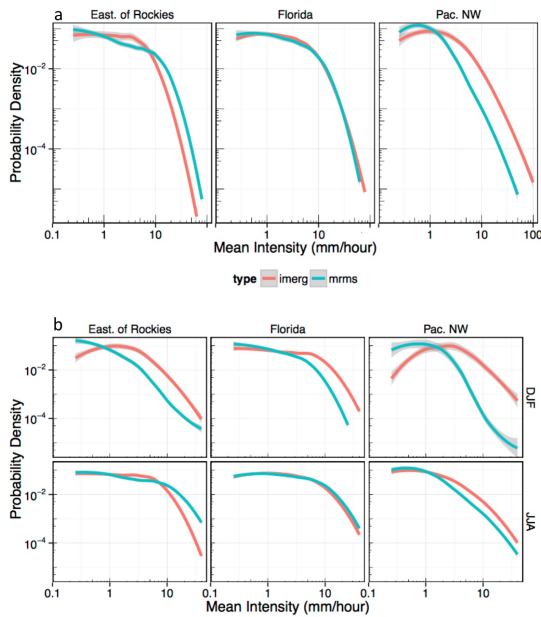


Figure 4-7 Kernel density estimate of intensity (mm/h) for precipitation events maintaining a rain rate above 0.2 mm/hr for (a) each region with JJA and SJF combined, (b) each region with DJF and JJA considered separately, from March 2014 to December 2015. Grey shading represents the standard error.

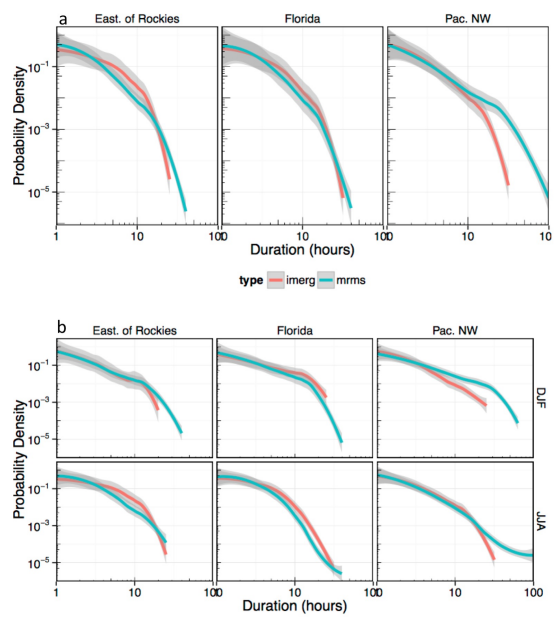


Figure 4-8 Kernel density estimate of duration (h) for precipitation events maintaining a rain rate above 0.2 mm/hr for (a) each region with JJA and SJF combined, (b) each region with DJF and JJA considered separately, from March 2014 to December 2015. Grey shading represents the standard error.

(Figure 4-6c), although the standard error is partially overlapping. The sharp drop-off in the longest-lived events may be partly due to morphing, which may smooth over rainfall and bring it below our detection threshold.

We also take a closer look at the intensity and duration in three regions, which represent regions in the west (Pacific Northwest), central (east of the Rockies), and southeastern United States (Florida). Figure 4-7a shows that each region exhibits disagreement with MRMS in terms of rain intensity, although it appears that the discrepancies are largely driven by winter observations (Figure 4-7b).

In terms of duration (Figure 4-8a), the disagreement is more evenly split between the two seasons. Florida's distribution is somewhat skewed toward longer events than MRMS, particularly during JJA, while the detected events are shorter over the Pacific Northwest. Their seasonal distributions are somewhat reversed east of the Rockies,

with more underestimation in the winter and more overestimation for moderate duration events (Figure 4-8b). However, duration errors east of the Rockies are large due to the small sample size (Figure 4-4). As more data become available, this distribution can be re-examined.

4.4.3 The diurnal cycle of rainfall

In addition to studying the IDF characteristics of rain events, we also examine the time when these events take place. Figure 4-9 shows the diurnal cycle of rainfall from

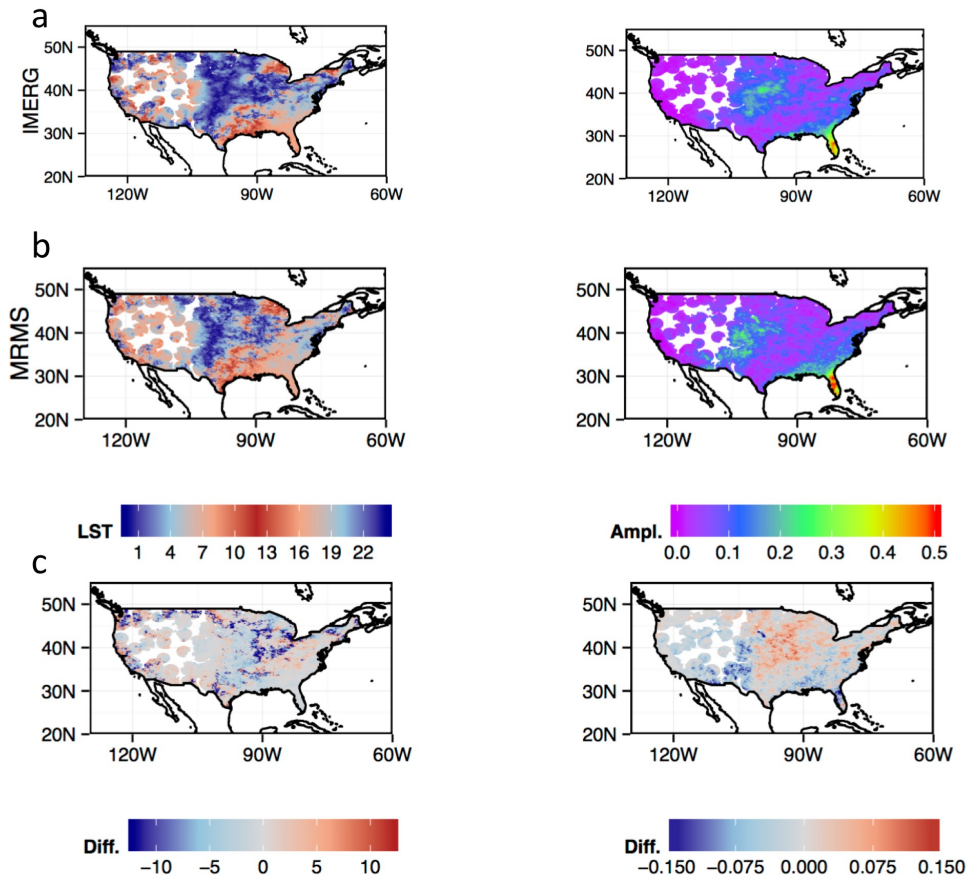


Figure 4-9 The JJA diurnal cycle maximum hourly rain in local standard time and the amplitude of the signal. Data in regions with an average quality index below 80% were excluded from this analysis.

the Fourier transform on daily average rainfall in JJA. Other seasons were excluded from the analysis because the amplitude of the diurnal cycle was significantly weaker in other seasons. In Figure 4-9a, both datasets show that the Rocky Mountains and adjacent Great Plains have a nocturnal maximum while an afternoon peak is generally found elsewhere, which is consistent with past studies [Dai, 1999]. There is also good agreement between IMERG and MRMS over the timing and amplitude over Florida. The IMERG amplitude is weaker over southern and southwestern CONUS, although the phase is reasonably well-captured when compared with MRMS.

While there is mostly agreement, IMERG’s probability density in Figure 4-10a shows

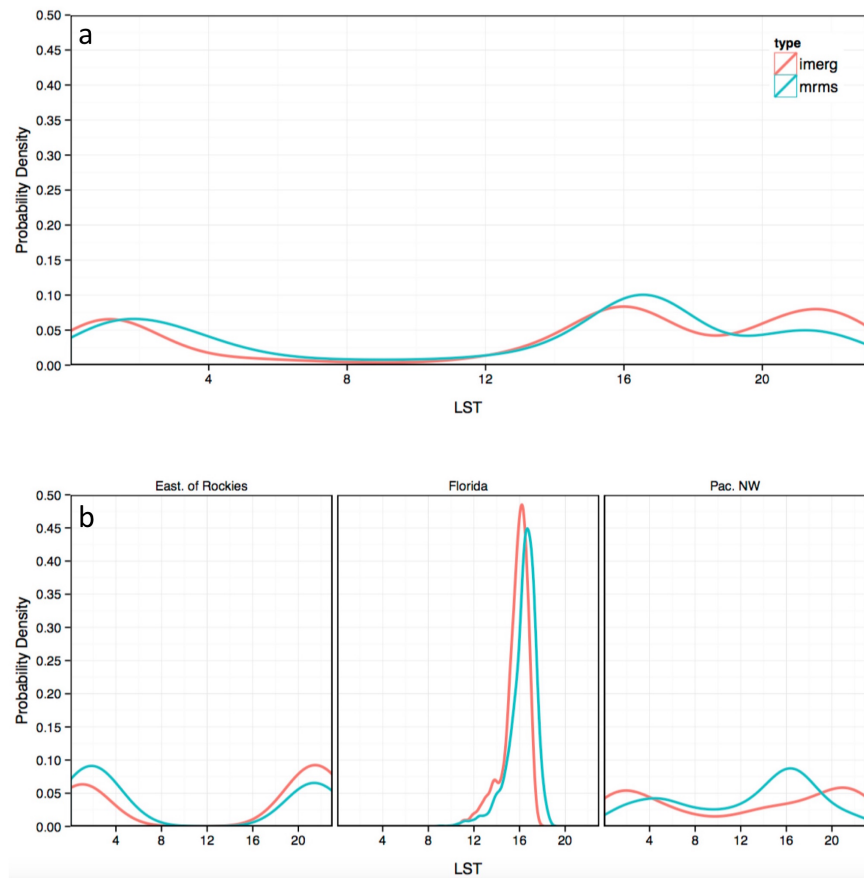


Figure 4-10 JJA kernel density estimate of the diurnal cycle hourly phase in local standard time for (a) all CONUS and (b) each region considered separately.

that the local solar time (LST) of rainfall peaks has a broader distribution in IMERG than in MRMS. IMERG has a peak centered at 18:00 LST, while in MRMS the peak occurs closer to 16:00 LST. As we saw in Figure 4-6c, IMERG tends to overestimate the duration of moderate strength events in JJA.

Unlike much of the United States, there is a nocturnal peak in rainfall east of the Rockies, and the pattern is faithfully captured by IMERG (Figure 4-10b). There is a strong diurnal peak in Florida, which occurs roughly an hour earlier in the IMERG dataset. Over the Pacific Northwest, there is an almost three-hour lag in the occurrence of peak precipitation.

4.5. Summary and Discussion

In this Chapter, we show that the IDF framework can be used to evaluate how rain characteristics from satellite precipitation datasets compare with ground truth. In terms of daily mean precipitation, agreement is good between the two sources, but IDF differences are region and season-specific, which we visually summarize in Figure 4-10. We show that over Florida, IMERG overestimates the intensity and overestimates duration, but underestimates the frequency of rainfall in the winter. Although seasonal averages of daily rain rates show good agreement east of the Rocky Mountains, when examining the event-based characteristics IMERG underestimates the intensity distribution and frequency, however duration is inconclusive due to sample size limitations. We found relatively good agreement in the diurnal cycle over CONUS, which is promising since Tang et al. [2016] found

IMERG overestimated the diurnal cycle in the afternoon and in the Tibetan Plateau and did not capture the cycle over Northwest China.

Wintertime overestimation (Figure 4-3) of rain intensity, particularly light rainfall, can arise from the difficulty of PMW sensors “seeing” warm rain processes above a warm land surface. Secondly, IR cannot detect warmer stratiform clouds [Vincente et al., 1998], which can lead to cloud motion vectors that follow only the coldest cloud features or miss the cloud altogether. Distinguishing rain from land surfaces remains a challenge to PMW retrievals [Ferraro et al. 1996]. Since we used a rain rate

	Intensity	Duration	Frequency	Diurnal Phase
All CONUS	General agreement of average precipitation at seasonal timescales			
DJF	>	mixed	<<	/
JJA	mixed	>	<	=
Pacific NW				
DJF	>>	<<	<	NA
JJA	>	>	<	+3 h
Florida				
DJF	>>	>	<	/
JJA	<	>	<	-1 h
East of Rocky Mountains				
DJF	>>	mixed	<	/
JJA	<<	mixed	<	=

Figure 4-11 Summary highlighting the major differences of IMERG vs MRMS between the magnitude of the intensity, duration, and frequency, based on primary features. Shading (red, grey, blue) and symbols (>, =, <) used in the table above indicate that IMERG events were larger, equal, or smaller in value than MRMS, respectively; mixed implies a great deal of regional variability or uncertainty in estimates.

threshold for duration in this study, inaccurate rain intensity estimates in the source data impact the duration and frequency of the event as well. Underestimation of the heaviest rain can result from poor Z-R relationships above the melting layer in the cloud. Florida had the best agreement, which is likely due to the regions relatively flat terrain and mild winters, which were also observed by Tian et al. 2007.

PMW measurements have the highest skill in measuring rainfall, but in the mid-latitudes, rain events will only have one or two PMW “best” estimates during their lifetimes. The skill of the IMERG precipitation estimate is related to the measurement source (passive microwave, morphing, or infrared). Morphing represents 67.5% of detected rain cases in the Mid-Atlantic and has a higher occurrence of falsely detected rain than in PMW and IR only estimates [Tan et al. 2016]. We speculate that morphing may be influencing the duration of events, particularly in the summer, when short-lasting convective events can quickly develop and dissipate. A future study can explore the impact of the three primary estimation techniques (PMW, morphing, IR) on the quality of the IDF estimation.

The present study cannot isolate the cause and effect of the discrepancies in IMERG and MRMS. However, past studies of TRMM-based datasets show that PMW-based observations tend to have a positive bias at daily time scales, with overestimation of low intensity rainfall (<50 mm/day), underestimation of high intensity rainfall [Jiang et al., 2016], and regional and seasonal dependencies of measurement errors were observed across the globe [Maggioni et al., 2016]. In CMORPH validation studies, it was found that daily precipitation totals were generally underestimated in DJF and

overestimated in JJA compared with radar, where the biases could exceed ± 5 mm/day [Tian et al., 2007].

There are several challenges related to this study. It is apparent that MRMS coverage is limited in the west, particularly in the boreal winter months, and radar artifacts mean that we had to limit our study to regions with a quality index of 80% more to compare with IMERG. At the time of writing, only two years of IMERG data were available due to the recent launch of GPM. Eventually, IMERG will be reprocessed back in time to the beginning of the TRMM-era. As with any new data product, improvements are being made very quickly and new versions of the dataset will be available.

Past studies on TRMM-based products have shown that precipitation retrieval errors can depend on the life cycle stage [Tadesse and Anagnostou, 2009]. Realistically, rain develops within clouds, not as fixed points on the ground, so it would be useful to track rain features continuously as they evolve, which would facilitate knowledge of the age and total lifetime of the system [Esmaili et al., 2016]. In the past object-based tracking of rainfall was possible but computationally intensive and complex [Skok et al., 2009]. When IMERG is processed back through the TRMM era, the resulting long-term, high-resolution satellite precipitation product will enable the more in-depth evaluation and new applications of precipitation features as objects.

Chapter 5. Conclusion

5.1 Summary and contribution to the scientific community

By following the trajectories and properties of individual clouds at short time scales, in this thesis I show how cloud life cycle evolution takes place in the time periods between low-earth orbit overpasses (Chapter 2). The location and intensity of clouds and rainfall can be modulated by dust aerosols, such as in proximity to Saharan dust outbreaks in the Atlantic (Chapter 3). Combined, these chapters show the complicated nature of cloud development. A simplified view of cloud evolution in merged rainfall retrievals is a possible source of errors, which can propagate in composite analysis. In Chapter 4, I investigate the intensity, duration, and frequency of precipitation in next-generation satellite precipitation products with ground observations over the contiguous United States. A summary of the questions and findings that resulted from this thesis can be found in Figure 5-1.

While I completed my thesis work under the guidance of my advisors, I took a lead role in developing, conducting, and analyzing the research described in this dissertation. The primary scientific contributions of this thesis include:

- Building off prior studies which primarily focused on the tropics, I produced the first statistical characterization of the number, size, and lifetime of clouds in the atmosphere, which can be useful for model output validation.

- I showed that the life cycle evolution of cloud size and temperature is non-linear. Next-generation satellite precipitation products use infrared-derived motion vectors to linearly propagate rainfall, thus these results can be applied to improving assumptions in merged precipitation datasets.

Questions	Findings
Chapter 2: Global Cloud Tracking and Life Cycle Evolution	
<ul style="list-style-type: none"> • At what rate do cloud characteristics such as size and temperature evolve over the life cycle? • At what time of day does development take place? 	<ul style="list-style-type: none"> • Evolution of cloud growth is non-linear; The maturity stage is extended for longer lasting clouds than shorter lasting clouds • Over the ocean, the diurnal cycle of maximum cloud frequency has two peaks, and the nocturnal peak is composed of longer lasting clouds
Chapter 3: Aerosol Impact on Evolution	
<ul style="list-style-type: none"> • Do large-scale Saharan dust outbreaks impact the location and the intensity of cloud clusters in the tropical Atlantic? 	<ul style="list-style-type: none"> • Position of the cloud development enhanced near dust outbreak regions • There is an increased probability of intense storms on dust outbreaks days
Chapter 4: Rain Event Evaluation	
<ul style="list-style-type: none"> • What are the differences between the intensity, duration, and frequency of satellite precipitation products (IMERG) and ground observations (MRMS)? 	<ul style="list-style-type: none"> • Agreement on seasonal scales, but overestimation of intensity from December to February, duration from June to August, and underestimation of frequency (both seasons).

Figure 5-1: Summary of the questions and findings that were reached in this thesis.

- I examined the diurnal cycle of cloud life cycle stage and total lifetime both globally, and examined the land and ocean differences over India and Western Africa. Past studies of the diurnal cycle found that rainfall is more intense for oceanic nocturnal storms. Because Lagrangian tracking enables knowledge of the clouds and storms' lifetimes, I could build on past studies to show that these systems in addition to having more intense rain rates, also have extended lifetimes.
- I show that large-scale Saharan dust outbreaks shift cloud trajectories closer to the dust outbreak source, and evidence that the intensity of cloud clusters in the tropical Atlantic is enhanced during outbreaks and reduced during low-dust conditions. These results provide observational support to prior modeling studies.
- Evaluated event-based characteristics (intensity, duration, and frequency, or IDF) of the IMERG satellite precipitation product with ground radar observations over the continental United States. These results show that while seasonal means might show agreement, the features have discrepancies: average rain rate are universally too high in the winter, durations are too high in the summer, and frequencies are too low in both seasons. This is the first study to evaluate the data quality of in the IDF framework.

The field of atmospheric science traditionally focuses on the Eulerian framework, however this thesis highlights how these two approaches can be complementary. Lagrangian methods can provide another means of evaluating global climate models (such as those shown in Figure 1-1) and I show how observed development unfolds in

high spatio-temporal scales. This research resulted in a publication to the Journal of Geophysical Research – Atmospheres and a manuscript submission to the Journal of Hydrometeorology.

5.2 Future Work

“Almost everything about science is changing because of the impact of information technology. Experimental, theoretical, and computational science are all being affected by the data deluge, and a fourth, “data-intensive” science paradigm is emerging. The goal is to have a world in which all of the science literature is online, all of the science data is online, and they interoperate with each other. Lots of new tools are needed to make this happen.”

–Jim Grey, 2007

Data and computing resources are a major driver of cutting edge research in the Earth sciences, and through data synthesis we can achieve the spatial and temporal scales needed to advance climate modeling and weather prediction. The problem highlighted in this thesis is that in spite of more earth observing satellite missions than ever before, there are still many gaps in our understanding, which then translate into errors and uncertainty in satellite precipitation products. As a first order solution, it is tempting to apply the newest statistical methods to solve problems, as was done with IMERG. Doing so actually was very successful at achieving the scientific community’s first-order goal of having high spatial and temporal resolutions which are needed to run atmospheric and flood models, but at the expense of data quality. To further refine the accuracy of data products, knowing how observed cloud systems

initiate, grow, mature, and decay can allow scientific concepts to be built into heuristic algorithms.

One area of improvement in the IMERG and other morphing algorithms is the treatment of development: the preceding chapters show how cloud size and temperature properties change with time, what the development differences are for storms versus small-scale clouds, and the daily timing of when events take place. These results can be useful for algorithm development and model evaluation, but can also be used to answer broader scientific questions, such as those related to the impact of coarse aerosols on cloud cluster development.

Clouds and rainfall development can be enhanced or inhibited by dust aerosols; large scale dust outbreaks can shift ITCZ development northward and potentially cause more intense storms to form over adjacent ocean regions. These chapters advance the hypothesis that event tracking more realistically depicts how cloud evolution unfolds, which is more complex than the statistical assumptions that are currently used in PMW-IR morphing schemes in precipitation data products, like IMERG.

A simplified view of cloud evolution is but one potential error source in merged rainfall retrievals, which then propagate into higher level analysis. While much past research was dedicated to examining the errors in individual sensors, combining satellites makes it difficult to determine the error source [Tan et al., 2016] and also how it propagates into analysis at longer time scales [Tian et al., 2007]. To examine the collective impact of these uncertainty, I investigate the intensity, duration, and frequency of precipitation events to see how IMERG compares with ground

observations over the contiguous United States. I show that even though there is reasonable agreement at seasonal scales, event-based analysis of IMERG demonstrates that IMERG systematically underestimates the number of events, overestimates the intensity of rainfall, particularly in the winter, and can under or over estimate how long events last and the timing in which they take place. These results can be used to provide a more detailed understanding of rainfall characteristics, and evaluate the strengths and weaknesses of satellite precipitation products as a reference to climate models. It is important to understand that although we raised some issues regarding IMERG, it is a relatively young data product. In TRMM's 15-year history, the TMPA dataset was reprocessed seven times to reflect new corrections and innovations [Chen et al., 2013]. New versions become rapidly become available and past validation studies can become obsolete. Thus, validation is not static in time, but rather an ongoing community effort.

As noted by Jim Grey in the quote opening this chapter, one of our duties as scientists in this data-driven era is to enable open access of data and publications. As a scientist, my ideas are shaped by a lifetime of experiences and training. The successes of satellite precipitation products were enabled by the large, international effort of the International Precipitation Working Group (IPWG) and other members of the scientific community. One outcome of this thesis is a public storm track database (<https://stormtracks.umd.edu>) to allow our international and interdisciplinary community of earth scientists to apply it to their areas of need.

IMERG will eventually be reprocessed back through the TRMM-era, resulting in the longest satellite precipitation dataset to date. By combining rainfall with data from the

storm track database, we can examine the cloud-precipitation system as a whole. In the past, the TRMM precipitation feature (TRMM-PF) dataset developed by Liu et al. [2008]. TRMM-PF has been extensively used to study the size and intensity of strong rainfall events. By combining long-term IMERG records with our IR-based cloud tracks, rain features can be studied in the context of their entire life cycle and trajectory. Additionally, the precipitation radars on the TRMM and GPM satellites enable a three-dimensional representation of rainfall structure within the storm. The combination of precipitation radar measurements with high-resolution infrared observations from geostationary satellites would allow precipitation profiles and surface rainfall to be studied in the context of its development stage. This would make it possible to answer scientific questions such as: *What are the vertical precipitation structures within the cloud and how do they evolve over time? How does surface rainfall change with other morphologic and thermodynamic characteristics during the storm's life cycle?* Answering these questions will deepen our understanding of the atmospheric water cycle, which in turn can be used to improve climate and meteorological models of such processes.

There are certainly limitations to the techniques used in this thesis, which can impact assessment of rain algorithms and future work. Cloud clusters are not interchangeable with rain features within the cloud, clouds do not always contain rain, and warm clouds can be indistinguishable from the surface and thereby avoid detection. Cloud clusters also do not behave coherently through the entirety of their life cycle, as they split and merge or drop below the temperature threshold. Early termination and erratic behavior can result. Moving forward, it will be important to address these

detection issues, particularly before combining with rainfall observations to study rain feature development.

On November 19, 2016, NASA and NOAA jointly launched GOES-16, a geostationary satellite that will produce imagery at twice the spatial resolution (2 km) and up to four times the temporal resolution (15 min) of previous GOES satellites [Schmit et al., 2005]. The improvements increase the time and spatial sampling, permitting a more detailed study of cloud cluster development and diurnal cycle. The mission will be centered over the Atlantic, enabling more examination of Saharan Air Layer and dust outbreaks on cloud cluster development and hurricanes. Previous GOES satellites could difference the 10.9 μm and 12 μm channels to detect SAL but this channel did not function on newer satellites. However, in time, it may be possible to consistently track large aerosol particles which trigger a variety of environmental effects that lead to the suppression of cloud development.

In closing, event-based analysis would not be possible before this data-driven era of earth observing satellites. Now, we can engage in “storm chasing” from the comfort of our workspace to test theories, enhance predictive models, and deepen understanding of the environment. However, it is through the creative combination of data, statistics, and science that we can truly push our boundaries of understanding.

Appendix A. Comparing Satellite-based and GEOS-5 Cloud Tracks, Characteristics, and Diurnal Cycle over the Atlantic Ocean

A.1 Datasets and methods

In Section 1.3.1, we show preliminary findings that illustrate some of the discrepancies between observations and models by comparing the trajectories obtained from observed brightness temperatures from geostationary satellites with outgoing longwave radiation (OLR) from the high-resolution nature run (7-km horizontal resolution, 30 min dataset) produced from the Goddard Earth Observing System Model, Version 5 (GEOS-5) system of Earth observing model. OLR measures the radiation emitted by earth, included atmospheric features such as clouds, and is important in describing the energy balance of our planet and can also indicate the presence of convective activity.

The trajectories were computing using the methods described in Section 2.3. To track systems similarly in both datasets, observed brightness temperature observations were rescaled to 7-km to match the spatial resolution of GEOS-5. The two datasets capture different variables, brightness temperature (K) and OLR (W/m^2), which can be related by the Stefan-Boltzman law:

$$OLR = \sigma T^4$$

Where $\sigma = 5.6693 \times 10^{-8}$, is the Boltzman constant. Thus, if we use the 235 K temperature threshold (see Section 2.3.1 for temperature threshold justification) as the

equivalent brightness temperature, the equivalent radiance was 173 W/m^2 . However, T_b is radiance at a specific band (10.9 μm) while OLR is radiance across all IR bands.

A.2 Differences in cluster properties

Figure 1-2 shows that there are more trajectories in the GEOS-5 OLR than in the geostationary brightness temperature. The GEOS-5 produces a broader ITCZ and the resulting trajectories are smoother in the model than in the geostationary observation results. While this does highlight some of the disagreement that exists between models and observations, a sensitivity study needs to be done to see if differences are due to the threshold parameters used in the tracking or due to a limitation of the model.

There are also dissimilarities in the cluster characteristics. In Figure 1-3a, we can see that clusters are smaller in the GEOS-5 OLR compared with brightness temperature observations, especially outside of the ITCZ region. However, GEOS-5 clusters typically last longer (Figure 1-3b) than observed clusters. GEOS-5 produces a surplus of clusters, particularly over the Caribbean and the Southeastern United States in comparison to (Figure 1-3c).

A.3 Diurnal cycle

The diurnal cycle of cloud cluster formation is poorly represented in the GEOS-5 OLR analysis when compared with observed brightness temperature clusters over the southeastern United States (Figure 1-4). Afternoon thunderstorms are common over the region in June, which is observed in the brightness temperature clusters, but not in

the GEOS-5 clusters. Features of the shortest time scales are the most difficult for models to reproduce [Dai et al.,1999]. The GEOS-5 nature run is available for two years (2005-2006), so further refinement may elucidate some of the differences between models and observations.

References

- Adler, R. F. et al. (2003), The Version-2 Global Precipitation Climatology Project (GPCP) Monthly Precipitation Analysis (1979–Present), *J. Hydrometeor.*, *4*(6), 1147–1167, doi:10.1175/1525-7541.
- Arguez, A., I. Durre, S. Applequist, R. S. Vose, M. F. Squires, X. Yin, R. R. Heim, and T. W. Owen (2012), NOAA’s 1981–2010 U.S. Climate Normals: An Overview, *Bull. Amer. Meteor. Soc.*, *93*(11), 1687–1697, doi:10.1175/BAMS-D-11-00197.1.
- Bell, T. L., D. Rosenfeld, K.-M. Kim, J.-M. Yoo, M.-I. Lee, and M. Hahnenberger (2008), Midweek increase in U.S. summer rain and storm heights suggests air pollution invigorates rainstorms, *J. Geophys. Res.*, *113*(D2), D02209, doi:10.1029/2007JD008623.
- Bengtsson, L., K. I. Hodges, and E. Roeckner (2006), Storm tracks and climate change, *J. Climate*, *19*(15), 3518–3543.
- Bengtsson, L., K. I. Hodges, and N. Keenlyside (2009), Will Extratropical Storms Intensify in a Warmer Climate?, *J. Climate*, *22*(9), 2276–2301, doi:10.1175/2008JCLI2678.1.
- Biasutti, M., and S. E. Yuter (2013), Observed frequency and intensity of tropical precipitation from instantaneous estimates, *J. Geophys. Res. Atmos.*, *118*(17), 9534–9551, doi:10.1002/jgrd.50694.
- Blamey, R. C., and C. J. C. Reason (2012), Mesoscale Convective Complexes over Southern Africa, *J. Climate*, *25*(2), 753–766, doi:10.1175/JCLI-D-10-05013.1.
- Boer, E. R., and V. Ramanathan (1997), Lagrangian approach for deriving cloud characteristics from satellite observations and its implications to cloud parameterization, *J. Geophys. Res.*, *102*(D17), 21383–21399, doi:10.1029/97JD00930.
- Braun, S. A. (2010), Reevaluating the Role of the Saharan Air Layer in Atlantic Tropical Cyclogenesis and Evolution, *Mon. Wea. Rev.*, *138*(6), 2007–2037, doi:10.1175/2009MWR3135.1.
- Bretl, S., P. Reutter, C. C. Raible, S. Ferrachat, C. S. Poberaj, L. E. Revell, and U. Lohmann (2015), The influence of absorbed solar radiation by Saharan dust on hurricane genesis, *J. Geophys. Res. Atmos.*, *120*(5), 2014JD022441, doi:10.1002/2014JD022441.
- Carvalho, L. M. V., and C. Jones (2001), A Satellite Method to Identify Structural Properties of Mesoscale Convective Systems Based on the Maximum Spatial

- Correlation Tracking Technique (MASCOTTE), *Journal of Appl. Meteorol.*, *40*(10), 1683–1701, doi:10.1175/1520-0450.
- Cattani, E., A. Merino, and V. Levizzani (2016), Evaluation of Monthly Satellite-Derived Precipitation Products over East Africa, *J. Hydrometeorol.*, *17*(10), 2555–2573, doi:10.1175/JHM-D-15-0042.1.
- Chen, S. et al. (2013), Evaluation of the successive V6 and V7 TRMM multisatellite precipitation analysis over the Continental United States, *Water Resour. Res.*, *49*(12), 8174–8186, doi:10.1002/2012WR012795.
- Chen, S. S., and R. A. Houze (1997), Diurnal variation and life-cycle of deep convective systems over the tropical pacific warm pool, *Q.J.R. Meteorol. Soc.*, *123*(538), 357–388, doi:10.1002/qj.49712353806.
- Chen, S. S., R. A. Houze Jr., and B.E. Mapes (1996), Multiscale variability of deep convection in relation to large-scale circulation in TOGA COARE, *Journal of the Atmospheric Sciences*, *53*(10), 1380.
- Dai, A., F. Giorgi, and K. E. Trenberth (1999), Observed and model-simulated diurnal cycles of precipitation over the contiguous United States, *J. Geophys. Res.*, *104*(D6), 6377–6402, doi:10.1029/98JD02720.
- Dinku, T., E. N. Anagnostou, and M. Borga (2002), Improving Radar-Based Estimation of Rainfall over Complex Terrain, *J. Appl. Meteorol.*, *41*(12), 1163–1178, doi:10.1175/1520-0450(2002)041<1163:IRBEOR>2.0.CO;2.
- Dunion, J. P., and C. S. Velden (2004), The Impact of the Saharan Air Layer on Atlantic Tropical Cyclone Activity, *Bull. Amer. Meteor. Soc.*, *85*(3), 353–365, doi:10.1175/BAMS-85-3-353.
- Ebert, E. E., J. E. Janowiak, and C. Kidd (2007), Comparison of Near-Real-Time Precipitation Estimates from Satellite Observations and Numerical Models, *Bull. Amer. Meteor. Soc.*, *88*(1), 47–64, doi:10.1175/BAMS-88-1-47.
- Elsebaie, I. H. (2012), Developing rainfall intensity–duration–frequency relationship for two regions in Saudi Arabia, *Journal of King Saud University - Engineering Sciences*, *24*(2), 131–140, doi:10.1016/j.jksues.2011.06.001.
- Engelstaedter, S., and R. Washington (2007), Atmospheric controls on the annual cycle of North African dust, *J. Geophys. Res.*, *112*(D3), D03103, doi:10.1029/2006JD007195.
- Ferraro, R. R., E. A. Smith, W. Berg, and G. J. Huffman (1998), A Screening Methodology for Passive Microwave Precipitation Retrieval Algorithms, *J. Atmos. Sci.*, *55*(9), 1583–1600, doi:10.1175/1520-0469(1998)055<1583:ASMFPM>2.0.CO;2.

- Fiolleau, T., and R. Roca (2013), An Algorithm for the Detection and Tracking of Tropical Mesoscale Convective Systems Using Infrared Images From Geostationary Satellite, *IEEE T. Geosci. Remot.*, *51*(7), 4302–4315, doi:10.1109/TGRS.2012.2227762.
- Futyan, J. M., and A. D. Del Genio (2007), Deep Convective System Evolution over Africa and the Tropical Atlantic, *J. Climate*, *20*(20), 5041–5060, doi:10.1175/JCLI4297.1.
- Guilloteau, C., R. Roca, and M. Gosset (2016), A Multiscale Evaluation of the Detection Capabilities of High-Resolution Satellite Precipitation Products in West Africa, *J. Hydrometeor.*, *17*(7), 2041–2059, doi:10.1175/JHM-D-15-0148.1.
- Guo, H., S. Chen, A. Bao, A. Behrangi, Y. Hong, F. Ndayisaba, J. Hu, and P. M. Stepanian (2016), Early assessment of Integrated Multi-satellite Retrievals for Global Precipitation Measurement over China, *Atmospheric Research*, *176–177*, 121–133, doi:10.1016/j.atmosres.2016.02.020.
- Harrison, D. L., S. J. Driscoll, and M. Kitchen (2000), Improving precipitation estimates from weather radar using quality control and correction techniques, *Met. Apps*, *7*(2), 135–144, doi:10.1017/S1350482700001468.
- Heinold, B., P. Knippertz, J. H. Marsham, S. Fiedler, N. S. Dixon, K. Schepanski, B. Laurent, and I. Tegen (2013), The role of deep convection and nocturnal low-level jets for dust emission in summertime West Africa: Estimates from convection-permitting simulations, *J. Geophys. Res. Atmos.*, *118*(10), 4385–4400, doi:10.1002/jgrd.50402.
- Hennon, C. C., C. N. Helms, K. R. Knapp, and A. R. Bowen (2011), An Objective Algorithm for Detecting and Tracking Tropical Cloud Clusters: Implications for Tropical Cyclogenesis Prediction, *J. Atmos. Ocean. Tech.*, *28*(8), 1007–1018, doi:10.1175/2010JTECHA1522.1.
- Hoskins, B. J., and K. I. Hodges (2002), New perspectives on the Northern Hemisphere winter storm tracks, *Atmos. Sci.*, *59*(6), 1041–1061.
- Hou, A. Y., R. K. Kakar, S. Neeck, A. A. Azarbarzin, C. D. Kummerow, M. Kojima, R. Oki, K. Nakamura, and T. Iguchi (2013), The Global Precipitation Measurement Mission, *Bull. Amer. Meteor. Soc.*, *95*(5), 701–722, doi:10.1175/BAMS-D-13-00164.1.
- Hou, A. Y., R. K. Kakar, S. Neeck, A. A. Azarbarzin, C. D. Kummerow, M. Kojima, R. Oki, K. Nakamura, and T. Iguchi (2013), The Global Precipitation Measurement Mission, *Bull. Amer. Meteor. Soc.*, *95*(5), 701–722, doi:10.1175/BAMS-D-13-00164.1.

- Houze, R. A., Jr., K. L. Rasmussen, M. D. Zuluaga, and S. R. Brodzik (2015), The variable nature of convection in the tropics and subtropics: A legacy of 16 years of the Tropical Rainfall Measuring Mission (TRMM) satellite. *Rev. Geophys.*, 53, doi:10.1002/2015RG000488.
- Hsu, K., H. V. Gupta, X. Gao, and S. Sorooshian (1999), Estimation of physical variables from multichannel remotely sensed imagery using a neural network: Application to rainfall estimation, *Water Resour. Res.*, 35(5), 1605–1618, doi:10.1029/1999WR900032.
- Hsu, N. C., S. C. Tsay, M. D. King, and J. R. Herman (2006), Deep Blue Retrievals of Asian Aerosol Properties During ACE-Asia, *IEEE Transactions on Geoscience and Remote Sensing*, 44(11), 3180–3195, doi:10.1109/TGRS.2006.879540.
- Huffman, G. J., D. T. Bolvin, E. J. Nelkin, D. B. Wolff, R. F. Adler, G. Gu, Y. Hong, K. P. Bowman, and E. F. Stocker (2007), The TRMM Multisatellite Precipitation Analysis (TMPA): Quasi-global, multiyear, combined-sensor precipitation estimates at fine scales, *Journal of Hydrometeorology*, 8(1), 38–55.
- Huffman, G.J., D. Bolvin, D. Braithwaite, K. Hsu, R. Joyce, and P. Xie (2013). NASA Global Precipitation Measurement (GPM) Integrated Multi-satellitE Retrievals for GPM (IMERG). Algorithm Theoretical Basis Doc., version 4.1, NASA, 29 pp.
http://pmm.nasa.gov/sites/default/files/document_files/IMERG_ATBD_V4.1.pdf.
- Janowiak, J. E., R. J. Joyce, and Y. Yarosh (2001), A Real-Time Global Half-Hourly Pixel-Resolution Infrared Dataset and Its Applications, *Bull. Amer. Meteor. Soc.*, 82(2), 205–217, doi:10.1175/1520-0477.
- Jiang, D., H. Zhang, and R. Li (2016), Performance evaluation of TMPA version 7 estimates for precipitation and its extremes in Circum-Bohai-Sea region, China, *Theor Appl Climatol*, 1–13, doi:10.1007/s00704-016-1929-0.
- Joyce, R. J., J. E. Janowiak, P. A. Arkin, and P. Xie (2004), CMORPH: A method that produces global precipitation estimates from passive microwave and infrared data at high spatial and temporal resolution, *Journal of Hydrometeorology*, 5(3), 487–503.
- Kendon, E. J., N. M. Roberts, H. J. Fowler, M. J. Roberts, S. C. Chan, and C. A. Senior (2014), Heavier summer downpours with climate change revealed by weather forecast resolution model, *Nature Clim. Change*, 4(7), 570–576, doi:10.1038/nclimate2258.
- Kidd, C., A. Becker, G. J. Huffman, C. L. Muller, P. Joe, G. Skofronick-Jackson, and D. B. Kirschbaum (2016), So, how much of the Earth’s surface is covered by rain gauges?, *Bull. Amer. Meteor. Soc.*, doi:10.1175/BAMS-D-14-00283.1.

- Kikuchi, K., and B. Wang (2008), Diurnal Precipitation Regimes in the Global Tropics, *Journal of Climate*, 21(11), 2680–2696, doi:10.1175/2007JCLI2051.1.
- Kim, K. M., K. M. Lau, Y. C. Sud and G. K. Walker (2010), Influence of aerosol-radiative forcings on the diurnal and seasonal cycles of rainfall over West Africa and Eastern Atlantic Ocean using GCM simulations, *Clim. Dyn.*, doi:10.1007/s00382-010-0750-1.
- Knippertz, P., and M. C. Todd (2010), The central west Saharan dust hot spot and its relation to African easterly waves and extratropical disturbances, *J. Geophys. Res.*, 115(D12), D12117, doi:10.1029/2009JD012819.
- Kubota, T., and S. Shige (2007), Global Precipitation Map Using Satellite-Borne Microwave Radiometers by the GSMaP Project: Production and Validation, *IEEE Trans. Geosci. Remote Sens.*, 45(7), 2259 – 2275, doi:10.1109/TGRS.2007.895337.
- Kummerow, C. et al. (2000), The Status of the Tropical Rainfall Measuring Mission (TRMM) after Two Years in Orbit, *J. Appl. Meteor.*, 39(12), 1965–1982, doi:10.1175/1520-0450(2001)040<1965:TSOTTR>2.0.CO;2.
- Kunkel, K. E., T. R. Karl, D. R. Easterling, K. Redmond, J. Young, X. Yin, and P. Hennon (2013), Probable maximum precipitation and climate change, *Geophys. Res. Lett.*, 40(7), 1402–1408, doi:10.1002/grl.50334.
- Laing, A. G., and J. Michael Fritsch (1997), The global population of mesoscale convective complexes, *Q.J.R. Meteorol. Soc.*, 123(538), 389–405, doi:10.1002/qj.49712353807.
- Lakshmanan, V., K. Hondl, and R. Rabin (2009), An Efficient, General-Purpose Technique for Identifying Storm Cells in Geospatial Images, *J. Atmos. Ocean. Technol.*, 26(3), 523–537, doi:10.1175/2008JTECHA1153.1.
- Lau, K.-M., K.-M. Kim, Y. C. Sud, and G. K. Walker, 2009: A GCM study of the response of the atmospheric water cycle of West Africa and the Atlantic to Saharan dust radiative forcing *Ann. Geophys.*, 27, 4023-4037.
- Li, J., K. Hsu, A. AghaKouchak, and S. Sorooshian (2015), An object-based approach for verification of precipitation estimation, *International Journal of Remote Sensing*, 36(2), 513–529, doi:10.1080/01431161.2014.999170.
- Liu, C., E. J. Zipser, D. J. Cecil, S. W. Nesbitt, and S. Sherwood (2008), A Cloud and Precipitation Feature Database from Nine Years of TRMM Observations, *J. Appl. Meteor. Climatol.*, 47(10), 2712–2728, doi:10.1175/2008JAMC1890.1.
- Liu, C., and E. J. Zipser (2009), “Warm Rain” in the Tropics: Seasonal and Regional Distributions Based on 9 yr of TRMM Data, *J. Climate*, 22(3), 767–779, doi:10.1175/2008JCLI2641.1.

- Liu, C., and E. J. Zipser (2015), The global distribution of largest, deepest, and most intense precipitation systems: largest, deepest and strongest storms, *Geophys. Res. Lett.*, *42*(9), doi:10.1002/2015GL063776.
- Liu, C., E. J. Zipser, D. J. Cecil, S. W. Nesbitt, and S. Sherwood (2008), A Cloud and Precipitation Feature Database from Nine Years of TRMM Observations, *J. Appl. Meteor. Climatol.*, *47*(10), 2712–2728, doi:10.1175/2008JAMC1890.1.
- Liu, Z. (2015), Comparison of Integrated Multisatellite Retrievals for GPM (IMERG) and TRMM Multisatellite Precipitation Analysis (TMPA) Monthly Precipitation Products: Initial Results, *J. Hydrometeorol.*, *17*(3), 777–790, doi:10.1175/JHM-D-15-0068.1.
- Lovejoy, S., and D. Schertzer (2006), Multifractals, cloud radiances and rain, *J. Hydrol.*, *322*(1-4), 59–88, doi:10.1016/j.jhydro.2005.02.042.
- Machado, L. A. T., and H. Laurent (2004), The convective system area expansion over Amazonia and its relationships with convective system life duration and high-level wind divergence, *Monthly weather review*, *132*(3), 714–725.
- Machado, L. A. T., M. Desbois, and J.-P. Duvel (1992), Structural Characteristics of Deep Convective Systems over Tropical Africa and the Atlantic Ocean, *Monthly Weather Review*, *120*(3), 392–406, doi:10.1175/1520-0493(1992)120<0392:SCODCS>2.0.CO;2.
- Machado, L. A. T., W. B. Rossow, R. L. Guedes, and A. W. Walker (1998), Life cycle variations of mesoscale convective systems over the Americas, *Mon. Weather Rev.*, *126*(6), 1630–1654.
- Maddox, R. A. (1980), Mesoscale Convective Complexes, *Bull. Amer. Meteor. Soc.*, *61*(11), 1374–1387, doi:10.1175/1520-0477.
- Mapes, B. E., and R. A. Houze (1993), Cloud Clusters and Superclusters over the Oceanic Warm Pool, *Mon. Weather Rev.*, *121*(5), 1398–1416, doi:10.1175/1520-0493.
- Mapes, B. E., T. T. Warner, and M. Xu (2003), Diurnal Patterns of Rainfall in Northwestern South America. Part III: Diurnal Gravity Waves and Nocturnal Convection Offshore, *Monthly Weather Review*, *131*(5), 830–844, doi:10.1175/1520-0493(2003)131<0830:DPORIN>2.0.CO;2.
- Morel, C., and S. Senesi (2002), A climatology of mesoscale convective systems over Europe using satellite infrared imagery. II: Characteristics of European mesoscale convective systems, *Q.J.R. Meteorol. Soc.*, *128*(584), 1973–1995, doi:10.1256/003590002320603494.

- Nesbitt, S. W., and E. J. Zipser (2003), The Diurnal Cycle of Rainfall and Convective Intensity according to Three Years of TRMM Measurements, *J. Climate*, *16*(10), 1456–1475, doi:10.1175/1520-0442-16.10.1456.
- Neu, U. et al. (2013), IMILAST: A Community Effort to Intercompare Extratropical Cyclone Detection and Tracking Algorithms, *Bull. Amer. Meteor. Soc.*, *94*(4), 529–547, doi:10.1175/BAMS-D-11-00154.1.
- Oliveira, R., V. Maggioni, D. Vila, and C. Morales (2016), Characteristics and Diurnal Cycle of GPM Rainfall Estimates over the Central Amazon Region, *Remote Sens.*, *8*(7), 544, doi:10.3390/rs8070544.
- Parzen, E. (1962), On Estimation of a Probability Density Function and Mode, *Ann. Math. Statist.*, *33*(3), 1065–1076, doi:10.1214/aoms/1177704472.
- Prospero, J. M. (1999), Long-term measurements of the transport of African mineral dust to the southeastern United States: Implications for regional air quality, *J. Geophys. Res.*, *104*(D13), 15917–15927, doi:10.1029/1999JD900072.
- Prospero, J. M., and P. J. Lamb (2003), African Droughts and Dust Transport to the Caribbean: Climate Change Implications, *Science*, *302*(5647), 1024–1027, doi:10.1126/science.1089915.
- Rienecker, M. M. et al. (2011), MERRA: NASA’s Modern-Era Retrospective Analysis for Research and Applications, *J. Climate*, *24*(14), 3624–3648, doi:10.1175/JCLI-D-11-00015.1.
- Rosenblatt, M. (1956), Remarks on Some Nonparametric Estimates of a Density Function, *Ann. Math. Statist.*, *27*(3), 832–837, doi:10.1214/aoms/1177728190.
- Sassen, K., P. J. DeMott, J. M. Prospero, and M. R. Poellot (2003), Saharan dust storms and indirect aerosol effects on clouds: CRYSTAL-FACE results, *Geophys. Res. Lett.*, *30*(12), 1633, doi:10.1029/2003GL017371.
- Schmit, T. J., M. M. Gunshor, W. P. Menzel, J. J. Gurka, J. Li, and A. S. Bachmeier (2005), Introducing the next-generation advanced baseline imager on goes-r, *Bull. Amer. Meteor. Soc.*, *86*(8), 1079–1096, doi:10.1175/BAMS-86-8-1079.
- Skok, G., J. Tribbia, J. Rakovec, and B. Brown (2009), Object-Based Analysis of Satellite-Derived Precipitation Systems over the Low- and Midlatitude Pacific Ocean, *Monthly Weather Review*, *137*(10), 3196–3218, doi:10.1175/2009MWR2900.1.
- Silva Dias, P. L., J. P. Bonatti, and V. E. Kousky (1987), Diurnally Forced Tropical Tropospheric Circulation over South America, *Mon. Wea. Rev.*, *115*(8), 1465–1478, doi:10.1175/1520-0493(1987)115<1465:DFTTCO>2.0.CO;2.

- Sinclair, M. R. (1994), An Objective Cyclone Climatology for the Southern Hemisphere, *Mon. Wea. Rev.*, 122(10), 2239–2256, doi:10.1175/1520-0493.
- Stephens, G. L., T. L'Ecuyer, R. Forbes, A. Gettleman, J.-C. Golaz, A. Bodas-Salcedo, K. Suzuki, P. Gabriel, and J. Haynes (2010), Dreary state of precipitation in global models, *J. Geophys. Res.*, 115, D24211, doi:10.1029/2010JD014532.
- Stephens, G. L., T. L'Ecuyer, R. Forbes, A. Gettleman, J.-C. Golaz, A. Bodas-Salcedo, K. Suzuki, P. Gabriel, and J. Haynes (2010), Dreary state of precipitation in global models, *J. Geophys. Res.*, 115, D24211, doi:10.1029/2010JD014532.
- Storer, R. L., S. C. van den Heever, and T. S. L'Ecuyer (2014), Observations of aerosol-induced convective invigoration in the tropical east Atlantic, *J. Geophys. Res. Atmos.*, 119(7), 3963–3975, doi:10.1002/2013JD020272.
- Sui, C.-H., K.-M. Lau, Y. N. Takayabu, and D. A. Short (1997), Diurnal Variations in Tropical Oceanic Cumulus Convection during TOGA COARE, *J. Atmos. Sci.*, 54(5), 639–655, doi:10.1175/1520-0469(1997)054<0639:DVITOC>2.0.CO;2.
- Tadesse, A., and E. N. Anagnostou (2009), The Effect of Storm Life Cycle on Satellite Rainfall Estimation Error, *J. Atmos. Ocean.*, 26(4), 769–777, doi:10.1175/2008JTECHA1129.1.
- Tan, J., W. A. Petersen, and A. Tokay (2016), A Novel Approach to Identify Sources of Errors in IMERG for GPM Ground Validation, *J. Hydrometeor.*, 17(9), 2477–2491, doi:10.1175/JHM-D-16-0079.1.
- Tang, G., Y. Ma, D. Long, L. Zhong, and Y. Hong (2016), Evaluation of GPM Day-1 IMERG and TMPA Version-7 legacy products over Mainland China at multiple spatiotemporal scales, *Journal of Hydrology*, 533, 152–167, doi:10.1016/j.jhydrol.2015.12.008.
- Tang, G., Z. Zeng, D. Long, X. Guo, B. Yong, W. Zhang, and Y. Hong (2015), Statistical and Hydrological Comparisons between TRMM and GPM Level-3 Products over a Midlatitude Basin: Is Day-1 IMERG a Good Successor for TMPA 3B42V7?, *J. Hydrometeor.*, 17(1), 121–137, doi:10.1175/JHM-D-15-0059.1.
- Tao, W.-K., J.-P. Chen, Z. Li, C. Wang, and C. Zhang (2012), Impact of aerosols on convective clouds and precipitation, *Rev. Geophys.*, 50(2), RG2001, doi:10.1029/2011RG000369.
- Teng, H.-F., C.-S. Lee, and H.-H. Hsu (2014), Influence of ENSO on formation of tropical cloud clusters and their development into tropical cyclones in the western North Pacific: Influence of ENSO on TCC Formation, *Geophysical Research Letters*, 41(24), 9120–9126, doi:10.1002/2014GL061823.

- Thorncroft, C., and K. Hodges (2001), African Easterly Wave Variability and Its Relationship to Atlantic Tropical Cyclone Activity, *J. Climate*, *14*(6), 1166–1179, doi:10.1175/1520-0442(2001)014<1166:AEWVAI>2.0.CO;2.
- Tian, Y., C. D. Peters-Lidard, B. J. Choudhury, and M. Garcia (2007), Multitemporal Analysis of TRMM-Based Satellite Precipitation Products for Land Data Assimilation Applications, *J. Hydrometeorol*, *8*(6), 1165–1183, doi:10.1175/2007JHM859.1.
- Tian, Y., and C. D. Peters-Lidard (2010), A global map of uncertainties in satellite-based precipitation measurements, *Geophys. Res. Lett.*, *37*(24), L24407, doi:10.1029/2010GL046008.
- Tian, Y., G. S. Nearing, C. D. Peters-Lidard, K. W. Harrison, and L. Tang (2016), Performance Metrics, Error Modeling, and Uncertainty Quantification, *Monthly Weather Review*, *144*(2), 607–613, doi:10.1175/MWR-D-15-0087.1.
- Trenberth, K. E., A. Dai, R. M. Rasmussen, and D. B. Parsons (2003), The Changing Character of Precipitation, *Bull. Amer. Meteor. Soc.*, *84*(9), 1205–1217, doi:10.1175/BAMS-84-9-1205.
- Trenberth, K. E., A. Dai, R. M. Rasmussen, and D. B. Parsons (2003), The Changing Character of Precipitation, *Bull. Amer. Meteor. Soc.*, *84*(9), 1205–1217, doi:10.1175/BAMS-84-9-1205.
- Twohy, C. H. (2014), Measurements of Saharan Dust in Convective Clouds over the Tropical Eastern Atlantic Ocean, *J. Atmos. Sci.*, *72*(1), 75–81, doi:10.1175/JAS-D-14-0133.1.
- Velasco, I., and J. Fritsch (1987), Mesoscale Convective Complexes in the America, *J. Geophys. Res.-Atmos.*, *92*(D8), 9591–9613, doi:10.1029/JD092iD08p09591.
- Vila, D. A., L. A. T. Machado, H. Laurent, and I. Velasco (2008), Forecast and Tracking the Evolution of Cloud Clusters (ForTraCC) using satellite infrared imagery: Methodology and validation, *Wea. Forecasting*, *23*(2), 233–245.
- Walsh, J. J., and K. A. Steidinger (2001), Saharan dust and Florida red tides: The cyanophyte connection, *J. Geophys. Res.*, *106*(C6), 11597–11612, doi:10.1029/1999JC000123.
- Westra, S., H. J. Fowler, J. P. Evans, L. V. Alexander, P. Berg, F. Johnson, E. J. Kendon, G. Lenderink, and N. M. Roberts (2014), Future changes to the intensity and frequency of short-duration extreme rainfall, *Rev. Geophys.*, *52*(3), 2014RG000464, doi:10.1002/2014RG000464.
- Wilcox, E., K. M. Lau, and K. M. Kim (2010), A northward shift of the North Atlantic Ocean Intertropical Convergence Zone in response to summertime

- Saharan dust outbreaks. *Geophys. Res. Lett.* 37, L04804, doi:10.1029/2009GL041774.
- Wilks, D. S. (2011), *Statistical methods in the atmospheric sciences*, International geophysics series v. 100, 3rd ed., Elsevier/Academic Press, Amsterdam ; Boston.
- Williams, M., and R. A. Houze (1987), Satellite-Observed Characteristics of Winter Monsoon Cloud Clusters, *Mon. Weather Rev.*, 115(2), 505–519, doi:10.1175/1520-0493.
- Wu, L. (2007), Impact of Saharan air layer on hurricane peak intensity, *Geophys. Res. Lett.*, 34(9), L09802, doi:10.1029/2007GL029564.
- Wu, M.-L. C., O. Reale, S. D. Schubert, M. J. Suarez, R. D. Koster, and P. J. Pegion (2009), African Easterly Jet: Structure and Maintenance, *J. Climate*, 22(17), 4459–4480, doi:10.1175/2009JCLI2584.1.
- Xie, P., and A.-Y. Xiong (2011), A conceptual model for constructing high-resolution gauge-satellite merged precipitation analyses, *J. Geophys. Res.*, 116(D21), D21106, doi:10.1029/2011JD016118.
- Zahraei, A., K. Hsu, S. Sorooshian, J. J. Gourley, Y. Hong, and A. Behrangi (2013), Short-term quantitative precipitation forecasting using an object-based approach, *J. Hydrol.*, 483, 1–15, doi:10.1016/j.jhydrol.2012.09.052.
- Zeng, N. (2003), Drought in the Sahel, *Science*, 302(5647), 999–1000, doi:10.1126/science.1090849.
- Zeng, N., J. D. Neelin, K.-M. Lau, and C. J. Tucker (1999), Enhancement of Interdecadal Climate Variability in the Sahel by Vegetation Interaction, *Science*, 286(5444), 1537–1540, doi:10.1126/science.286.5444.1537.
- Zhang, J. et al. (2011), National Mosaic and Multi-Sensor QPE (NMQ) System: Description, Results, and Future Plans, *Bull. Amer. Meteor. Soc.*, 92(10), 1321–1338, doi:10.1175/2011BAMS-D-11-00047.1.
- Zhang, J., Y. Qi, C. Langston, and B. Kaney (2011), Radar Quality Index (RQI)—A combined measure of beam blockage and VPR effects in a national network, ResearchGate, 351.
- Zipser, E. J. et al. (2009), The Saharan Air Layer and the Fate of African Easterly Waves—NASA’s AMMA Field Study of Tropical Cyclogenesis, *Bull. Amer. Meteor. Soc.*, 90(8), 1137–1156, doi:10.1175/2009BAMS2728.1.
- Zipser, E. J., D. J. Cecil, C. Liu, S. W. Nesbitt, and D. P. Yorty (2006), Where are the most intense thunderstorms on earth?, *Bull. Amer. Meteorol. Soc.*, 87(8), 1057, doi:10.1175/BAMS-87-8-1057.

Zolina, O., and S. K. Gulev (2002), Improving the Accuracy of Mapping Cyclone Numbers and Frequencies, *Mon. Wea. Rev.*, *130*(3), 748–759, doi:10.1175/1520-0493.

Zuidema, P. (2003), Convective Clouds over the Bay of Bengal, *Mon. Wea. Rev.*, *131*(5), 780–798, doi:10.1175/1520-0493(2003)131<0780:CCOTBO>2.0.CO;2.